THE FACULTY OF ENGINEERING AND THE BUILT ENVIRONMENT

Department of Mechanical Engineering

Thermodynamic Analysis and Performance Evaluation of PTC Receiver with External Annular Fins.

By

Jacob Mator Aketch

A dissertation submitted to the Department of Mechanical Engineering, University of Cape Town in partial fulfilment of the requirements for the degree of Master of Science in Mechanical Engineering

Declaration

I, Jacob Mator Aketch, know the meaning of plagiarism and declare that all the work in the document, save for that which is properly acknowledged, is my own. This thesis/dissertation has been submitted to the Turnitin module, and I confirm that my supervisor has seen my report and any concerns revealed by such have been resolved with my supervisor.

Signed by candidate

Jacob Mator Aketch
Date: 02-12-2023

Abstract

Title:	Thermodynamic Analysis and Performance Evaluation of PTC Receiver with Annular External Fins.
Author:	Jacob Mator Aketch (AKTJAC001)
Supervisor:	Prof. Tunde Bello-Ochende
University:	University of Cape Town
Department:	Mechanical Engineering
Degree:	Master of Science in Mechanical Engineering (M.Sc. Mech. Eng.)

Since the advent of industrial revolution, the main source of energy has been fossil fuels, and it has resulted in adverse environmental impacts. With the depletion of fossil fuels and greenhouse effect, the utilization of solar energy has attracted increasing attention owing to the distinct advantages, including cleanliness, sustainability, inexhaustibility. This has motivated extensive research and innovation to foster a shift to renewable energies, of which concentrated solar power presents itself as the most promising option. Given the unrivalled abundance of solar energy, the source has a potential to meet a substantial portion of future energy demand.

This research investigates the influence of external annular fins on the thermal and thermodynamic performance of parabolic trough collector receiver. The objective is achieved by developing thermal and fluid flow model with geometry of varied fin length and fin numbers in different range of Reynolds number and inlet temperature. The model was implemented in commercial ANSYS Fluent software and validated with existing literature—Forristall (2003) that yielded significant agreement.

The results showed that introduction of fins increases thermal efficiency of the receiver. An increase of 2.26 percent for T_{in} = 350 K, 2.21 percent for T_{in} = 400 K and 2.22 percent for T_{in} = 500 K was recorded for varying Reynolds numbers. Also, the thermal efficiency in t = 10 mm was higher than t = 5 mm with values in the range of 88 - 90.5 percent while smooth receiver fell in the range of 84 - 86 percent. Additionally, thermal enhancement factor showed slight improvement.

What’s more, exergy efficiency showed an improvement with introduction of fins. It was noted that the enhancement increased the exergy efficiency by 2.44 percent for *Re* = 5000, 2.30 percent for *Re* = 10000, and 2.30 percent for *Re* = 20000.

Similarly, entropy generation reduced with fins variations. The entropy generation rate decreases with increasing fin length. The smooth absorber tube has the highest entropy generation rate whereas the absorber tube with largest fin length has the lowest. Heat transfer irreversibility has been found to be dominant at lower turbulence and variation of annular fin length and numbers reduces it.

In summary, the introduction of passive enhancement of external annular fins was shown by the results to be thermally and thermodynamically favourable, regardless of the degree of improvement. Therefore, this enhancement technique can be combined with other methods to design a high performing PTC receiver—an endeavour that will contribute to implementation of a stand-alone reliable PTC power plants.

Keywords: Annular fins, ANSYS Fluent, Bejan number, CFD, Concentrated solar power, Entropy generation, Exergy, Parabolic trough collector, PTC receiver, Renewable energy, Thermal efficiency.

Dedication

This work is dedicated to the loving memory of

Kɔkɔk, ***Ang'ok Kuir Khoc****.*

May her unconditional love for people around her, and a passion to serve her community with utmost integrity and dignity eternally live on in us—those whose lives she profoundly touched.

Acknowledgements

I would like to acknowledge and extend my heart-felt gratitude to the following individuals and entities:

- **Almighty God** for giving me good health and serenity of mind during this research.
- My supervisor, *Prof. Tunde Bello-Ochende*, whose meticulous expert guidance offered this work the value it possesses. Grateful for the mentorship!
- *Dr. Majak D'Agoot* for his wise advice, unwavering support, and consistent encouragement to keep continuous education at the core of self-improvement and life endeavours.
- *Dr. Tanimu Jatau* for his generous assistance in learning ANSYS Fluent Software, and for providing moral support by giving general advice on the right attitude to have when approaching scientific investigation—something that was very helpful.
- *Denise Botha* for being exceptionally resourceful with administrative needs during the span of this research.
- My colleagues in the lab who offered conducive, friendly, and socially nurturing environment during this research.
- *Mastercard Foundation* for providing scholarship to pursue this postgraduate program, without which the dream of attaining this qualification would have been a mere mirage.

Table of Contents

List of Figures

List of Tables

Acronyms

EES	Engineering equation solver
CFD	Computational Fluid Dynamics
CLFC	Central Linear Fresnel Collector
CSP	Concentrated Solar Power
HCE	Heat Collector Element
HTF	Heat Transfer Fluid
IEA	Internatinal Energy Agency
LFR	Linear Fresnel Reflector
LFC	Linear Fresnel Collector
PEC	Performance Evaluation Criteria
PTC	Parabolic Trough Collector
RANS	Reynolds Average Naviers-Stokes
RNG	Re-Normalization Group
SEGS	Solar Energy Generating System
TES	Thermal Energy Storage

Nomenclature

A	Area, m^2
A_a	Collector's aperture area, m^2
A_r	Absorber tube's outer surface area, m^2
A_{wet}	Absorber tube's inner surface area, m^2
Be	Bejan number.
C_1, C_2, C_μ	Turbulent model constants
c_f	Skin friction coefficient
c_p	Specific heat capacity, J kg^{-1} K^{-1}
C_R	Concentration ratio
DNI	Direct normal irradiance, W/m^2
d_{gi}	Glass cover inner diameter, m
d_{go}	Glass cover outer diameter, m
d_{ri}	Absorber tube inner diameter, m
d_{ro}	Absorber tube outer diameter, m
f	Fluid friction factor
G	Mass flux, kg/m^2s
G_k	Generation of turbulence kinetic energy due to mean velocity gradients, kg $m^{-1}s^{-3}$
h	Heat transfer coefficient, W $m^{-2}K^{-1}$
h_w	Wind convection heat transfer coefficient, Wm^{-2} K^{-1}
I_b	Direct solar radiation. W m^{-2}
k	Turbulent kinetic energy, m^2 s^{-2}
L	Length, m
$\dot{m}$	Mass flow rate, kg/s
Nu	Nusselt number
P	Pressure, Pa
Pr	Prandtl number
q'	Heat transfer rate per meter length, W/m
q''	Heat flux, W m^{-2}

Re	Reynolds number
t	Fin length
S	Modulus of the mean rate-of-strain tensor, s^{-1}
S_{ij}	Rate of linear deformation tensor, s^{-1}
S_{gen}	Entropy generation rate due to heat transfer and fluid friction, W/K
S'_{gen}	Entropy generation due to heat transfer and fluid friction per unit length, W/m K
$(S_{gen})_H$	Entropy generation due to heat transfer, W/ K
$(S_{gen})_F$	Entropy generation due to fluid friction, W/ K
$(S'_{gen})_H$	Entropy generation due to heat transfer per unit length, W/ m K
$(S'_{gen})_F$	Entropy generation due to fluid friction per unit length, W/ m K
T	Temperature, K
u_m	Mean velocity, m s^{-1}
V	Volume, m^3
V_w	Wind speed, m/s
u_i, u_j	Averaged velocity components, m s^{-1}
u', v', w'	Fluctuations from mean velocity, m s^{-1}
u_τ	Friction velocity, m s^{-1}
$\dot{V}$	Volumetric flow rate, m^3/s
W_a	Collector aperture width, m
$\dot{W}_p$	Pumping power, W
x_i, x_j	Spatial coordinates, m
x,y,z	Cartesian coordinates
y^+	Dimensionless wall coordinate
$-\rho\overline{u_i'u_j'}$	Reynolds stresses, N m^{-2}
ΔP	Pressure drop, Pa

Greek letters

α Thermal diffusivity, $m^2\ s^{-1}$

α_t Turbulent thermal diffusivity, $m^2\ s^{-1}$

δ_{ij} Kronecker delta

ε Turbulent dissipation rate, $m^2\ s^{-3}$

λ Fluid thermal conductivity, $Wm^{-1}\ K^{-1}$

η Turbulence model parameter = Sk/ε

η_{th} Thermal efficiency, %

φ_r Rim angle

ϕ Absorber tube's circumferential temperature difference, K

ρ Density, $kg\ m^{-3}$

α_t Turbulent thermal diffusivity, $m^2\ s^{-1}$

σ_ε Turbulent Prandtl number for ε

$\sigma_{h.t}$ Turbulent Prandtl number for energy

σ_k Turbulent Prandtl number for k

τ_g Glass cover transmissivity

τ_w Wall shear stress

θ Receiver circumferential angle

μ Viscosity, Pa s

μ_t Turbulent viscosity, Pa s

μ_τ Friction velocity, m/s

μ_{eff} Effective viscosity, Pa s

v Kinematic viscosity, $m^2\ s^{-1}$

χ Thermal enhancement factor

Subscripts

amb	Ambient state
abs	Absorber
bulk	Bulk fluid state
col	Collector
en	Enhanced absorber tube
in	Absorber tube inlet
out	Absorber tube outlet
i, j, k	General spatial indices
p	Plain absorber tube
r_i	Absorber tube inner wall
r_o	Absorber tube outer wall
sky	Sky

Superscripts

$\bar{}$	Mean value
$\tilde{}$	Dimensionless value

Chapter One

Chapter 1: Introduction

1.1. Background

Since the advent of industrial revolution, the main source of energy has been fossil fuels, and it has resulted in adverse environmental impacts. With the depletion of fossil fuels and greenhouse effect, the utilization of solar energy has attracted increasing attention owing to the distinct advantages—cleanliness, sustainability, inexhaustibility [1]. This has motivated extensive research and innovation to foster a shift to renewable energies, of which concentrated solar power is the most promising option. Solar energy positions itself to meet both present and future energy demands, given its unparalleled abundance. The International Energy Agency (IEA) expects the concentrated solar power (CSP) technologies to be highly competitive by 2030, and it projects that by 2050,11.3% of total global electricity could be provided by these means, leading to a reduction in CO2-emission of 2.1 gigaton per year, if fully exploited [2].

Due to unsustainability of fossil fuels, and their adverse propagation of climate change, it has proven necessary to evolve energy consumption towards more environmentally friendly sources [3]. Being inexhaustible, clean, and plentiful, solar energy is the best alternative, but its intermittency and costliness limits its widespread use [4]. The intrinsically intermittent and diurnal nature of the solar resource and the strong influence of meteorological phenomena drastically reduce the effective availability of CSP power plants [5]. This problem can be solved by hybridization and increasing the reliability of the system by optimizing the most critical components.

Notable innovations such as hybridization are still at their nascency, with investigation being within the domain of academic investigations. Most studies focus on numerical and theoretical assessment of thermodynamics and economics of hybridization of diversified types of CSP system by investigating influence of the design parameters on energy, exergy efficiencies, and cost of production of plants such as desalination plants [6]. These kinds of CSP system tend to be on a small scale, when implemented.

To scale up the systems and ensure high reliability of the plants, the receiver needs a study on how its performance can be maximized, since it is the most critical component.

To ensure augmented reliability of parabolic trough collector in generating electricity, it is coupled with heat cycle process, gas turbine plant, electric generator Stirling, and biomass catalytic hydrothermal reforming process [7]

Although hybridization is an effective means to achieve high yield factor, it is advantageous to have stand-alone PTC system with relatively high reliability. To improve the performance of the system, various heat transfer enhancements are applied. For example, a twisted tape insert in PTC receiver is usually used. The swirling flow the tape insert generates enable effective heat exchange heat transfer, but it equally facilitates high pressure drop [8]. Despite its effectiveness in augmenting the performance, spike in pressure drop demands higher pumping power which is costly. Other design parameters such as concentration ratio influence performance of the receiver system. Increasing concentrator sizes and concentration ratios of the collector is one way of improving performance and reducing costs [9]. Like other heat transfer enhancement methods of performance improvement, extensive designs and studies concentrating on concentration ratio have been conducted.

The PTC system being considered in this study is in configuration as shown in Fig.1. 1

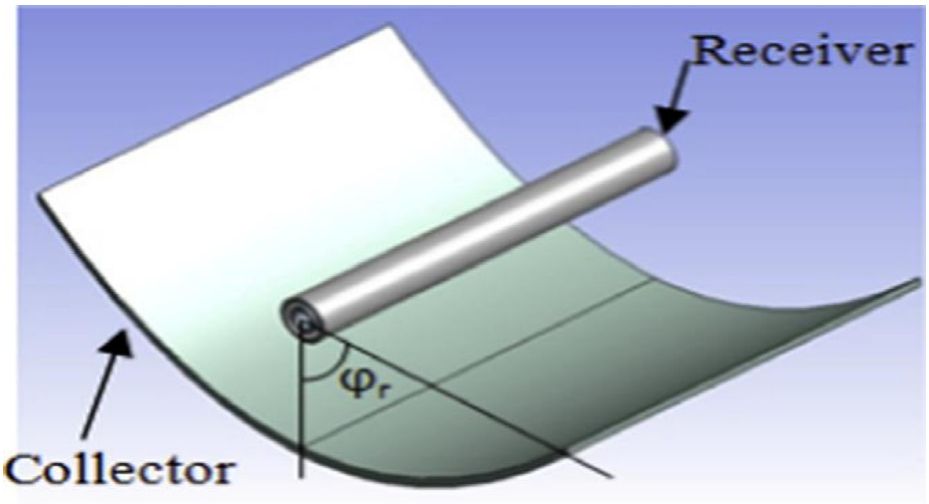

Fig.1. 1: Parabolic trough collector system [9]

This study focuses on the receiver. The research delves into the means of passively enhancing the geometry of the receiver to improve its performance.

1.2. Motivation

Success of energy transition depends on the capacity of the renewable energy technologies deployed. So far, most technologies in operation are not sufficiently efficient to independently generate power without supplement from the traditional fossil fuels.

To achieve the robustness of renewable technologies, scientific research needs to focus on the innovations with the highest potential. Concentrated solar power is one of those technologies that can revolutionize the energy sector, thus curtailing the effect of climate change.

Parabolic trough collector system as one of many CSP technologies has been sufficiently developed and operationalized in many countries on large scale. Despite its cost-effectiveness and ability to generate enough power, its reliability is still not at the optimum. To ensure the maximum reliability is achieved, critical components responsible for energy generation such as receiver should be optimally designed and improved.

The design of the PTC receiver is done with thermal and optical losses in consideration. The critical elements considered are composed of aggregate thermal losses and exergy destruction, and the final useful work (exergy) as represented in Fig.1. 2.

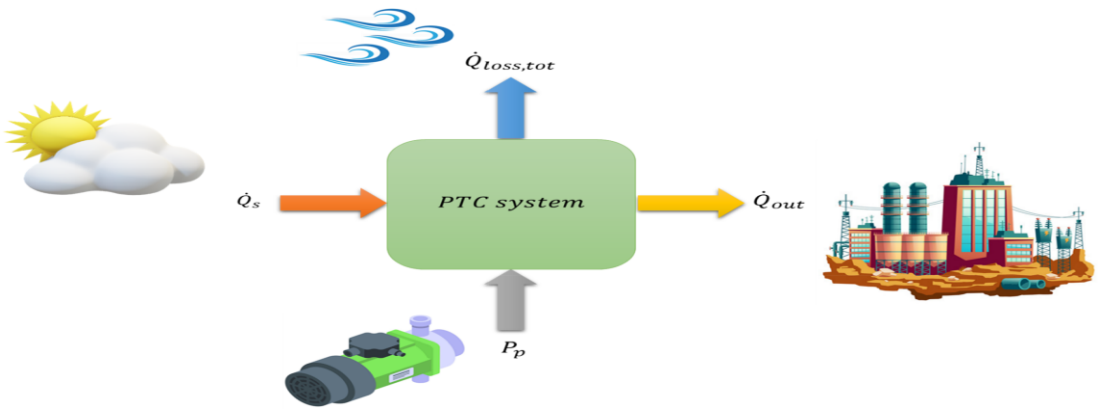

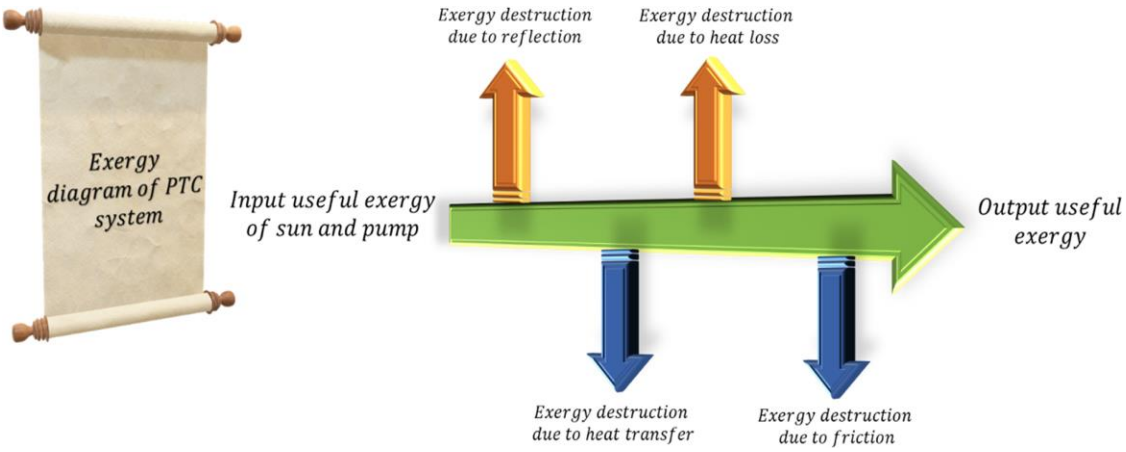

Fig.1. 2: Energy and exergy representation as extracted from Vahedi et al. [10]

Although the schematic shown above is just a system representation, it reflects what happens at the component level. Thermal losses and exergy destruction in individual vital components contribute to lower performance of the whole system. The most critical component involved in these processes in the case of the parabolic trough collector system is the receiver. Therefore, improving its thermal and thermodynamic performance consequently improves the aggregate system reliability.

Adding external fins to the conventional cylindrical receiver increases the surface area and that has a potential of enhancing the conductive heat transfer. Investigating its influence on the performance of the receiver definitively establishes its potential in enhancing the whole system's reliability.

At the current stage of the parabolic trough collector system operationalization, it is oftentimes coupled with the fossil-fuel power plants as mentioned in *section 1.1* due to its unstable performance. It ensures delivery of power on demand and continuously and reliably produces electricity [11].

In addition to many variations of heat transfer enhancements, numerous studies have been conducted to maximize the heat transfer through appropriate receiver design with high absorption properties and low emittance through a selective coating attached to collector with accurate tracking mechanism [12]. This contributes to the effort of making the system independent and thus fostering a complete shift to renewable energy, which consequently mitigates the looming impacts of climate change.

1.3. Problem Statement

As mentioned in *section 1.1* of this work, the environmental degradation because of reliance on fossil fuels as source of the energy has made it pressing to shift to clean and sustainable energy. It is established that if the average global temperature rises above two degrees Celsius, the result will be catastrophic. Therefore, intensive research has been initiated by academic institutions and governments to address the challenge.

As illustrated in *chapter 2* of this work, extensive research has been conducted on concentrated solar power as it is the most sustainable solution due to abundance of energy resource from the Sun.

Despite the extensive innovations, this source is still not self-sufficient as a source of energy due to inherent factors that affect the solar radiation supply. Therefore, it is necessary to study the means to maximize the energy generation with novel design of the system. Such design targets critical components like the receiver system—an element on which much of plants' reliability depends.

This research tries to investigate some enhancements of the receiver system aimed at the maximization of energy generation to improve the general reliability the concentrated solar power.

1.4. Objective

The general objective of this research is to investigate the influence of external annular fins on the thermal and thermodynamic performance of the PTC receiver. To accomplish this objective, a comparative analysis with unenhanced receiver is carried out. Some of the performance evaluation criteria considered include thermal and exergy efficiencies, entropy generation, thermal enhancement factor, and Bejan number.

1.5. Summarized Methodology

To achieve the objectives of this study, the author utilizes the following methodology:

- Thermal model and computational fluid dynamics model were developed and implemented in a commercially available ANSYS Fluent software.
- Various simplifying assumptions were made to develop the models to reduce the complexity.

- The numerical results obtained from the developed models were validated with trustworthy simulation data that have extensively been used in model validation of similar CFD studies to establish their accuracy and trustworthiness.
- Targeted geometries were subjected to iterative simulations and the results obtained were subjected to comparative analysis using performance evaluation criteria (PECs) based on the first and second laws of thermodynamics.
- Conclusions were then established from the analysis.

1.6. Organization of the thesis

The thesis has been laid out as follows:

Chapter 1**:** *Introduction.* It gives the background information of the study, its motivation, the literature gap it aims to bridge, and objectives that need to be tested.

Chapter 2: *Literature study*. It explores the body of knowledge available on concentrated solar power and the relevant research that has been conducted on the design and performance of parabolic trough collector receiver. The objective of the chapter is to offer background knowledge necessary to fully understand this source of energy.

Chapter 3: *Numerical modelling and theoretical framework*. It delves into the theory of the research and the methodology that is applied to test the specific objectives of this study.

Chapter 4: *Model validation*. The chapter tests the accuracy of the developed models by conducting comparative analysis with the well-established and trustworthy literature.

Chapter 5: *Performance evaluation based on the First Law of Thermodynamics*. This chapter utilizes the performance evaluation criteria based on the First Law of Thermodynamics to evaluate the thermal and thermodynamic performance of the receiver.

Chapter 6: *Performance evaluation based on the Second Law of Thermodynamics*. Just like chapter 5, it uses PECs based on the Second Law of Thermodynamics to examine the performance of the designed receiver.

Chapter 7: *Summary, conclusion, and recommendations*. The chapter presents a summary of the entire work, draws conclusions from the findings, and suggests recommendations for future study.

Chapter Two

Chapter 2: Literature Study

2.1. Background

Numerous concentrated solar power technologies have been fully developed and deployed. The main CSP technologies includes linear Fresnel reflector, parabolic trough collector (PTC), parabolic dish, and solar tower [13]. Extensive research has been conducted on these technologies.

The purpose of this chapter is to offer the exploratory discussion on these technologies and provide highlights of the most important research conducted on parabolic trough collector (PTC) with special focus on the thermal and thermodynamic enhancements of the receiver. It also explores various modelling techniques that have been applied to past and ongoing research and the relevant findings generated.

At the final section of the chapter, a discussion of various performance evaluation criteria based on the first and second laws of thermodynamics is done, among which are utilized in this research. This establishes a better understanding of the technical underpinnings of the considered PECs.

2.2. Concentrated solar power overview.

2.2.1. Parabolic dish

As mentioned in *section 2.1*, Parabolic Dish (Dish-Stirling) is one of the CSP technologies presently deployed in either the small-scale or large-scale production of renewable energy. The parabolic dish is a CSP technology performing an efficient conversion of direct normal irradiance (DNI) into electricity [2]. Its major components consist of paraboloidal dish, power conversion unit that compartmentalizes alternator, Stirling engine and receiver, and solar tracking system.

According to Backes *et al*. [2] parabolic dish is made up of 104 independent glass mirrors, installed on a steel structure that collect and focus the incident solar beam radiation to a focal point placed at more than seven meters from its vertex, mirrors of high reflectivity, and Stirling engines with high conversion efficiency that reach higher

that 30 % with DNI above 900 W/m^2. This optimal design ensures attainment of the optimal specific yield of the system.

As shown in Fig.2. 1, parabolic dish is designed in a way that maximizes both optical and thermal efficiency which translates to more power output. The parabolic dish is usually fitted with direct steam generation receivers coupled to off-grid engines or on-grid steam power plants [14].

Fig.2. 1: The Ominium-G Parabolic Dish collector [14]

Operationally, the receiver is placed at the focal point of the reflector and firmly supported in that place with steel girders. It functions as a converting mechanism for radiative energy concentrated by the reflector at the focal point. The radiation is converted to thermal energy captured in HTF which is then transferred to module where heat transfer is done to directly heat up the working fluid for power generation.

Just like any other system, an optimal design does not always ensure the high efficiency over life cycle of such system. The maximum optical efficiency of the concentrator is assured by a periodical mirror cleaning [2].

Several performance assessments have been conducted on this system and clear mathematical parameterization has been established to accurately model the system. Subramani *et.al* [15] outlines the critical parameters in eq.(2.1 and (2.2).

$$x^2 = 4yf \tag{2.1}$$

$$f = \frac{w}{4\tan\left(\frac{\theta}{2}\right)} \quad (2.2)$$

The formulae are oftentimes utilized in numerical simulations as well as in physical designing the system.

Performance of parabolic dish has been extensively studied. For instance, Msaddak *et al*. [16] utilized Lattice Boltzmann Method coupled with net radiation method to determine heat loss from cavity receiver of the parabolic dish and concluded that convective losses are increased by increasing the inclination angle whereas radiative heat losses are unchanged by inclination angle changes. They also established that while an increase in surface emissivity marginally reduced natural connective losses, it also linearly increases the radiative losses. From this conclusion, a system can be optimized to reduce the aggregate losses that can potentially affect the efficiency of the cavity receiver which is widely used. Wang *et al*. [17] enhanced the similar system with spillage skirts and secondary reflector and found that the spillage skirts reduced cavity receiver dimensions while decreasing spillage loss. The secondary reflector was found to have similar effects of reducing aperture while decreasing spillage loss. The attempt in optimization of this system is geared toward reducing the heat losses—a factor that has adverse effects on the general performance of the system.

Since this research is not dealing with parabolic dish systems, these highlights provide sufficient grounding in its design, operation, and enhancement.

2.2.2. Linear Fresnel collector

Developed from the concept of linear Fresnel Lens, the collector is made of arrays of flat, slightly curved, mirrors that reflect and concentrate solar radiation at the absorber tube located at the focal point of the mirrors. Physically, the system is composed of optically perfect reflecting surfaces and thermally stable secondary surfaces and a tracking mechanism with high accuracy and reliability over time, even in adverse environmental conditions [12]. This ensures the optical efficiency of the system is kept in the optimal state for maximum reliability.

The linear Fresnel collector (LFC) has been harnessed and its power plants have been constructed in some countries. Like other CSP technologies, LFC plants ensure the

conversion of solar radiation to thermal energy that does work to generate electricity. The main equipment are organized in four major entities: solar boiler, steam turbine generator, cooling system, and feedwater system [18]. All the plant components perform specialized functions that enable it to produce requisite power.

The Linear Fresnel Collector plant is conventionally configured as shown in Fig.2. 2.

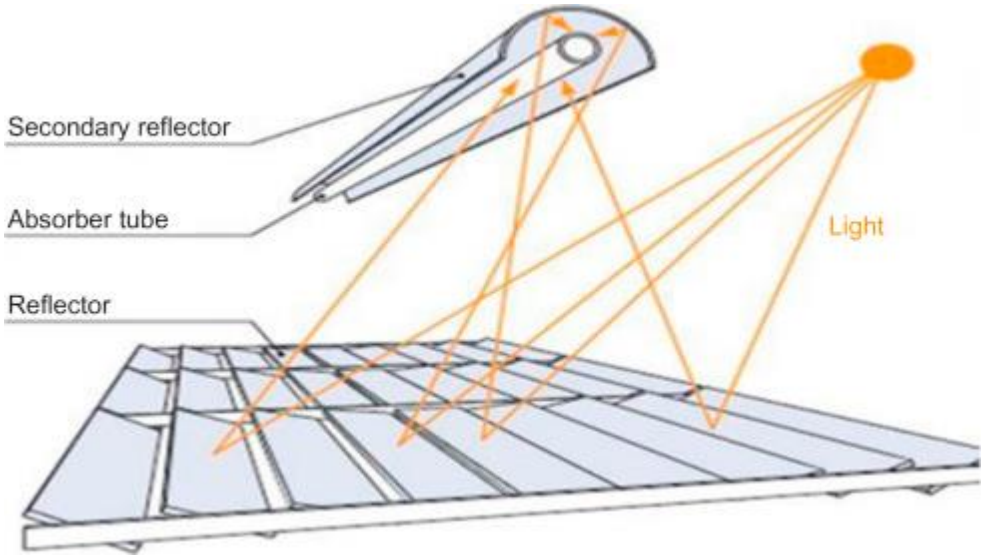

Fig.2. 2: Linear Fresnel Reflector system [19]

To achieve the best configuration of the LFC plant, the following considerations are put into account as outlined in Benmarraze *et al*. [18]:

- mass flow rate— This is induced in the loop by high predefined enthalpy and loop length. For instance, too-short loops lead to low mass flow rates which induces thermal shocks and overheating due to phase stratification; and too-long loops result in high steam velocities that consequently raises pressure drops and increases internal erosion.
- solar field pressure drop—Long header pipes due to wide solar field and high mass flow rates induce head losses. This spikes pressure drops leading to adverse high parasitic consumption for the circulation's pumps.
- optical end losses—Low sun positions in winter lead to important end losses at the inlet or outlet of the solar field.

Comparatively, LFC plants command an advantage over other renewable sources such as parabolic trough collector due to relatively simple construction, low wind loads

and significantly lower costs. Like most other concentrated solar power systems, absorber tube is an important component that immensely contributes to reliability and availability of LFC system. As observed by Schlipf *et al*. [20], the absorber tube provides an attenuation coefficient of nearly 95 % and an emissivity factor of maximum 10 % and the amount of the reflected irradiance depends on the panel reflectivity and glass cover transmittance and cleanliness of the components. It confirms the great contribution of absorber tube and by extension a requisite attention it demands during system design.

Since the inception of the LFC technology, numerous research has been conducted on the elements that impact its performance. For example, Montes *et al*. [21] looked at single-tube receiver with secondary reflector and conducted optical analysis by tweaking geometrical parameters to determine performance and also compared central LFC and compact LFC. The study found that in all configurations that shading is greater for denser mirror fields. They also observed lower shading is achieved in CLFC configurations. The results point toward the configurations that can yield the best energy output for the system.

In separate study, Montes *et al*. [22] investigates thermal performance of single-tube LFC receiver by using energy and exergy efficiency. The study reports the energy and exergy efficiency decreases as thermal emittance increases. Both factors decrease are due to the higher radiation losses as the temperature increases, and linear increase of the tube thermal emittance with the temperature. The same study found that both efficiencies remain practically constant in the evaporation zone, but they follow opposing trends in the other zones where energy efficiency decreases, and exergy efficiency increases with increasing temperature.

Looking at annual optical efficiency, mean flux intensity, and circumferential flux intensity homogeneity of LFC with different secondary reflector and made comparison to PTC receiver, Abbas *et al*. [23] observed higher efficiency in parabolic trough collectors than LFC with secondary reflector. However, they also found that selected designs of LFC achieve higher flux intensities, and thermal efficiency. This ensures optimal performance and cost-effectiveness of the system.

2.2.3. Central Tower Receiver

The solar tower system also known as central tower system uses series of flat mirrors called heliostats that focus solar irradiance on receivers positioned at the center of the heliostats arrays. The concentrated solar irradiance is converted into thermal energy and transferred by heat transfer fluid to working fluid that generates useful work for power generation.

The frequent heat transfer fluid used is molten salt. In a molten-salt solar power tower, liquid salt is pumped from a “cold” storage tank through the receiver where it is heated to 565°C and subsequently pumped to a steam generating system that produces superheated steam for useful work [24]

The figure below shows the typical central tower system.

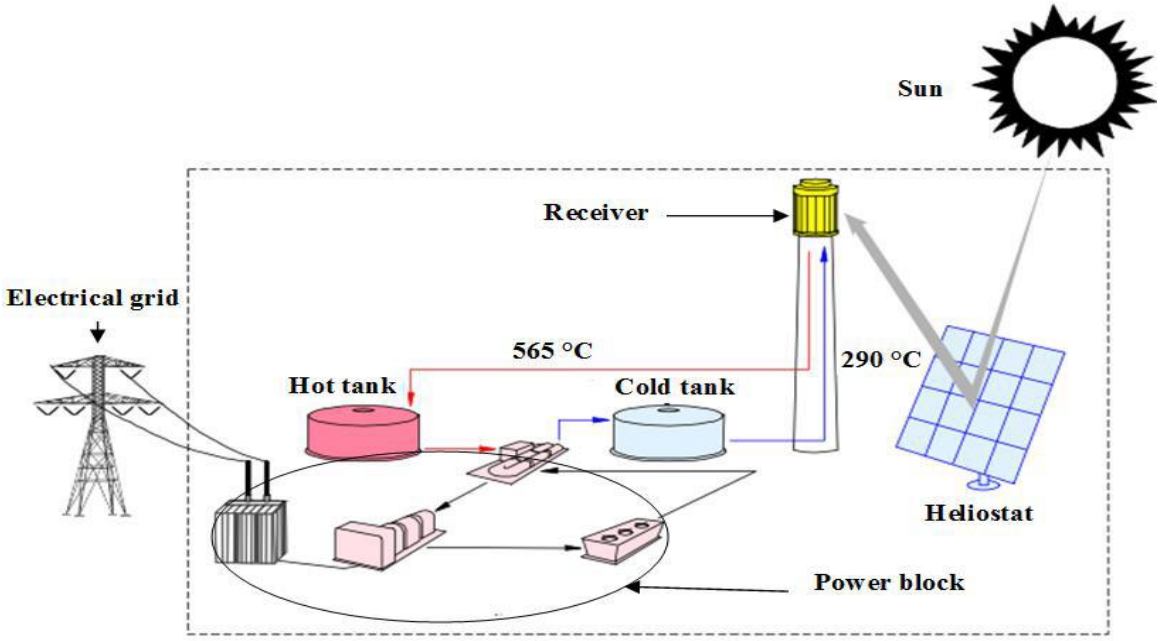

Fig.2. 3: Central tower system extracted from Oukili et.al [24]

As shown above, receiver plays a critical role in the availability of the central tower system and therefore its efficiency is a pivotal factor to monitor. In Binotti *et al*. [25] this factor is observed, and the obtained efficiency is comparable with the one estimated for Rankine cycle.

Equally important is heliostats, and thus its optimization contribute to reliability of the system. Awan *et al*. [26] considered an optimized plant containing 9745 heliostats compared to 6818 heliostats in the initial design and found the year one energy output

of the optimized plant is a 35.6% improvement. The results demonstrate the influence of this element.

Generally, to ensure the system is at its best performance, heliostats and receiver demands optimal design. The technology, just like other concentrated solar power, has the advantage of generating clean renewable energy which makes it a perfect system to utilize to maintain good environmental balance.

2.2.4. Parabolic Trough Collector System

Since this research is on the parabolic trough collector (PTC) system, an in-depth literature study is dedicated to it. The PTC system is the most developed and commercially harnessed. The biggest application of this type of system is the Southern California power plants, known as Solar Electric Generating Systems (SEGS) [27].

Parabolic trough solar thermal power plant consists of reflectors, heat collector element with HTF, Rankine steam turbines, and TES [28]. In-built tracking system enables the PTC receiver to move in tandem with the sun as it daily crosses the sky, from sunrise to sunset which increases the thermal efficiency and maximizing the energy yield of the system [29]

The typical parabolic trough collector plant is configured as shown below.

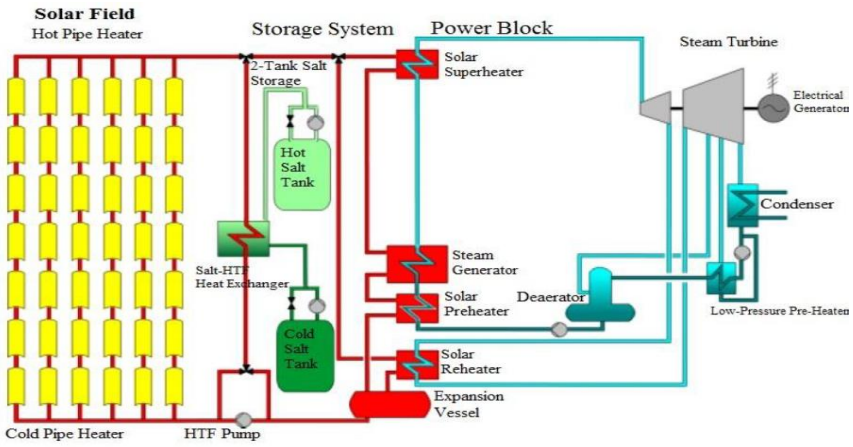

Fig.2. 4: Conventional parabolic trough collector plant as extracted from Prieto & Cabeza [30]

The energy yield of PTC system is also influenced by the heat transfer fluid used. Commonly, non-pressurized thermal oil with a maximum temperature of 350^{0}C is used as heat transfer fluid [5]. The desired characteristics of HTF are high temperature stability, good heat transfer tendencies, and low melting point [31]. Another HTF

applies in an equal fashion is molten salt. While current commercial projects are dominated by DSG and molten nitrate salt concepts, more efficient systems involve higher temperature which makes salt ineffective [31]

Power extracted from PTC technology is reliable, clean and environmentally friendly [32]. In addition to this advantage, the flexibility of PTC helps in the integration into the grid of other renewable energy technologies, such as solar photovoltaics. The integration of more renewable energy help in maximizing the power production to meet the energy demand of modern societies. What's more, the thermal energy storage system incorporated in PTC plants enhances its performance and availability. Thermal energy storage should characteristically accommodates large generated daily heat to generate power at night to meet the demand [33]. Generally, high-temperature thermal storage enhances power efficiency by producing high-temperature steam [34]. This efficiency is not constant throughout the lifecycle of the system. It should be noted that thermal degradation occurs in PTC power plants over the time of operation [28]. This thermal strain amongst other factors such as state of the collectors sometimes leads to decreasing efficiency as the system operates over the time.

Excessive use of fossil fuels in power generation and locomotive fueling has caused serious damage to the environment [35]. The adverse effects demand a shift to renewable energy sources and the PTC system has proven itself a valuable alternative.

Since this research is on the numerical modelling of PTC receiver, the proceeding sections will be exclusively dedicated to the literature exploration on the receiver.

2.3. Parabolic Trough Collector (PTC) Receiver

The receiver is a specially designed system that is placed at the focal point of the parabolic trough collector to absorb the reflected solar radiation from the reflector and convert it into thermal energy that does useful work to generate electricity. The absorber tube is one of the most important elements in a PTC system because of its influence on CSP plant reliability and the energy production cost [36]. To supplement the reliability of the system, solar tracking system is applied to give an incident angle that depends on the location coordinates and solar angles [37]. This maximizes the irradiance and heat flux which contribute to maximization of the generated power.

2.3.1. PTC Receiver Design

The PTC receiver is designed with thermal losses as the major factor in consideration. The receiver consists of absorber composed of a stainless steel tube with high absorptance surface and low emissivity [38]. The applied selective coatings enable high energy absorption and minimizing energy emission [28]. In addition to absorber, a specialized glass envelope is placed around it to create an annulus space. It prevents oxidation, minimizes convective thermal losses, thus improving thermal and thermodynamic performance of receiver [27], [38]. The receiver thermal loss depends on the vacuum quality in the receiver's annulus space, geometry of the glass envelope and receiver ends, absorber tube temperatures, and properties of the glass [9]. The annulus is also airtight with specially designed insulators at the ends.

The figure below illustrates the generic design of the PTC receiver.

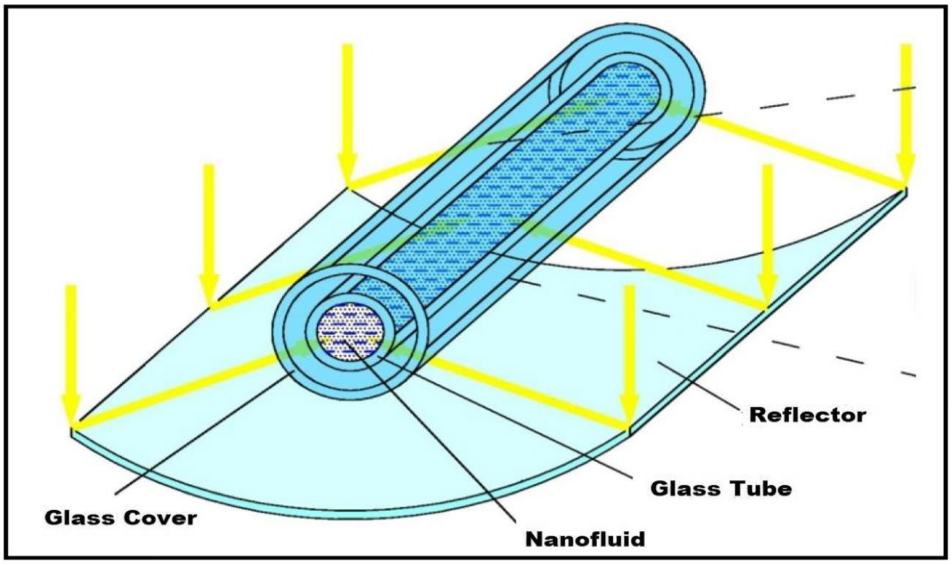

Fig.2. 5: Generic PTC receiver as extracted from Naveenkumar et al. [7]

As shown above, the glass functions as an envelope against heat losses. However, in some cases high temperature gradients will generate large thermal stresses that results in destructive deformation on glass cover that induces thermal loss [39]. The problem persists to be one of the challenges when it comes to designing the most reliable receiver that can endure a wide range of temperature and the resultant thermal stress.

Different designs of the receiver have been proposed to foster the enhancement of heat transfer and consequently enhance thermal and thermodynamic performance.

Fahim *et al*. [40], for instance, placed a series of internal obstacles within receiver and investigated the influence of geometrical parameter, obstacles' orientation and spacing on the performance of the receiver. They established obstacles in the absorber have a favorable influence on Nusselt number, and adverse effect on friction factor—the friction factor is inversely proportional to the value of P/D. Similarly, Mwesigye *et al*. [41] examined the impact of the geometrical concentration ratios on the general performance of an enhanced receiver and found that an increase in concentration ratios leads to an increased entropy generation rates due to the spike in finite temperature differences as concentration ratios increase.

The proceeding sub-sections delves in some of the influences of the heat transfer enhancement techniques of receiver and other associated parameters such as rim angle and concentration ratios on the general thermal and thermodynamic performance of the system as assessed in the existing literature.

2.3.2. Receiver Geometry

Geometry influences the performance of engineering functions in thermal systems. Different researchers have examined not only the local geometry of the receiver, but also the geometry of the collector and interrogated how it influences the performance of the receiver itself.

Mwesigye *et al*. [42] investigated the influence of a geometrical parameter of collector known as rim angle on the receiver temperature, and observed that as the rim angle increases, the absorber tube circumferential temperature differences reduce. This has implications on the performance of the receiver since a high circumferential temperature significantly enables high thermal losses. Other geometric parameters of collector such as concentration ratio affects the receiver performance as well. Mwesigye *et al*. [43] examined impacts of concentration ratio on the Reynolds number and found that an increase in concentration ratio leads to an increase in optimal Reynolds number.

Other researchers have modified the geometry of the absorber tube to attain the most performing geometry. Considering the traditional cylindrical absorber tube, Zou *et al.* [44] investigated the effect of the receiver diameter (D) of the SEGS LS-2 PTC module on the local concentration ratio (C_R) and discovered inverse proportionality. This is

because the smaller the diameter, the higher the interaction of heat transfer fluid with the absorbed thermal energy.

2.3.3. Receiver Efficiency

The absorber tube is one of the most important elements in a PTC system whose thermal efficiency affects both plant reliability and cost [39]. It calls for critical study of the factors that influence not just thermal efficiency, but also exergy efficiency. Abdulhamed *et al*. [45] outlines the following factors that influence the receivers' efficiencies:

- Receiver geometrical modifications such as internal fins enhance thermal efficiency.
- Heat transfer coefficient, optical efficiency, adsorption, heat flux, transmission, collector length, and absorber diameter affect receiver efficiencies.

It should be noted that it is not only the above-mentioned factors that exclusively determine the performance of receiver. Padilla *et al*. [38] also considered the following operating conditions that tend to dramatically affect the efficiencies of the system:

- Inlet temperature of heat transfer fluid affects the exergy leakage due to thermal losses.
- Friction of the viscous fluid and heat transfer from high to low temperatures result in exergy destruction.

As Bellos *et al*. [46] observed for inlet temperature equal to 650 K, the exergy efficiency for Syltherm-800 is 37.71% and for Syltherm-800-CuO is 37.98%, presenting an enhancement of 0.72%. It proves that inlet temperatures enable higher efficiency. Increasing the temperature to higher levels will lead higher efficiencies, but current thermal oil based HTFs degrade at temperatures above 400 C [4]. This further implies that efficiency and applicability of HTF for heat transfer applications is hinged on their trade-off of thermophysical and rheological properties [47]. Therefore, different heat transfer fluid such as water of nano-fluid are explored.

In case of water as heat transfer fluid, it is determined that as mass flow rate increases, heat absorption is augmented because as water flows quickly, more volume of water absorbs more heat with less heat loss, resulting in enhanced efficiency of the collector [48]. Another limiting factor with regards to a choice of heat transfer fluid is rate of

decomposition. Some HTF such as water decompose when temperatures exceed about 400^0C, therefore getter is provided to absorb the resultant hydrogen [43]

As previously mentioned, friction factor influences the efficiency of the receiver. Mwesigye *et al*. [43] observed that fluid friction irreversibility increases with an increase in Reynolds number but does not change with changing concentration ratio, whereas the heat transfer irreversibility decreases with increasing Reynolds numbers and increases significantly as the concentration ratios increase.

2.3.4. Thermal and Thermodynamic Analysis of PTC Receiver

2.3.4.1. Mathematical Modelling of the Receiver System

Like any other engineering system, the PTC receiver system has a fundamental mathematical foundation that describes its thermal and thermodynamic behavior. As elaborated in [49]–[52], eq. (2.3)-(2.20) lay the important foundation to mathematically model the flow and thermodynamics of the receiver.

The collector receives the available solar irradiation described by eq. (2.3).

$$Q_S = A_a.I_b \tag{2.3}$$

Where A_a = collector aperture area, I_b = Direct beam solar irradiation

Not all the irradiations are absorbed by the absorber tube as some energy is lost through various energy loss mechanisms. The only useful energy of solar collector gained by the heat transfer fluid is determined by eq. (2.4).

$$Q_u = m_c.c_p\left(T_{out} - T_{in}\right) \tag{2.4}$$

Alternatively, the useful energy can be quantified by considering convective heat transfer formulation as shown by eq. (2.5).

$$Q_u = h.A_{ri}\left(T_r - T_{fm}\right) \tag{2.5}$$

Where T_{fm}= mean fluid temperature, which is an average of inlet and out temperature depicted in eq. (2.6).

$$T_{fm} = \frac{\left(T_{out} + T_{in}\right)}{2} \tag{2.6}$$

Therefore, to determined thermal efficiency of the receiver system, a ratio of the useful energy and available solar irradiance is taken as shown by eq. (2.7).

$$\eta_{th} = \frac{Q_u}{Q_s} \tag{2.7}$$

As previously mentioned, not all the available solar energy is absorbed by the absorber. Some are lost due to optical efficiency of the collector. The amount of absorbed solar energy from the absorber is determined by eq. (2.8) and (2.9).

$$Q_{abs} = Q_u + Q_{loss} \tag{2.8}$$

$$Q_{abs} = Q_s.\eta_{opt} \tag{2.9}$$

Where η_{opt} = collector optical efficiency

The thermal loss in the receiver system can be reduced by evacuating the annulus area. With evacuated annulus, the loss is through radiation and due to steady state, the loss to cover is equal to loss to ambient as shown here:

$$Q_{loss} = \frac{A_{ro}.\sigma\left(T_r^4 - T_c^4\right)}{\frac{1}{\varepsilon_r} + \frac{1-\varepsilon_c}{\varepsilon_c} + \frac{A_{ro}}{A_{ci}}} \tag{2.10}$$

On similar fashion, cover loss to the environment through radiation and convection is described by eq. (2.11).

$$Q_{loss} = h_{co}.A_{co}\left(T_c - T_{am}\right) + A_{co}.\sigma.\varepsilon_c\left(T_c^4 - T_{am}^4\right) \tag{2.11}$$

The same references provided mathematical formulations on the flow of the heat transfer fluid. Three major flow parameters are Reynolds number, Prandtl number, and Nusselt number as they describe the nature of a flow. They are formulated as follows:

Reynold number,

$$\mathrm{Re} = \frac{4m_c}{\pi.D_{ri}.\mu} \tag{2.12}$$

Prandtl number,

$$\mathrm{Pr} = \frac{\mu.c_p}{k} \tag{2.13}$$

Nusselt number,

$$Nu = \frac{h.D_{ri}}{k} \tag{2.14}$$

For smooth tube, a Nusselt number can be best described by Dittus-Boelter Equation which relates it to Prandtl number.

$$Nu = 0.023\,\mathrm{Re}^{0.8}.\mathrm{Pr}^{0.4} \tag{2.15}$$

Another important flow parameters are friction factor and pressure drop as they indicate the amount of power required to pump the fluid. They are quantified as follows for smooth absorber tube:

Pressure drops,

$$\Delta p = f_r.\frac{L}{D_{ri}}.\left(\frac{1}{2}.\rho.u^2\right) \tag{2.16}$$

Where the mean velocity of fluid in the absorber tube is,

$$u = \frac{m_c}{\rho.\left(\pi.\frac{v_{ri}^2}{4}\right)} \tag{2.17}$$

Friction factor,

$$f_r = \frac{1}{\left[0.79\ln(\mathrm{Re}) - 1.64\right]^2} \tag{2.18}$$

Sky Temperatures determined,

$$T_{sky} = 0.0552T_{am}^{1.5} \tag{2.19}$$

Coefficient of convective heat transfer as reported in Mwesigye *et.al* [9] given ambient temperature 300 K.

$$h_w = V_w^{0.5} d_{go}^{0.42} \tag{2.20}$$

Where V_w is wind velocity.

Pressure drop and pumping power can be related using this formula:

$$W_p = \pi \frac{D^2}{4} u_m \Delta P \tag{2.21}$$

Most of the discussed mathematical formulations will be used in the modelling and analysis chapters of this work.

2.3.4.2. Thermal and Thermodynamic Assessment

The fundamental research that has been carried out with relation to performance and reliability of PTC receiver has predominantly been on the how to optimize thermal and thermodynamic performance. They have scrutinized the thermodynamic variables that can be considered when designing the receiver. These variables include heat flux distribution, thermal energy, heat transfer coefficient, and thermophysical parameters of materials.

Determination of heat flux distribution on the receiver is crucial to the analysis of the thermal performance of the system [9]. This is because the heat flux dictates the temperature distribution whose gradient influences performance of the system. Manipulating convective heat transfer coefficient, an appropriate temperature gradient is achieved. Risk of breakage and hydrogen built-up in receiver can be reduced through reduction of circumferential temperature and peak temperatures with improved heat transfer [42]. In PTC receivers, the non-uniformity of the absorber tube's circumferential temperature leads to thermal stresses which results in breakage and this requires optimal design that minimizes it [9].

To minimize temperature gradient and ensure optimal thermal and thermodynamic performance of the receiver system, an enhancement is done on the receiver system. Mwesigye *et al*. [53] investigated the influence of perforated inserts on the performance of the receiver and observed that the use of perforated plate inserts is shown to increase the modified thermal efficiency of the receiver in the range 1.2% and 8% depending on the insert spacing, insert size and Reynolds number. The finding validates the fact that an enhanced heat transfer generally reduces the temperature gradient, hence minimizing the thermal losses.

Temperature difference can also be optimized by optimizing the rim angle of the reflector. As Mwesigye *et al.* [42] found that as the rim angle increases, the

circumferential temperature reduces which consequently results in increased thermal and thermodynamic efficiency.

Besides temperature gradient, thermal strain constitutes a factor that influences the overall thermal performance of a PTC receiver. As investigated by Fuqiang *et al*. [28] with asymmetrically corrugated parabolic trough receiver, it is established that using asymmetric outward convex corrugated metal tube to replace the smooth tube for tube receiver as tube receiver can reduce the von-Mises thermal strain up to 26.8%. The modification of the conventional tube that result in this improvement translates to general reliability of the receiver.

Just as the referenced study compares the thermal and thermodynamic performance of smooth and corrugated receiver tube, Abdullahi *et al.* [54] introduced a novel concept of investigating the comparative performance of single-tube receiver to double-tube receiver at constant optical efficiency. The study showed that double tube configurations outperformed single counterpart with a daily average of 21%, 19.8% and 18.3% increase in heat delivered to the cooling water for HPCPC30, HPCPC40 and HPCPC60 respectively for seven hours of operations as indicated below.

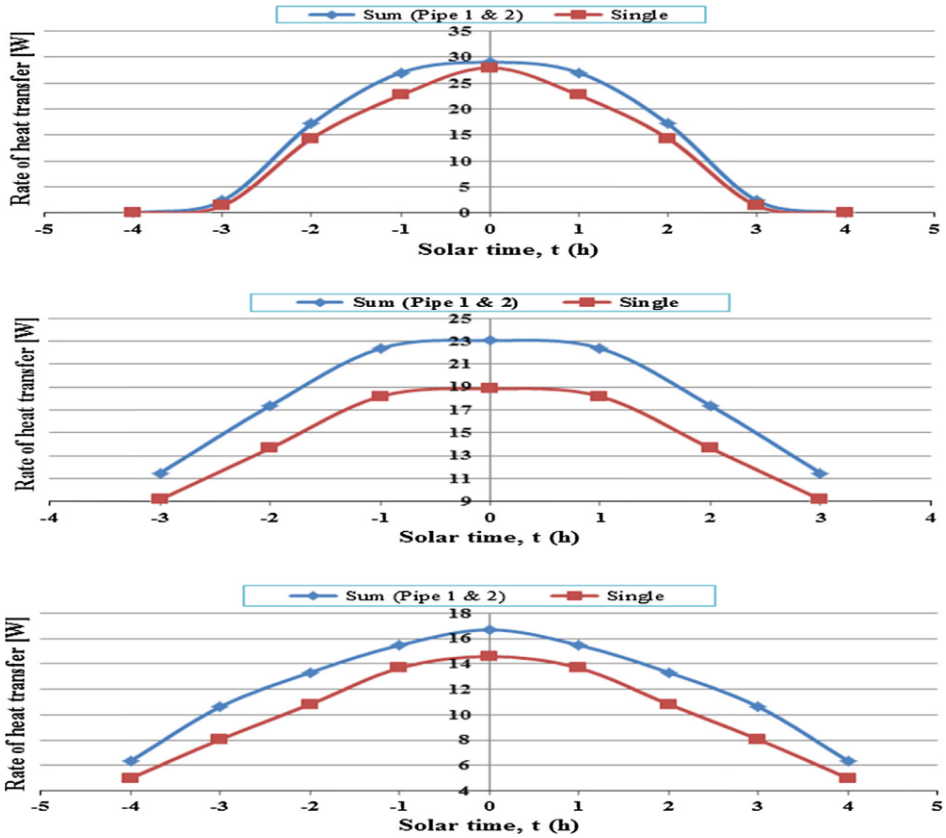

Fig.2. 6: Comparative rate of heat transfer in double and single tube configuration [54]

The difference is due to the minimization of thermal losses due to increased area upon which concentrated irradiance lands on.

Novel design of parabolic trough receiver has contributed to the overall efficiency of the receiver system. Some studies are devoted to a design that consider the heat transfer thermal enhancement to improve the performance of the receiver. One of the critical studies is Bellos *et al*. [55] that examined the impact of longitudinal fins on the performance of the receiver by using performance criteria such as thermal efficiency and Nusselt number. The study established that an increase in length of the internal fins increase thermal efficiency as indicated below.

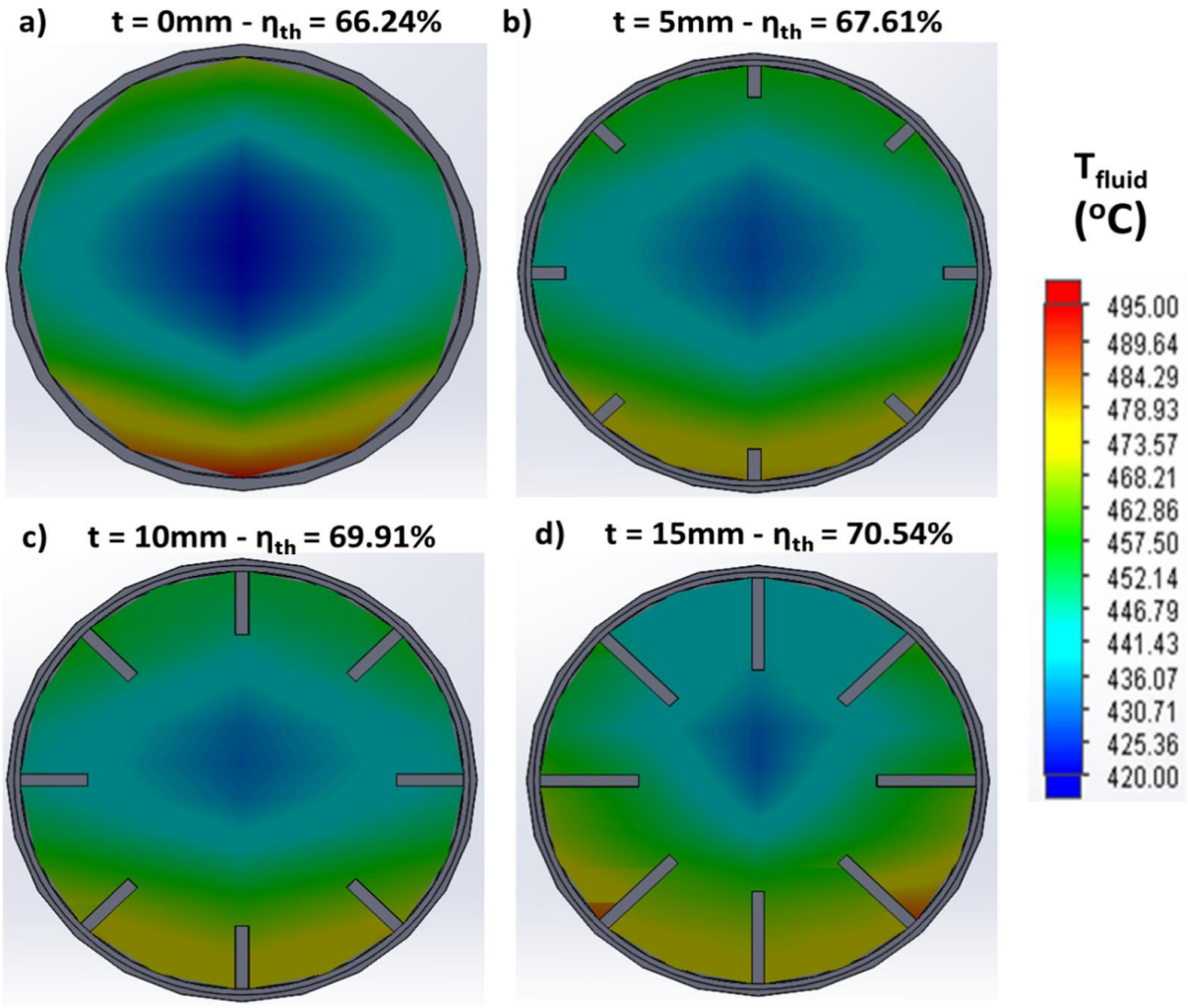

Fig.2. 7: Influence of the length of internal longitudinal fins [49]

The same study concluded that the most suitable fin exergetically is the one with 10 mm length, and comparatively more energetically (higher thermal efficiency) is the one with 15 mm length. In other words, the higher fin length leads to higher thermal performance, but the exergetic performance is maximized for a specific fin length. The

reason for this conclusion is based on the increase in pressure drop for the longer fin. The same study looked at the pressure drop as a performance criterion and found that it increases with the increase in the fin length which is attributable to increased turbulence induced by decreasing internal volume.

Apart from modifying the absorber tube to improve the receiver performance, some studies examined a modified glass cover with internal shield. Hassan *et al*. [56] studied internally shielded receiver as shown in figure below.

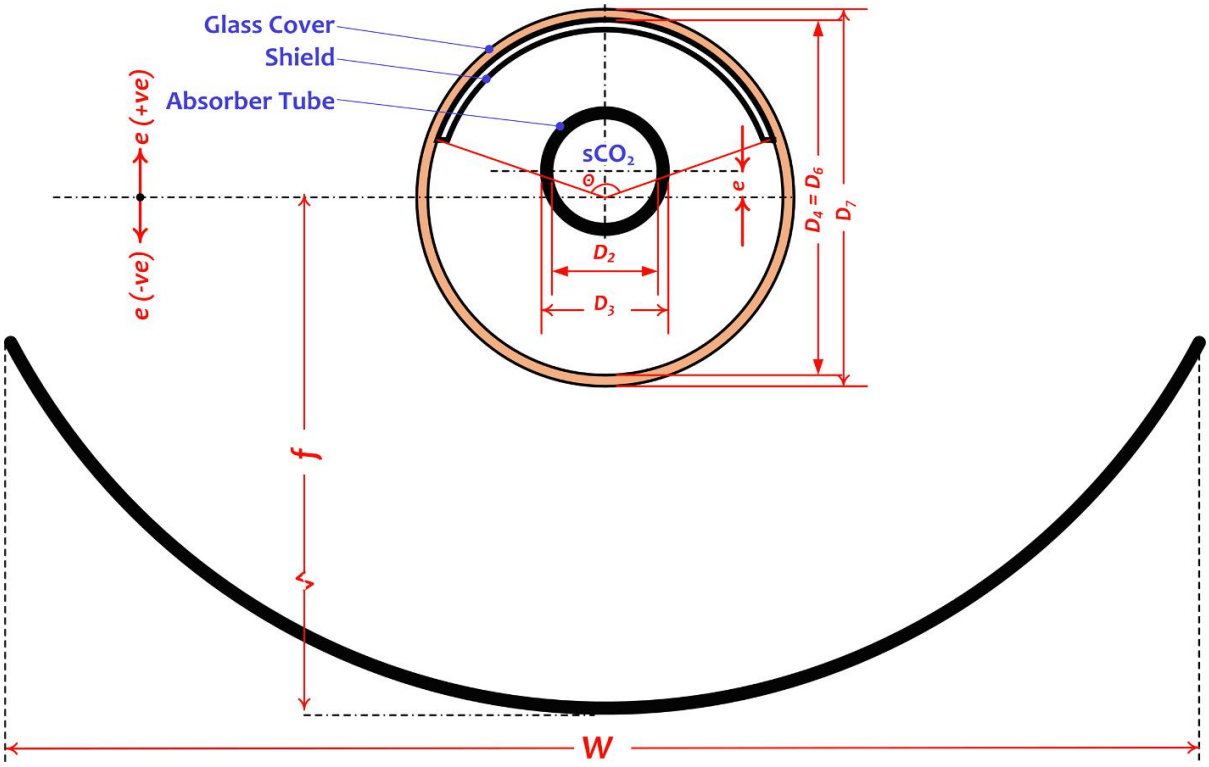

Fig.2. 8: Novel designed receiver with internally shielded glass cover [56].

The study concluded that:

- Absorber diameter increase reduces performance sensitivity to tubular eccentricities hence adversely affecting thermal efficiency.
- With large heat shield, eccentricities lower than 15 mm can be acceptable.
- Shielding the receiver is favourable for opening angles of no larger than 160^0
- Optical efficiency is affected by heat shield compared to thermal efficiency.

2.3.5. Performance Evaluation Criteria

2.3.5.1. PECs based on the First Law

The First Law of Thermodynamics is pivotal in evaluating the dynamics of energy in a thermal system. For various systems, the following performance evaluation criteria derived from the first law are used:

- Thermal efficiency.

This performance criterion evaluates the efficiency of energy conversion. Thermal efficiency can be improved by either enhancing the heat transfer mechanism or devising means to reduce losses. For instance, Zhao *et al*. [57] cascadingly applied selective-coatings on an absorber of PTC and performed two-dimensional model simulation to investigate its influence on the thermal efficiency. The study found that multi-section systems which have higher emissivity compared to conventional systems have less heat loss which translates to higher thermal efficiency. On similar note, Shinde *et al*. [58] after conducting numerical simulation of novel receiver with especial insulation over absorber tube established that the novel receiver shows substantially lower efficiency when compared with the Schott receiver.

As mentioned, heat transfer enhancements improve thermal performance of the receiver. One of the enhancements is combination of inserts with special heat transfer fluid composed of nanofluid. Mohammed *et al*. [59] investigated thermohydraulic and thermodynamic performance of insert of wavy tape using numerical simulation and found thermal efficiency rises up to a specific value and then it starts to diminish with the increase of temperature parameter. This is due to the increment of pumping power as Reynolds number increases which gets remarkably higher than the useful heat gain.

In addition to using nanofluid, Samiezadeh *et al*. [60] placed some internal fins at the lower interior of a the absorber tube and observed that thermal efficiency dramatically increases as the nanoparticles are introduced and equally increased with the fin length and number of fins. This is due to improved heat transfer mechanism. Just like fins, a twisted tape inserts with nanofluid improves heat transfer. It was furthermore established that the PEC values always increase by growth of nanoparticles volume fractions. It was clear that for all studied conditions the PEC values of model LWRC always rise by intensification of Reynolds numbers [61].

- Pressure drops.

Pressure drop is one of the important parameters used to measure the performance of receiver because it determines the friction factor and pumping power of the system. Sani *et al.* [62] evaluated pressure drop of absorber with wavy twisted strips insert with hybrid nanofluid HTF which established that pressure drop increases with Reynolds numbers and equally increases with tape height. This has implications for an elevated pumping power of the system which could have adverse consequences on the system performance.

Similarly, Ibrahim *et al.* [63] conducted numerical study combining twisted turbulator and two-phase nanofluid. The study observed that as the pitch ratio value increases, the curvature in the turbulator rises and, as a result, the flow lines become more curved. Besides, the amount of pressure is intensified significantly by raising the pitch ratio [64].

2.3.5.2. PEC based on the Second Law

- Exergy efficiency

Exergy of a receiver system determines its effectiveness in maximizing useful energy. For receiver system, many studies have been conducted to evaluate its performance using this parameter. For instance, Allouhi *et al*. [65] performed numerical study using nanofluid as HTF and observed that the exergy efficiency varied between 3.05% and 8.5 % for the base fluid case and gets improved more remarkably when nanofluids are employed. The study discovered the peak exergy efficiency is attained by the CuO based nanofluid and is about 9.05%. This means the useful energy absorbed significantly increase with introduction of nanofluid as heat transfer fluid.

- Entropy generation rate

Like exergy efficiency, entropy generation rate and by extension entropy generation number are performance evaluation criteria hinged on the Second Law of Thermodynamics. They examine influences of irreversibility on the performance of a system. Many studies, experimental and numerical studies, have been done on these factors. For example, Goyal & Reddy [66] numerically studied entropy by modelling a receiver with supercritical carbon dioxide. The study observed that the rate of entropy generated due to heat transfer irreversibility dominates at low Reynolds number, and

with increasing Reynolds number, the contribution of heat transfer reduces and the contribution of fluid friction on the entropy generation increases.

2.4. Summary and conclusion

The chapter has explored the fundamentals of concentrated solar thermal power and the development it has undergone to be proven as a promising and reliable source of energy. Different types of CSP technologies have been discussed to give an appreciation of the applicability of each with regards to the capabilities to supply demanded energy.

Thermal and thermodynamic analysis and the mathematical models that underpin it have been discussed to lay foundation for the framework needed in the subsequent chapters of this work. Some of these formulations will be necessary in the construction of thermal and CDF models and later in analysis and synthesis of the simulation results.

Since research is usually a tangential deviation from the existing literature, various relevant previous research has been highlighted to establish the unique niche for this work. By so doing, credence is afforded to the work and its importance established.

As a conclusion, the chapter examine various performance evaluation criteria that are often used to evaluate the thermal and thermodynamic performance of concentrated solar thermal system. Some of these criteria will be applied in this work.

The subsequent chapters involve using the general knowledge assessed here to develop the framework, test it, and evaluate the results.

Chapter Three

Chapter 3: Numerical Modelling and Theoretical Framework

3.1. Introduction

Computational fluid dynamics utilizes complex tools in solving physical problems. The usefulness and applicability of the tools can be appreciated by comprehensively understanding the underpinning theories. This research uses a CFD tool called ANSYS Fluent in performing the numerical simulation. To appreciate its power in modelling the considered flow regime and the thermal models applied, this chapter delves into the relevant theoretical framework that forms the basis of this study.

It explores mathematical equations applied, CFD and thermal models, Finite Volume Method (FVM), and mesh generator analysis.

3.2. Mathematical Formulation

Fluid flow is one of prevalent natural phenomena. The process is precisely modelled to determine the behaviour and how it influences the state of nature and subsequently its harnessing. Three major mathematical formulations that fully describe fluid flow of any nature and form the basis of the Navier's Stokes equations are: continuity equation, momentum equation, and energy equation. Not only do they precisely determine the nature of the flow, but also model vital elements of flow that are utilized in fluid flow applications.

3.2.1. Conservation of Mass

The conservation of mass hinges on the law that states the mass in a domain cannot be created nor destroyed. It models the flow with the mass continuum in consideration. Also known as continuity equation, it has different variation, but its generic form is as in eq. (3. 1)

$$\frac{d\rho}{dt} + \nabla.(\rho u) = 0 \qquad (3.\ 1)$$

The equation describes the conservation of mass which posits that the mass inflow equals the mass outflow. This is underpinned by the mass balance described by the

mass balance equation that forms the basis of eq. (3. 1). From it, some of the Navier's Stokes equations—system of formulations that describes fluid flow—are derived.

For steady state, extensive and intensive properties are time-independent, therefore the terms in the equation that depend on time disappears.

3.2.2. Conservation of momentum

Also referred to as momentum equation, it is an expression of the second law of motion that represents force balance in a flow. It describes the action of all forces on the flow. The equation posits that a rate of change of momentum of micro unit in flow field equals all the external forces acting on the unit [67]. It is derived from the Newton Second law of motion.

The generic form of momentum equation can be either represented in differential or vector form. Due to its compactness, it is the vector form that is usually reported as shown in eq. (3. *2*).

$$\rho\left(\frac{\partial V}{\partial t}+V.\nabla V\right)=-\nabla p+\mu\nabla^2 V+\rho g \qquad (3.\ 2)$$

Just like in continuity equation of the fluid flow, some of the Navier's Stokes are derived.

3.2.3. Energy Equation

Derived from the First Law of Thermodynamics, energy equation describes the conservation of energy in the fluid flow. It relates the behaviour of internal energy of the system and the external energy that influences energy transport of the system.

The compact generic vector form of the energy equation is as shown in eq. (3. 3)

$$\rho\frac{De}{Dt}=-\rho\nabla.u+\nabla.(k\nabla T)+\phi \qquad (3.\ 3)$$

3.3. Turbulent Modelling

3.3.1. Reynolds Average Navier's Stokes Equation

As mentioned previously, Navier-Stokes equations are the fundamental mathematical formulations of the fluid dynamics. They are derived from the governing equations

briefly discussed in *section 3.2* of this work. Despite the robustness of the Navier-Stokes equations, their application in CFD modelling in their original form proves to be challenging due to time-dependence in some of the terms. To circumvent the challenge, time-averaging of the terms has been carried out and the resultant set of equations are referred to as Reynolds Average Navier-Stokes (RANS) equations. The simplification is done by neglecting the correlations with fluctuations of molecular transport and thermodynamics coefficients such as viscosity and specific heat capacity [68]. These equations effectively govern steady and fully developed flow. As reported in Mwesigye *et al*. [43] the continuity equation, and momentum equation take the following differential forms shown in eq. (3. 4) and (3. 5).

Continuity equation

$$\frac{\partial(\rho u_i)}{\partial x_i} = 0 \tag{3. 4}$$

Momentum equation

$$\frac{\partial}{\partial x_j}(\rho u_i u_j) = \frac{\partial P}{\partial x_i} + \frac{\partial}{\partial x_j}\left[\mu\left(\frac{\partial u_i}{\partial x_j} + \frac{\partial u_j}{\partial x_i}\right) - \frac{2}{3}\mu\frac{\partial u_i}{\partial x_i}\delta_{ij} - \rho\overline{u_i' u_j'}\right] \tag{3. 5}$$

Similarly, the conservation of energy equation is time-averaged to conform with the RANS equations presented in eq. (3. 4) and (3. 5).

Energy equation

$$\frac{\partial}{\partial x_j}(\rho u_j c_p T) = \frac{\partial}{\partial y_j}\left(\lambda\frac{\partial T}{\partial x_J} + \frac{\mu_t}{\sigma_{h,t}}\frac{\partial(c_p T)}{\partial x_j}\right) + u_j\frac{\partial P}{\partial x_j} + \left[\mu\left(\frac{\partial u_i}{\partial x_j} + \frac{\partial u_j}{\partial x_i} - \frac{2}{3}\mu\frac{\partial u_i}{\partial x_i}\delta_{ij} - \rho\overline{u_i' u_j'}\right)\right]\frac{\partial u_i}{\partial x_j} \tag{3. 6}$$

Where T is time-averaged temperature, P is time-averaged pressure, λ is the fluid thermal conductivity and u_i, u_j, are respectively time-averaged velocity components in *i*-and-*j* directions. Thermal stress term ($-\rho\overline{u_i' u_j'}$) shows up in both momentum and energy equation and is defined according to Boussinesq approach.

$$-\rho\overline{u_i' u_j'} = \mu_t\left(\frac{\partial u_i}{\partial x_j} + \frac{\partial u_j}{\partial x_i}\right) - \frac{2}{3}\left(\rho k + \mu_t\frac{\partial \mu_k}{\partial x_k}\right)\delta_{ij} \tag{3. 7}$$

Turbulent kinetic energy per unit mass (k) in eq. (3. 7) is given by:

$$k = \frac{1}{2}\left(\overline{u'^2} + \overline{v'^2} + \overline{w'^2}\right) \quad (3.\ 8)$$

From numerous CFD simulations of fluid flow, it has been established that Boussinesq approach, especially *k-ε* model, is computationally less costly and is therefore usually a popular choice for numerical study. In this approach, standard *k-ε* model and realisable *k-ε* model present themselves equally robust. However, since realisable *k-ε* model is based on analytic method, its results tend to be more accurate. In realizable *k-ε* model additional equations of kinetic dissipation and kinetic energy are solved.

Turbulent kinetic dissipation,

$$\frac{\partial}{\partial x_j}\left(\rho \varepsilon u_j\right) = \frac{\partial}{\partial x_j}\left[\left(u + \frac{\mu_t}{\sigma_\varepsilon}\right)\frac{\partial \varepsilon}{\partial x_j}\right] + \rho C_1 S_\varepsilon - \rho C_2 \frac{\varepsilon^2}{k + \sqrt{\nu\varepsilon}} \quad (3.\ 9)$$

Turbulent kinetic energy k,

$$\frac{\partial}{\partial x_j}\left(\rho k u_j\right) = \frac{\partial}{\partial x_j}\left[\left(\mu + \frac{\mu_t}{\sigma_k}\right)\frac{\partial k}{\partial x_j}\right] + G_k - \rho\varepsilon \quad (3.\ 10)$$

Where G_k is production turbulent kinetic energy, which is a function of thermal stress.

$$G_k = -\rho\overline{u_i' u_j'}\frac{\partial u_j}{\partial x_i} \quad (3.\ 11)$$

Further simplification of eq. (3. 11) using thermal stress equation yields the following relation:

$$G_k = \mu_t S^2 \quad (3.\ 12)$$

Where μ_t is eddy viscosity which is a function of turbulent dissipation and kinetic energy.

$$\mu_t = \rho C_\mu \frac{k^2}{\varepsilon} \quad (3.\ 13)$$

Additional constants are required to fully solve all the governing equation in realizable *k-ε* model. As presented in *Ref*. [67], these constants are defined as follow:

$$C_1 = \max\left[0.43, \frac{\eta}{\eta+5}\right], \quad \eta = S\frac{k}{\varepsilon}, \quad S = \sqrt{2S_{ij}S_{ij}}, \quad C_2 = 1.9, \quad \sigma_k = 1, \quad \sigma_\varepsilon = 1.2$$

Where S_{ij} is the rate of linear deformation of fluid element represented according to *Ref.* [69].

$$S_{ij} = \frac{1}{2}\left(\frac{\partial u_i}{\partial x_j} + \frac{\partial u_j}{\partial x_i}\right) \tag{3. 14}$$

Eq.(3. 14) being a tensor, it has nine components decomposable into shearing and elongation deformation.

3.3.2. Near-wall Treatment

For turbulence flow, the near-wall region is critical as shear stress and viscosity are prominent. At the wall-fluid interface, viscous damping reduces tangential velocity variation and kinematic blacking equally affects normal velocity gradient [67]. Because of that influence, viscosity, velocity, and length in the near-wall region are defined as shown in eq.(3. 15)-(3. 17).

Cell-wall distance (Length):

$$y = \frac{y^+ \mu_f}{\rho u_\tau} \tag{3. 15}$$

Where u_τ is the average turbulent velocity in the region and is function of wall shear stress and fluid density.

$$u_\tau = \sqrt{\frac{\tau_w}{\rho}} \tag{3. 16}$$

Wall shear stress

$$\tau_w = 0.5 C_f \rho U_\infty^2 \tag{3. 17}$$

Where C_f is the fluid skin friction defined as:

$$C_f = \frac{0.026}{\mathrm{Re}^{1/7}} \quad (3.\ 18)$$

Determining cell-wall distance helps in ensuring the first node of the flow lies between viscous sublayer and outer layer which ensures accurate prediction of pressure drop and velocities of the turbulence flow. It is computationally determined by the non-dimensional y^+ value. In CFD modelling of flow, appropriate y^+ values are approximated using the wall function represented in figure below.

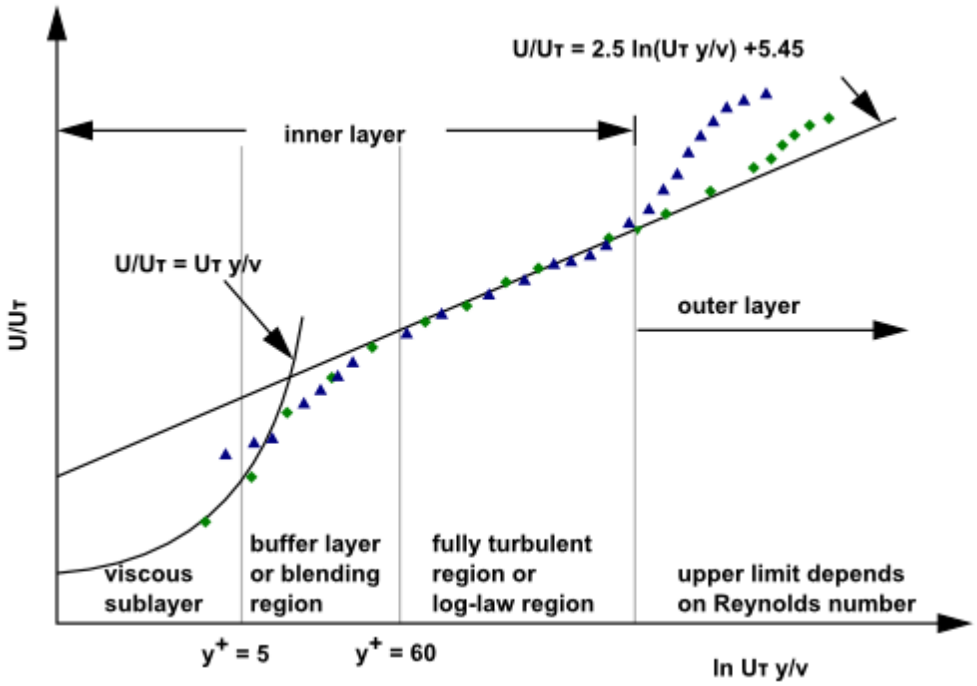

Fig.3. 1: Y-plus function as distributed in viscous layer [67]

As shown in the above logarithmic function, the appropriate y^+ value is dictated by the nature of the turbulence. For instance, a fully developed turbulence would appropriately do well with the value greater the 60. The choice of y^+ value is nonetheless determined by the turbulent model being used.

3.4. Computational Fluid Dynamics Thermal Model

All CFD thermal models are based on the heat transfer mechanisms of conduction, convection, and radiation.

Thermal conduction involves spontaneous heat transfer from hot region to cold region all governed by the natural law of thermodynamics. In CFD model, the thermal conduction is modelled using the heat equation (Fourier law of conduction).

$$q = -k\Delta T \tag{3. 19}$$

Eq. (3. 19) implies that the heat transfer rate in the media is proportional to the temperature difference, which means the greater the temperature differences of participating media the higher the rate of heat transfer through conduction. That has direct implication in designing thermal system.

Convective mechanism, similarly, naturally occurs or forced. Although most practical engineering simulations are forced, naturally convection inherently occurs depending on the Reynolds number of the flow. Natural convection is heat transfer caused by fluid buoyancy forces that result from local temperature difference [70]. Both natural and forced convection are mathematically modelled using Newton law of cooling

$$q = hA\Delta T \tag{3. 20}$$

As depicted by eq.(3. 20), the heat transfer through convective mechanism is influenced explicitly by the surface area and the temperature difference between the surface and the fluid. In most flow regime, the velocity at the contact of surface and the fluid is zero due to viscous effects. The phenomenon results into convective heat transfer by heat diffusion (conduction) and heat transfer by fluid bulk flow (advection). In case of highly turbulent flow advection tends to be prominent.

Both conductive and convective heat transfer mechanisms rely on the medium. However, not all heat transfer mechanisms that need media; some occur through electromagnetic mechanisms. This constitutes radiative heat transfer. Despite inherent ability to occur in absence of media, radiation also occurs in porous media, and this is indeed the realm where most engineering applications lies. Porous media radiative heat transfer are generally high [71]. This is modelled using the Boltzmann's radiation formulation and its modification.

$$E = \sigma A(T^4 - T_0^4) \tag{3. 21}$$

Just like convective heat transfer, the areas and temperatures of the surfaces involved play defining role in radiative mechanism of heat transfer.

Based on the abovementioned heat transfer mechanism, useful CFD thermal models have been developed to study complex thermal system. The most powerful models are radiation models. They include Discrete ordinate radiation model, Rosseland radiation model, and Surface-to-surface radiation model. All the models solve the radiative transport equation (RTE) shown in equation below under different conditions.

$$\mu \frac{\partial I}{\partial \tau}(\tau, \mu, \phi) = I(\tau, \mu, \phi) - J(\tau, \mu, \phi) \quad (3.\ 22)$$

Where; I is the diffuse radiance, τ is the optical depth, μ is cosine of zenith angle, Φ is Zenith angle, and J is source function.

A choice of the appropriate model to apply usually depends on the optical depth. For instance, Surface-to-surface model is applicable in a case with thin optical depth whereas Discrete Ordinates (DO) model works best in a relatively longer optical depth.

Given the fact that most radiation phenomenon model has longer optical depth, discrete ordinate tends to be a useful tool. In computational domain using DO model, the directional relation of the RTE is taken care of by executing an angular discretization followed by an integral over the solid angle through numerical quadrature [67]. This positively affects computational cost.

3.5. Modelling of Fluid Flow

Most of real-world fluid dynamics tends to be turbulent. To model them, scientists have devised CFD models to accurately predict the flow behaviour.

One of the most useful turbulence models include: Standard k-ε model, RNG k-ε model, and realizable k-ε model. Although the models operate on similar principles of solving additional turbulent kinetic energy and dissipation equation in addition to the global governing equations, they possess inherent differences in their designed. While standard and RNG k-ε models are formulated from stochastic relations, realizable k-

ε model is derived from the exact equation for the mean-square vorticity fluctuation and Reynolds stresses constraints to the physics of the model with an assumption of fully-developed turbulence and effect of molecular viscosity being negligible [67]. The deterministic nature of the model which capture the actual physics of the problem makes it more accurate and therefore a popular choice in model turbulence flow.

3.6. Finite Volume Method

Finite Volume Method (FVM) is a numerical method used to solve complex partial differential equations. Given the prevalence of these equations in engineering applications, the method is very handy in engineering simulations, especially in complex system involving fluid flow, heat transfer, and electromagnetics.

Major components of FVM include discretization over computational domain, flux calculation on discrete volume, and application of those fluxes to the whole system.

The method procedurally performs discretization on structured and unstructured grids with exceptional versatility and geometric adaptability [72]. It enables efficient simulation of complex fluid flow system. Unlike Finite Difference Method (FDM), this numerical method is relatively flexible and can be applied to complex systems such as fluid flow, heat transfer, electromagnetics, and acoustics. Its versatility results from its unstructured grids.

Most engineering simulations tools available such as ANSYS Fluent utilizes FVM in its computation.

3.7. Solution Algorithms and Discretization Schemes

For computational solver to solve complex differential equations at computational domain, an algorithm is required to perform integrations of velocity. In CFD codes, ANSYS Fluent, pressure-based and density-based algorithms are available.

The algorithms are designed for specific suitability. While pressure-based algorithm is developed for low incompressible flow, the density-based algorithm is meant for compressible flow. Another difference lies in the extraction of velocity and pressure fields. In density-based approach, the velocity field is extracted from momentum equation, whereas in pressure-based approach, the pressure field is extracted by

solving a pressure or pressure correction equation which is obtained by manipulating continuity and momentum equations [67].

Despite the differences in the structure and suitability, both algorithms operate on similar techniques of control-volume. This involves division of the domain into discrete control volumes using a computational grid and apply the following procedure according to *Ref*. [67]:

- Integration of the governing equations on the individual control volumes to construct algebraic equations for the discrete dependent variables.
- Linearization of the discretized equations and simultaneously solve them.

As mentioned above, pressure-based approach suits incompressible flow and since many of engineering simulations involve incompressible fluid owing to it less complexity in modelling, this algorithm is commonly used. Therefore, it is worth delving into its procedural structure. As present in *Ref*. [67], the flow chart looks as follows:

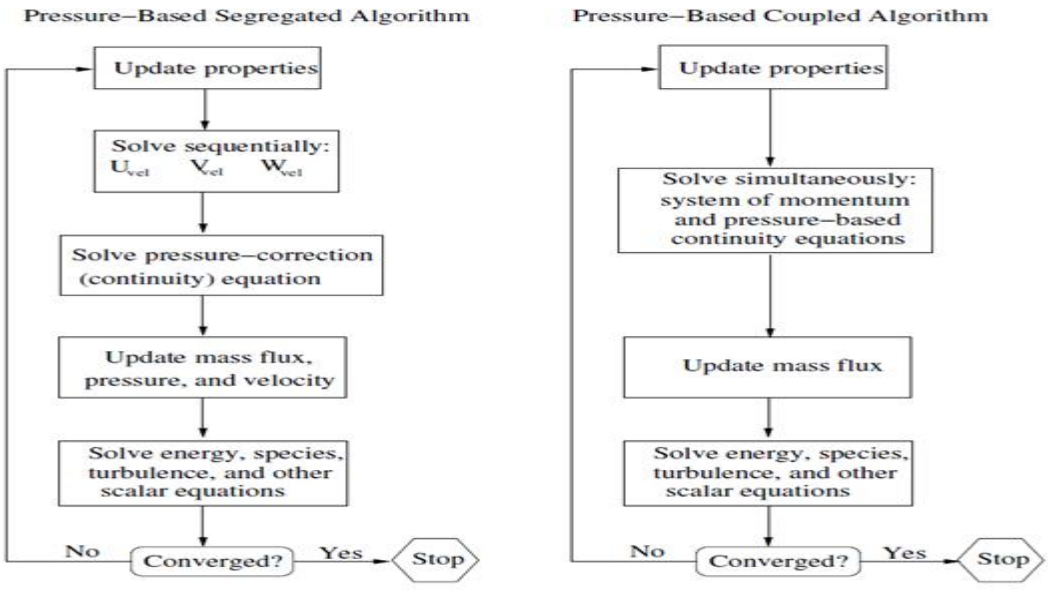

Fig.3. 2: Pressure-based couple algorithm as extracted from Ref. [67].

As show in the figure above, the pressure-based approach can be either segregated or coupled. For segregated approach, the momentum equation and continuity equation are solved separately, whereas in coupled scheme, both momentum and continuity equations are solved simultaneously. The segregation of these governing equations induces difficulties in the convergence of the solution thus making it less

appealing. On the other hand, pressure-based coupled algorithm exhibits more robustness.

As discussed in *section 3.6* of this work, the Finite Volume Method operates on the principle of discretization. The process integrates and converts scalar transport equations into linear equations to be iteratively solved over computational domain. The types of discretization used in most CFD codes are spatial discretization and temporal discretization. In spatial discretization, the operation is done in space within the element whereas in temporal discretization a time dimension is introduced.

In steady flow, spatial discretization is usually appropriate. It can be visualized in presentation of generic control volume as shown in figure below illustrating the centre-oriented discretization.

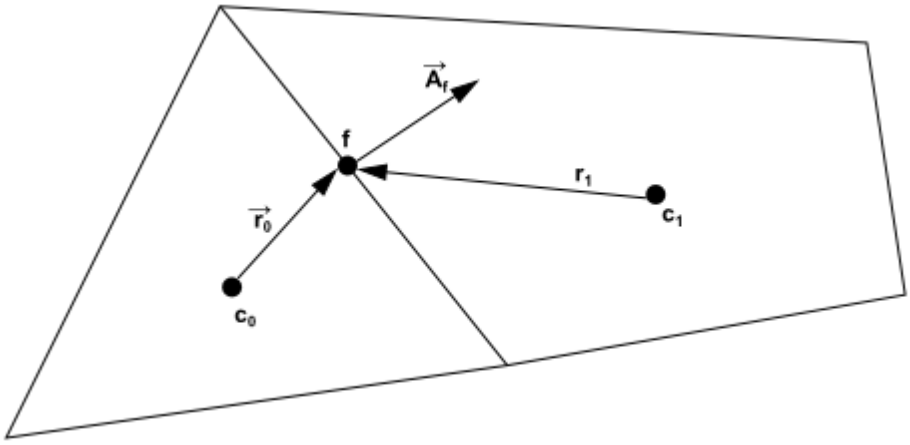

Fig.3. 3: Spatial discretization illustration as extracted from ANSYS, (2013)

In discretization process an upwind scheme is used to integrate the pressure and velocity. It can be first-order or second-order upwind. First-order upwind set face value of *Q* angle equal to cell-centre value of *Q*. That means, all the operations carried out with centre of the cell as a reference. Second-order upwind, on the other hand, applies multidimensional linear reconstruction. This makes the solution obtained more accurate and subsequently eases the solution convergence. Since the accuracy of solution bears an importance in any simulation, second upwind proves to be more robust and a better choice.

3.8. Pressure-volume Coupling

As mentioned in *section 3.7* of this work, using pressure-based coupled algorithms is more desirable as it simultaneously solve both momentum and continuity equations. The operation is possible because of pressure-velocity coupling.

Many algorithms available for CFD simulation such as Simple, Simplec, PISO, and Fractional Step Method and Coupled algorithm are all pressure-based segregated algorithm. To improve their robustness, especially when dealing with incompressible flow, pressure-velocity coupling is performed.

Improved velocity–pressure coupling is achieved by making use of a regularized form of the divergence-free constraint, which recognizes the pressure as a Lagrange multiplier enforcing the divergence-free constraint [73]

3.9. Summary and conclusion

The chapter delved into theoretical underpinnings of the computational fluid dynamics. It explored the fundamental governing equations of a flow regime and their explicit applications.

To develop theoretical framework that will be tested in this research, a concept of Reynolds (ensembled) averaging was discussed. These results in an in-depth exploration Reynold Average Navier's Stokes (RANS) equations that are essentially modified versions of governing equations applicable for turbulence flow.

Due to pervasive applications of Finite Volume Method in numerical modelling of fluid flow, this concept has been briefly examined. Some of its off-shooting elements such as discretization schemes and pressure-velocity coupling have also been discussed.

In conclusion, the chapter lays a conceptual foundation that will be the basis for the subsequent part of this work. The conceptual framework of numerical modelling of turbulence flow will be tested in the proceeding chapters.

Chapter Four

Chapter 4: Model Validation

4.1. Introduction

Computational Fluid Dynamics (CFD) is a complex field whose tools iteratively solve complex equations that defines physical phenomena. The tool used in this investigation, ANSYS Fluent, works on the similar principle. It solves Navier's Stokes equations in combination with other complementary equations under specified boundary conditions.

Operationally, the system has a capacity to produce a solution, however inaccurate. To build a trust in the sensibility and accuracy of obtained solution, a validation must be carried out. It involves comparing the solutions of a developed model with the similar existing solutions in literature. This chapter is dedicated to the validation process of the developed models for this study.

Parabolic trough collector being an extensively researched technology, there are several experimental and numerical studies on the performance of its receiver system available in literature. In this study, Forristall [74] is used to validate the developed models. Due to the precise accuracy and extensiveness of the study, it has been a popular validating literature on the performance evaluation and optimization of novel PTC receivers. Most of the literature cited in *chapter two* of this work have been validated using this literature. Moreover, the study is a pioneering numerical investigation of PTC receiver system carried out by National Renewable Energy Laboratory (NREL) operated by the US Department of Energy and the models were verified and validated using experiment data from Dudley *et al*. [75], an experimental study conducted at the Sandia National Laboratory on SEGS LS-2. These make it a trustworthy literature to check the accuracy of results obtained from numerical study of the system.

4.2. Description of the Validating Simulation

The validating literature [74] as mentioned in the introduction is a numerical study carried out at NREL and its results rigorously validated with experimental data from SEGS LS-2 experiments presented in Dudley *et al*. [75]. The computational model was constructed in EES.

Just like several other models conducted in investigating the improvement of performance of the PTC receiver system, the model used here is comprehensive and it consists of thermodynamic elements: forced convection between heat transfer fluid and inner surface of absorber, conduction within the walls of absorber, natural convection, radiation and/or vacuum in the annulus space, conduction within the walls of glass envelope, and radiation and/or natural convection on the outer wall of the glass cover. This model offers all comprehensive cases possible for holistic examination of the receiver performance. It examines the thermal and thermodynamic performance in the case where:

- Annulus space is filled with air, hydrogen, or Argon.
- Annulus space is evacuated.
- Glass cover is removed.

Additionally, the outer surface of absorber tube is covered with selective coating whose optical and thermal properties influence the overall performance. The selective coatings include:

- Luz black chrome
- Luz Cermet
- Solel UVAC Cermet

For the computational setup, one-dimensional and two-dimensional energy balance models were performed. The dimensions, optical, and physical properties of the modelled system is represented in Table 4. 1.

Table 4. 1: Model dimensions and optical and physical properties [74]

Properties	Values
• Absorber inner diameter (m)	• 0.066
• Absorber outer diameter (m)	• 0.070
• Glass envelope inner diameter (m)	• 0.109
• Glass envelope outer diameter (m)	• 0.115
• Projected aperture width (m)	• 5.0
• Mirror reflectivity	• 0.90
• Optical efficiency (%)	• 74.13
• Coating absorbance	• 0.98
• Glass envelope transmittance	• 0.97
• Coating emittance at 100 C, 400 C	• 0.04, 0.1

The geometry described by the dimensions illustrated in the Table 4. 1 is shown by this physical model represented by Fig.4. 1.

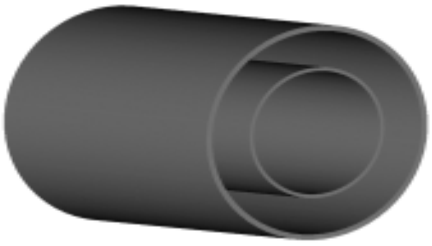

Fig.4. 1: Physical model [74]

Considering all the assumptions and simplifications, simulations for these two models were performed and the results validated with experimental results from Dudley *et al* [75] and perfect accuracy was established. The relevant results are reported *in sub-section 4.3*.

The heat transfer fluid used here was Syltherm-800 whose physical properties are temperature-dependent as reported in Mwesigye *et al*. [43]

For;

$$233.15 \leq T \leq 673K$$

$$c_p = 1.10787 + 1.70736x10^{-3}T(kJkg^{-1}K^{-1})$$
$$\ell = 1.2691x10^{3} - 1.52115T + 1.7913x10^{-3}T^{2} - 1.67145x10^{-6}T^{3}(kgm^{-3})$$
$$\lambda = 1.90134x10^{-1} - 1.88053x10^{-4}T(Wm^{-1}k^{-1})$$

Viscosity is given by piecewise polynomials.

For;

$$233.15 \le T \le 343K$$
$$\mu = 5.14887x10^{4} - 9.61656x10^{2}T + 7.50207T^{2} - 3.12468x10^{-2}T^{3} + 7.32194X10^{-5}T^{4} - 9.14636x10^{-8}T^{5} + 4.75624x10^{-11}T^{6}(mPas)$$

For;

$$\mu = 9.88562x10 - 7.30924x10^{-1}T + 2.21917x10^{-3}T^{2} - 3.42377X10^{-6}T^{3} + 2.66836x10^{-9}T^{4} - 8.37194X10^{-13}T^{5}(mPas)$$

4.3. Results of the Validating Simulation

Under various operating and boundary conditions, number of simulation trials were performed, and the consistent results obtained are reported in Table 4. 4. Two major boundary conditions were that the upper half periphery of the absorber tube receives the direct normal irradiance (DNI) whereas the lower half is subjected to non-uniform heat flux modelled from optical ray tracing method (Monte Carlo Ray Tracing).

Table 4. 2: Simulation results from the NREL study conducted by Forristall [74]

Case	I^b (W/m^2)	T_{am}(K)	V (L/min)	T_{in}(K)	T_{out}(K)	ΔT (C)	η_{th}
1	933.7	294.4	47.7	375.4	397.2	21.80	72.51
2	968.2	295.6	47.8	424.2	446.5	22.30	70.90
3	982.3	297.5	49.1	470.7	492.7	22.00	70.17
4	909.5	299.5	54.7	527.9	542.6	14.70	70.25
5	937.9	299.4	55.5	571.0	589.6	18.60	67.98
6	880.6	302.0	55.6	570.2	590.4	20.20	68.92
7	903.2	300.7	56.3	629.1	647.2	18.10	63.82

To complete the validation of the developed model in this work, some of these results are juxtaposed with results obtained in *section 4.4*.

4.4. The Developed Model for This Work

4.4.1. Model Description

Physically, the receiver system is composed of absorber tube and glass cover as described in *section 4.2*.

The model developed in this work is a simplified model that consider forced convective heat transfer in absorber tube, conduction in the walls of the absorber tube, and radiative heat transfer between outer surface of absorber tube and inner surface of glass cover. An important assumption regarding the annulus space between absorber tube and glass cover is that it is evacuated to eliminate natural convective heat loss, thus allowing only radiative heat exchange between absorber and glass cover.

Just as presented in *Section 4.2* of this work, the absorber tube is made of stainless steel and glass cover of Pyrex glass. Unlike in that work, the physical and optical properties of the material are temperature-independent, and no special coating applied. These assumptions were made for simplification purpose. The lateral and cross-sectional representation of the described model is shown in the figure below.

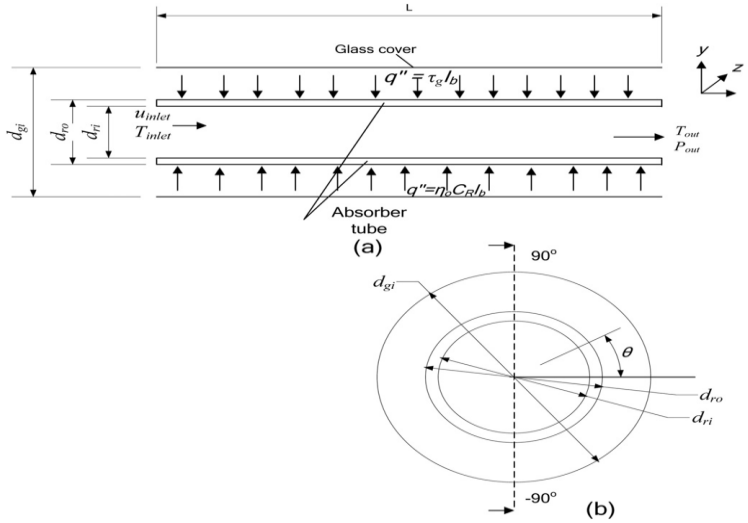

Fig.4. 2: Literal and cross-sectional representation of physical model [53]

4.4.2. Boundary Conditions and Solution Methodology

The computational simulation was implemented in engineering simulation software, ANSYS Fluent R2, that utilizes CFD codes. The physical geometry, a three-dimensional physical model of the absorber tube, was constructed in the SpaceClaim. Discretization and meshing were conducted using hexahedral element in the software meshing environment.

Turbulence flow was modelled using realizable *k-ε* model and radiative exchange between outer surface of the absorber and inner surface of the glass cover modelled using discrete ordinate (DO) model. Enhanced wall-treatment was chosen to model near-wall functional behaviour of the turbulence due to relatively low Reynold number of the flow and y^+ values were not specified because the model is insensitive to y^+ values as discussed in *chapter 3*, and thus failure to specify it does not affect the solution accuracy [67].

Boundary conditions for the simulation were applied over computational domain. Dimensions and operational conditions applied to the geometric construction and the subsequent boundary conditions are represented in table 4.3. The constants were extracted from Forristall [74].

Table 4. 3: Dimension, optical and thermal properties of receiver system

Properties	Values
• Absorber inner diameter (m)	• 0.066
• Absorber outer diameter (m)	• 0.070
• Glass envelope inner diameter (m)	• 0.109
• Glass envelope outer diameter (m)	• 0.115
• Projected aperture width (m)	• 7.8
• Aperture area m^2	• 39.0
• Mirror reflectivity	• 0.90
• Optical efficiency (%)	• 50
• Absorber absorbance	• 0.97
• Glass envelope transmittance	• 0.96
• Glass envelope emittance	• 0.86
• Absorber emittance	• 0.075
• Rim angle	• 90^0
• Concentration ratio	• 71

To computationally set up the simulation, simplifying assumptions were made. They include:

- Uniform heat flux

- The lower half of the absorber tube receives concentrated heat flux from the collector and the upper half receives flux from direct normal irradiation from the sun. These fluxes were calculated using the following formulae:

  - Flux applied on upper half.

$$q'' = \alpha \tau_g I_b \quad \text{[28]} \tag{4. 1}$$

Where α is permittivity of the absorber.

τ_g is transmissivity of the glass.

I_b is direct normal irradiance.

  - Flux applied on the lower half.

$$q'' = \eta_0 C_R I_b \quad \text{[43]} \tag{4. 2}$$

Where η_0 is optical efficiency of the collector.

C_R is concentration ratio.

I_b is direct normal irradiance.

- Fully developed turbulent flow.
- No-slip boundary conditions.
- Evacuated annulus space and no wind on the outside of the glass cover with negligible natural convective loss. (Meaning: the only thermal loss to be accounted for is radiative loss between the absorber and glass cover)

The operating and boundary conditions specified in *section 4.3* of this work were applied. Heat flux on the upper and lower halves of the absorber tube were calculated in accordance with eq. (4. 1) and (4. 2) and respectively applied.

The exterior of glass cover was assumed to be taking the ambient temperature. The rest of boundaries were coupled with the system to interact according to the other applied boundary conditions. The Simple algorithm was chosen to integrate pressure and velocity fields, and hybrid initialization was chosen to initialize the solution. Continuity, momentum, DO, and *k-ε* equations convergence was obtained at residual less than 10^{-5} and energy at less than 10^{-7}.

4.5. Numerical Solutions and Comparison

Based on the operating and boundary conditions discussed, the simulations were carried out and the results obtained are presented in Table 4. 4.

Table 4. 4: Results of the developed model for this study

Case	I_b (W/m^2)	T_{am}(K)	V (L/min)	T_{in}(K)	T_{out}(K)	ΔT (C)	η_{th}
1	933.7	294.4	47.7	375.4	397.7	22.28	73.27
2	968.2	295.6	47.8	424.2	447.0	22.80	71.97
3	982.3	297.5	49.1	470.7	493.3	22.65	71.43
4	909.5	299.5	54.7	527.9	547.2	19.25	71.09
5	937.9	299.4	55.5	571.0	591.1	20.11	70.68
6	880.6	302.0	55.6	570.2	589.0	18.84	70.78
7	903.2	300.7	56.3	629.1	649.3	20.24	70.21

To check the accuracy and correlation of the results, a comparison to the results presented in Table 4. 2 in *section 4.3* of this work was carried out. The juxtaposition was done using the outlet temperatures, change in temperature, and thermal efficiency. The charts below represent the comparison.

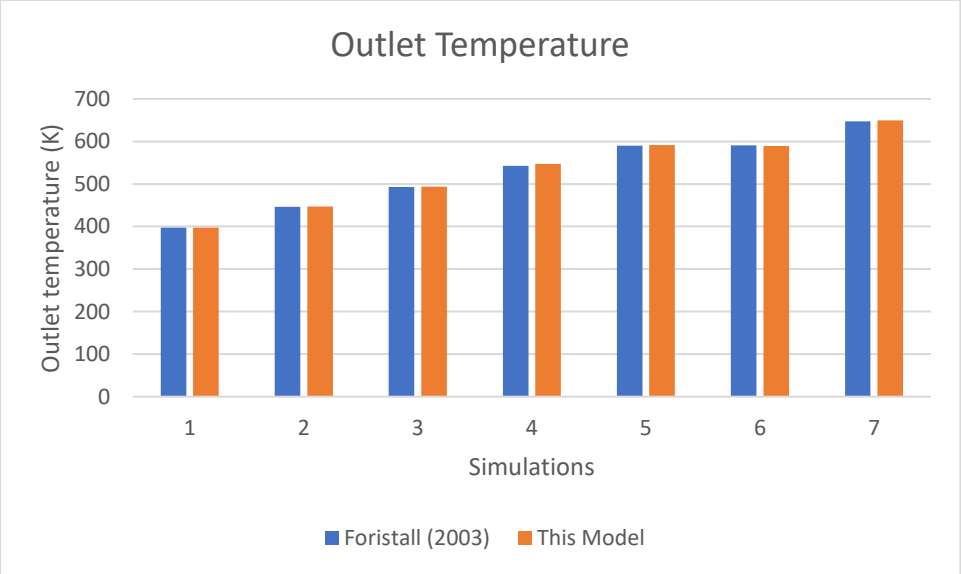

Fig.4. 3: Comparison of outlet temperature of the developed model and Forristall, (2003)

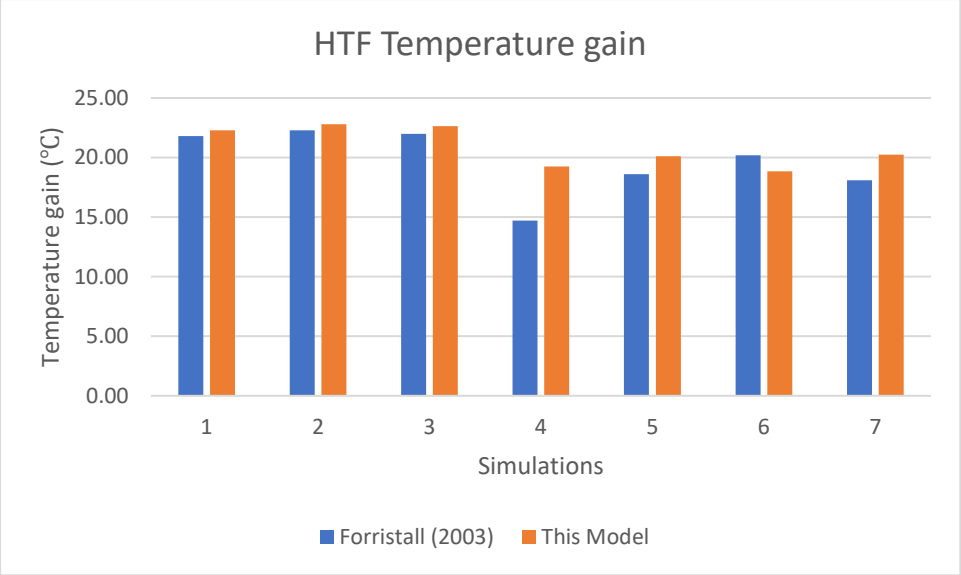

Fig.4. 4: Comparison of temperature change of the developed model and Forristall, (2003)

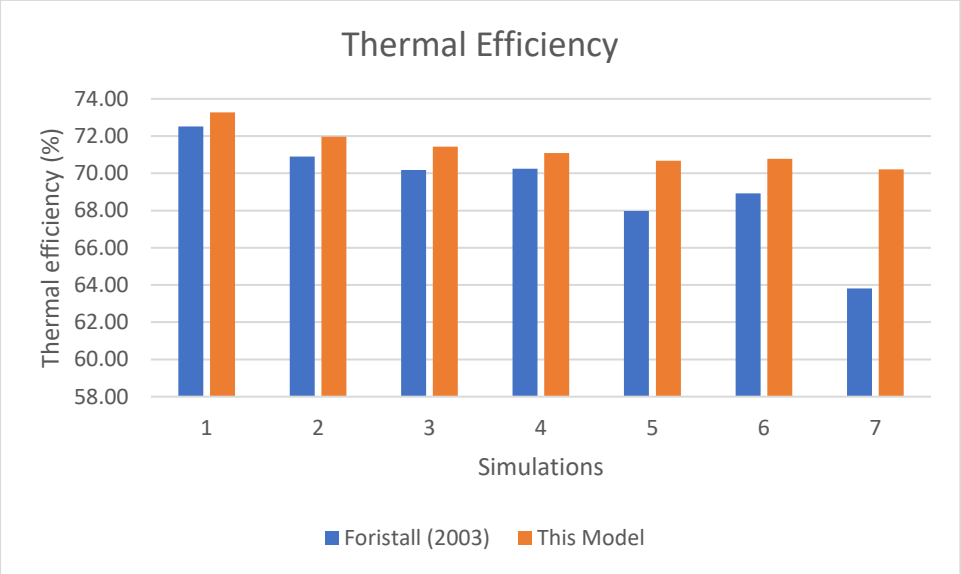

Fig.4. 5: Comparison of Thermal Efficiency of the developed model and Forristall, (2003)

4.6. Discussion

As shown by the results, the outlet temperatures, temperature gains, and thermal efficiencies in the two studies significantly correlate.

Table 4. 5: Error distribution for the tested parameters

For. (2003)	This Model		For. (2003)	This Model		For. (2003)	This Model	
$T_{out}(K)$	T_{out}(K)	Error (%)	ΔT (℃)	ΔT (℃)	Error (%)	η_{th}	η_{th}	Error (%)
397.2	397.7	0.12	21.80	22.28	2.19	72.51	73.27	1.05
446.5	447.0	0.11	22.30	22.80	2.22	70.90	71.97	1.51
492.7	493.3	0.13	22.00	22.65	2.94	70.17	71.43	1.80
542.6	547.2	0.84	14.70	19.25	30.95	70.25	71.09	1.19
589.6	591.1	0.26	18.60	20.11	8.10	67.98	70.68	3.97
590.4	589.0	-0.23	20.20	18.84	-6.71	68.92	70.78	2.69
647.2	649.3	0.33	18.10	20.24	11.85	63.82	70.21	10.01
Average		0.22			7.36			3.17

The average percentage deviation of outlet temperature, temperature gain, and thermal efficiency are 0.22 %, 7.3% and 3.17% respectively as shown in Table 4. 5, which are minimal. The deviation is due to the difference in the some of the boundary conditions in the two studies. The consequential differences are shown in Table 4. 6.

Table 4. 6 : Differences in the models that result in deviation.

Forristall (2003)	This model
• Absorber tube is coated with special coatings. • Physical properties of absorber tube and glass cover are temperature-dependent. • Heat flux applied was non-uniform and it was modelled using MC Ray Tracing. • Included the convective and radiative loss outside of the glass cover	• Polished stainless steel without special coatings. • Physical properties of absorber tube and glass cover temperature-independent • The model assumed uniform heat flux that are calculated out of assumed optical and thermal parameters of reflector. • Neglect the convective and radiative loss outside the glass cover

The differences mentioned in the *Table 4. 6* have significant implications in the deviations obtained in the two models. However conspicuous the percentage error in some of the cases above, the trend remains consistent in both studies. For instance,

the assumption of insignificant convective and radiative loss outside the glass cover ensures higher values of the heat gain in the developed model, hence higher outlet temperature, heat gain, and thermal efficiency. The similarity in the trend and the closeness of the values of the parameters examined validate the accuracy of the developed model and the result obtained from it can be scientifically trusted.

4.7. Summary and Conclusion

Having looked at the correlation between the developed model and the existing literature, the results from model can be trusted and thus replicable. Therefore, the geometry of the novel receiver model with annular fins will be inserted into the model and simulation carried out with consideration of specific parameters, some of which include Reynolds numbers and inlet temperatures, and other boundary conditions.

This chapter lays the foundation for the subsequent part of this research as the theoretical framework developed in *chapter three* has been successfully tested here, and therefore can be used in the proceeding chapters.

Chapter Five

Chapter 5: Performance Evaluation Based on the First Law of Thermodynamics

5.1. Introduction

First law of thermodynamics contextually examines thermodynamic processes using the lens of energy conservation. By thermodynamically enhancing the receiver, some of these processes are influenced. This chapter evaluates the performance of the PTC receiver by applying criteria based on the First Law of Thermodynamics.

The chosen performance evaluation criteria include, entropy generation rate, entropy distribution along the length of the receiver, entropy generation number, Bejan number, exergy efficiency, and exergy destruction rate.

5.2. Model Description

5.2.1. Physical Model

The physical model investigated is as described in *sub-section 4.4.1* of this work. It consists of an absorber tube with external annular fins arbitrarily placed along its length at equal distance. The number of fins used in this study are 9 fins and 19 fins. The numbers were arbitrarily chosen to investigate the effect of changing the number of fins.

The fin length was equally varied by choosing 5 mm and 10 mm. Just as the fin number was varied, this fin length variation is aimed at studying the influence of changing the fin length on the performance of the receiver. The dimensions, thermal and optical properties of the absorber as presented in Table 5. 1.

The absorber tube is enveloped in glass cover with dimensions, thermal and optical properties also listed in Table 5. 1. The glass cover is meant to reduce convective heat loss, as this improves the performance of the receiver. The sample physical representations of this model are shown in *appendix A.6.1 to A.6.3*

The collector was constructed in a way its rim angle (φ_r) is 90^0 and geometrical concentration ratio (C_r) of 86 as reported by Mwesigye *et al* [43]**.** As presented in Table 4. 3, some of these dimensions, optical, and thermal properties extracted from the cited literature has been combined with fittingly chosen properties and applied to this physical model. All the dimensions and material properties are listed in Table 5. 1

Table 5. 1: Dimension, optical and physical properties

Properties	Values
• Absorber inner diameter (m)	• 0.066
• Absorber outer diameter (m)	• 0.070
• Glass envelope inner diameter (m)	• 0.109
• Glass envelope outer diameter (m)	• 0.115
• Aperture length (m)	• 5.0
• Aperture area (m^2)	• 44.58
• Mirror reflectivity	• 0.90
• Optical efficiency (%)	• 75.4
• Direct Normal Irradiance (W/m^2)	• 1000
• Absorber absorbance	• 0.97
• Glass envelope transmittance	• 0.96
• Glass envelope emittance	• 0.86
• Absorber emittance (polished stainless steel)	• 0.075
• Rim angle	• 90^0
• Concentration ratio, C_R	• 86
• Fin length (mm)	• 5, 10
• Fin width (mm)	• 10
• Number of fins (~)	• 9, 19

The physical model constructed using these dimensions and physical properties is used in the subsequent part of this work.

5.2.2. Boundary conditions

The operating conditions of the model are set at atmospheric pressure, and ambient temperature of 300 K.

The simulation was set up such that the inlet mass flow rate is calculated from the targeted Reynolds number based on *eq.* (2.12*)*. The Reynolds numbers in the range of 5000-35000 were considered for this model. The turbulence flow was chosen because most flow regime in this kind of problem tends to be fully developed turbulence. As stated in *sub-section 4.4.2* of this work, the flow was subjected to no-slip boundary constraint. Also, at inlet the gauge pressure was constrained at zero and therefore the static pressure at the inlet is the resultant pressure due to the inlet flow rate. The inlet temperatures varied in the range of 350-600 K.

All the simplifying assumptions discussed in *sub-section 4.4.2* were applied.

Heat flux was computed using *eq. (4.1 and 4.2)* and applied at the lower and upper peripheries of the absorber tube as discussed in *sub-section 4.4.2.*

5.2.3. Grid Independence Test

To ensure the variation in number of elements in the simulation does not influence the accuracy of the results, a grid independence test was carried out with inlet temperature of 350 K and Reynolds number of 5000 with varied number of elements in the range of 190,000 - 1,000,000 cells and the results are presented in Table 5. 2.

Table 5. 2: Parameters considered for the grid-independence test.

Parameters	Mesh 1	Mesh 2	Mesh 3	Mesh 4	Mesh 5	Mesh 6	Mesh 7
Cells	194799	246313	302104	400620	546761	693960	957822
T_{out}	377.96	378.13	378.25	378.49	378.69	378.83	378.94
Error (%)	0.04	0.03	0.06	0.05	0.04	0.03	Baseline
T_r	489.15	492.01	493.92	496.79	497.70	497.57	497.29
Error (%)	0.58	0.39	0.58	0.18	-0.03	-0.06	Baseline
ΔP	139.83	135.90	132.96	125.98	118.42	113.59	109.56
Error (%)	-2.81	-2.16	-5.25	-6.00	-4.08	-3.55	Baseline

As observed in Table 5. 2, the percentage error induced by changing the number of elements of mesh is minimal across all the tested parameters and using all the cells tested does not induce any substantial error in the solution. Therefore, the range of

the number of elements chosen for this work was 200,000 - 600,000 since this range ensure the computational cost is minimized.

5.2.4. Solution Procedure

As mentioned in *sub-section 4.4.2*, the numerical simulation was implemented in engineering simulations software, ANSYS Fluent R2, that utilizes CFD codes. Discretization, meshing, and radiative model was implemented as described in the same sub-section.

Dimensions, material properties, and operational conditions applied to the geometric construction are discussed in *sub-section 5.2.1* of this work, and were extracted from *Refs*. [74]–[76] as previously mentioned.

The first batch of simulation involved varying Reynolds number ranging from 5000-35000 at inlet temperature 350 K, 400 K and 500 K.

The operating, boundary conditions, and assumptions are discussed in *sub-section 5.2.2* of this work.

Regarding thermal model, the calculated heat fluxes are applied at outer surface of the respective halves of the absorber tube. The rest of the absorber tube is coupled with the system to freely interact with the rest thermally and thermodynamically.

For radiation model, the Discrete Ordinate (DO) model is applied to the receiver system with absorber tube and glass cover as the participating agents. The temperature outside the glass cover is set to a temperature equaling the ambient temperature of 300 K. Emissivity of the Pyrex glass is assumed to be 0.86 whereas that of the polished stainless steel used in absorber tube is set at 0.075 as used in various literature.

The Simple algorithm was chosen to integrate pressure and velocity fields. The solution was initialized using hybrid initialization.

Scaled residuals were used to monitor the convergence. Convergence was achieved at scaled residuals less than 10^{-5} for continuity, momentum, discrete ordinate, and k-ε equations, while energy converged at the residuals less than 10^{-7}. The sample of the scaled residual is shown in *Appendix A.1* of this work. In addition to scaled residual, mass imbalance was monitored to ensure the conservation of mass was achieved.

The simulations were iteratively run for varied inlet temperatures in 350 - 600 K range for Reynolds number 5000, 10000 and 20000 for externally enhanced absorber tube and smooth one for comparison. The same was done for Reynolds numbers in 5000-35000 range at inlet temperature of 350 K, 400 K and 500 K. The number of fins was then arbitrarily increased from 9 to 19 and fin length at 5 mm to 10 mm and subjected to previous boundary conditions.

5.3. Effect of Fins on Thermal Efficiency

To investigate the effect of fins and their variations on the thermal efficiency of the receiver, inlet temperature is varied in the range of 350 - 600 K at Reynolds numbers of 5000, 10000, and 20000 for both smooth absorber tube and absorber tube with nine annular fins with fin length of 5 mm arbitrarily placed at equal distance along its length. As shown in Fig. 5. 1, the thermal efficiency for *Re* = 5000 steadily decreases for inlet temperature in the range of 350 - 400 K and no significant change for 400 - 500 K. Exponential increase in thermal efficiency occurs at 500 K inlet temperature. As expected, the enhanced receiver has higher thermal efficiency. This is because fins increase the surface area for the applied heat flux hence, higher conductive heat transfer. The results of *Re* = 10000 and 20000 exhibit similar trend but with higher thermal efficiency, and smooth exponential behaviour. With increase in flow turbulence, the convective heat transfer increases therefore high energy is transferred to the heat transfer fluid thus increasing thermal efficiency.

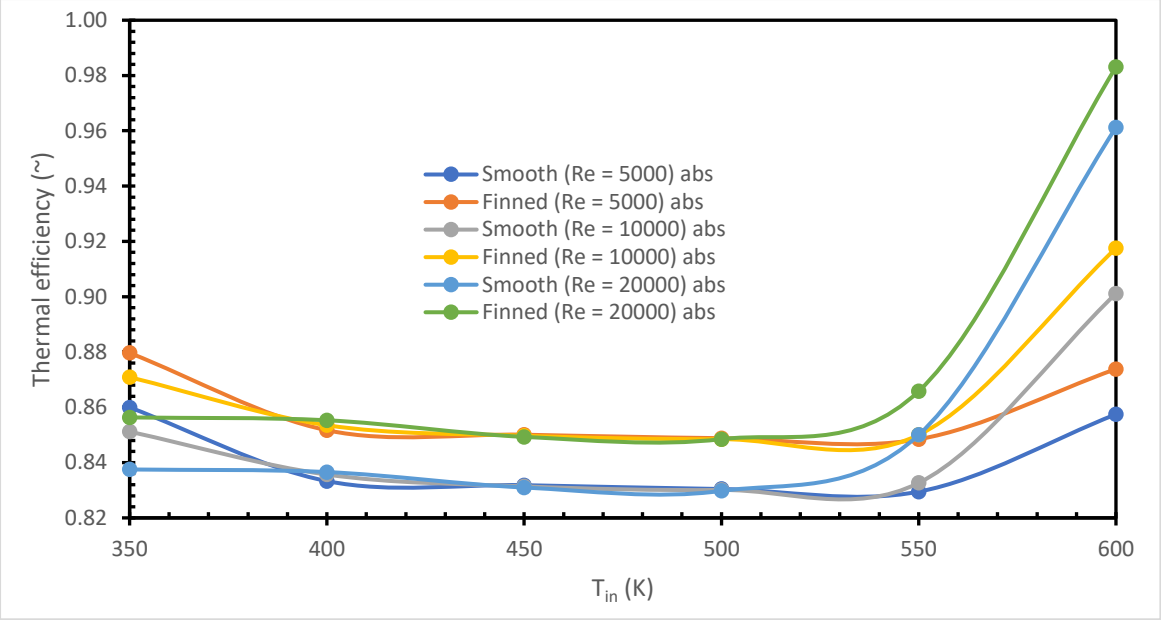

Fig. 5. 1: Thermal efficiencies as function of inlet temperatures for Re = 5000, 10000, 20000

For comprehensiveness, thermal efficiency of enhanced and smooth receiver was comparatively examined as functions of Reynolds numbers. This was done by varying the turbulence at inlet temperatures of 350 K, 400 K, and 500 K.

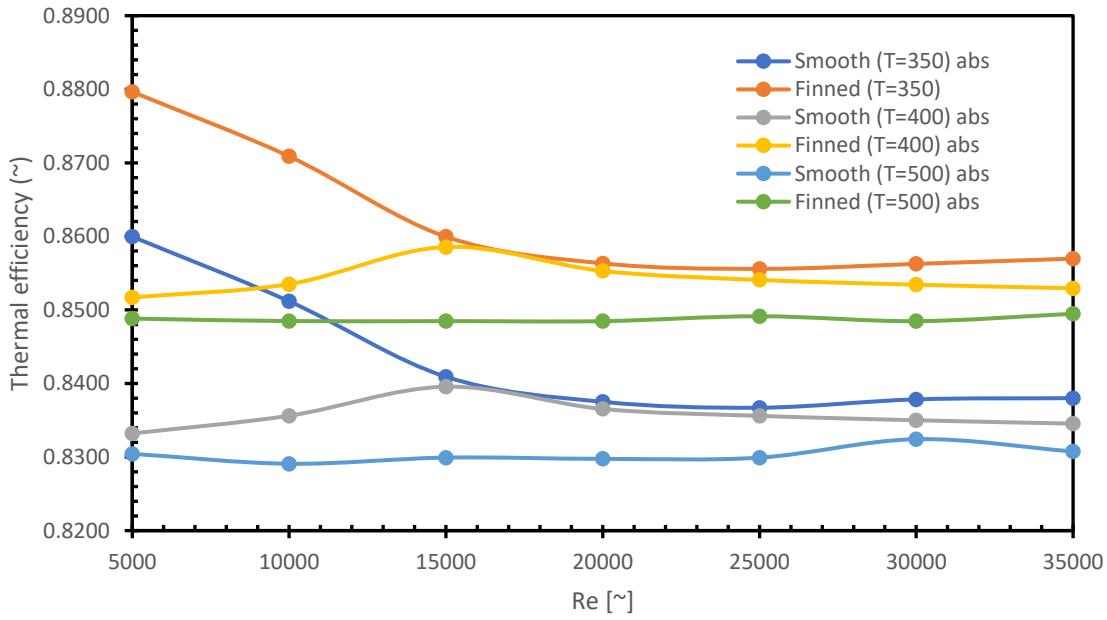

Fig. 5. 2: Thermal efficiencies as function of Reynold numbers for T_{in} = 350 K, 400 K, 500 K

As shown in Fig. 5. 2, the thermal efficiency steadily decreases with increase in Reynolds number for 350 K inlet temperature. An increase of 2.26 percent for T_{in} = 350 K, 2.21 percent for T_{in} = 400 K and 2.22 percent for T_{in} = 500 K is recorded. The increase, though not substantial, is due to the increase in conductive heat transfer owing to increased surface area.

Unlike T_{in} = 350 K, the results of T_{in} = 400K, 500 K show a rather constant thermal efficiency with increase in Reynolds numbers. The trend is due to relatively high turbulence caused by high inlet temperature. Since the heat transfer fluid properties are temperature-dependent, no significant change in thermal efficiency is expected as both inlet temperature and Reynolds number increase.

Despite the constancy of the thermal efficiency with increasing inlet temperatures and Reynolds numbers, the introduction of fins increases the thermal efficiency due to similar reasons mentioned in this section and that influence is shown in Fig. 5. 3.

Looking at influence of introducing just external annular fins is insufficient. A variation in the number of fins and their fin lengths further paint clearer picture. To implement this, the number of fins were arbitrarily increased from nine to nineteen and placed at equal distance along the absorber tube. Similarly, the fin length was increased from 5 mm to 10 mm. Inlet temperatures and Reynolds numbers were varied accordingly to generate the turbulence and the results are shown in Fig. 5. 3 and Fig. 5. 4. The tests were carried out at T_{in} = 350 K while varying the Reynolds number.

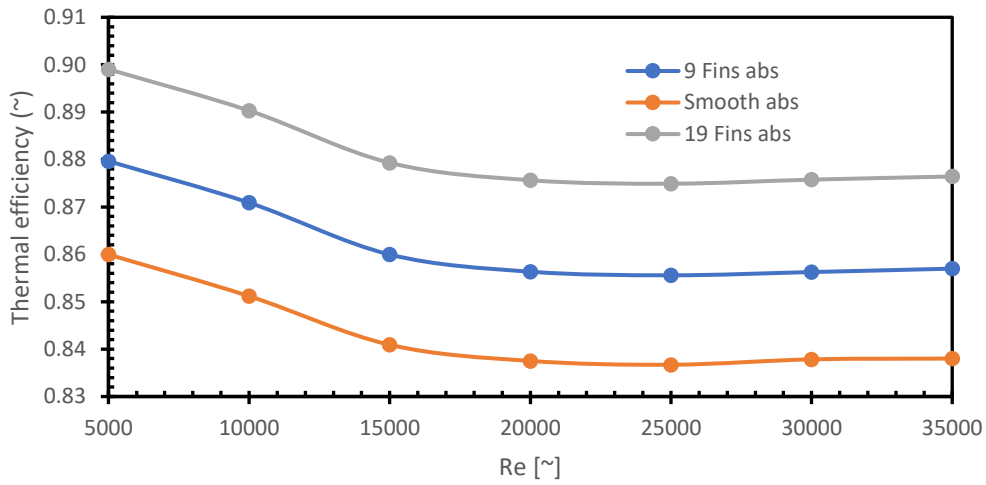

Fig. 5. 3: Variation of thermal efficiency from increasing the number of the external annular fins at T_{in} = 350 K.

Doubling the number of fins has positive impact on thermal efficiency. Thermal efficiency in the receiver with 19 fins is higher than the one with 9 fins and smooth one has the lowest as depicted in Fig. 5. 3. Increasing the number of fins increases the external surface area of the absorber tube and that allows more heat flux to be absorbed and conducted to the heat transfer fluid. Consequently, an increase in the amount of energy absorbed in HTF increases thermal efficiency due to their direct proportionality formulated in *eq.* (2.7).

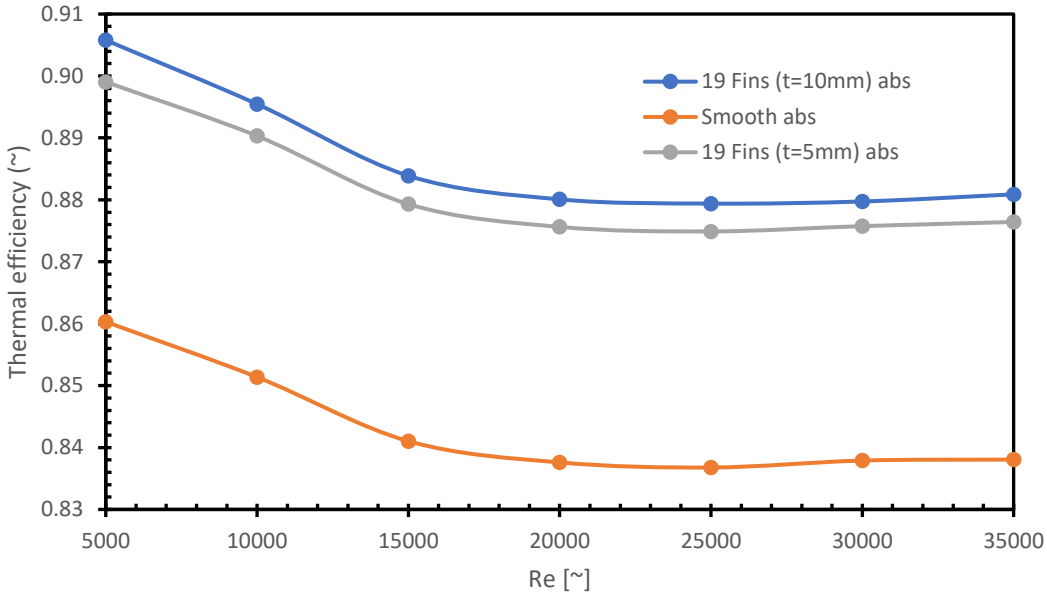

Fig. 5. 4: Thermal efficiency as influenced by increase fin length at T_{in} = 350 K.

Similar trend is observed in Fig. 5. 4 with a doubling of the fin length. As depicted on the graph, the efficiency in t = 10 mm is higher than the t = 5 mm with efficiencies lying in the range of 88 - 90.5 percent while smooth receiver falls in the range of 84 - 86 percent. The appreciation in thermal efficiency is the positive influence of increasing absorber surface area on the heat transfer.

5.4. Influence of Fins on Thermal Enhancement Factor

The motivation for introducing external annular fins hinges on enhancing thermal heat transfer. One of the criteria to measure this is thermal enhancement factor. To determine how the novel receiver perform against this performance evaluation criteria, a simulation was conducted by varying Reynolds number at inlet temperatures of 350 K and 400 K. As Fig. 5. 5 shows, the thermal enhancement factor peaks at 15,000

Reynolds number while at the minimum at 25,000. Its average thermal enhancement factor is 1.0042, which indicates 0.42 percent thermal enhancement.

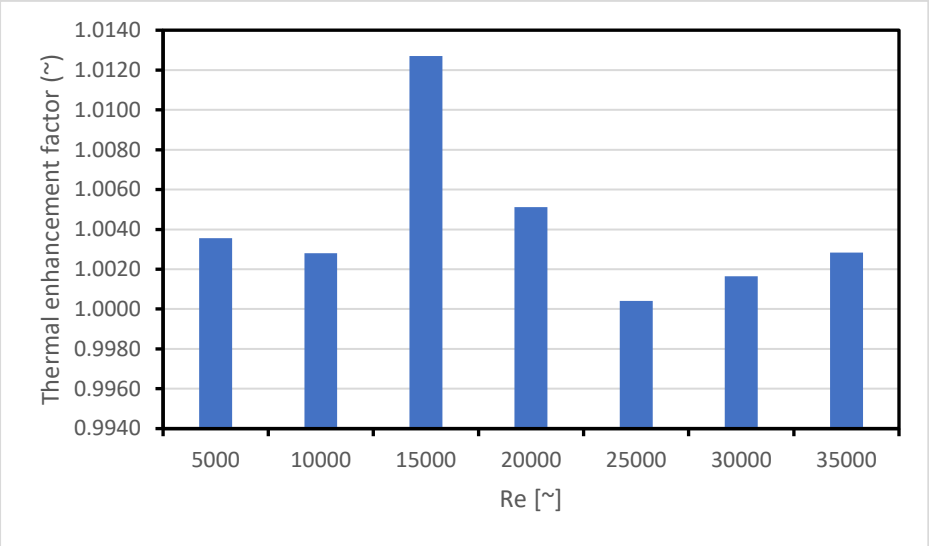

Fig. 5. 5: Thermal enhancement factor at 350 K inlet temperature

The results of 400 K inlet temperature show, an average thermal enhancement factor at 1.0036 which reflects 0.36 percent thermal enhancement with maximum and minimum as depicted in Fig. 5. 6.

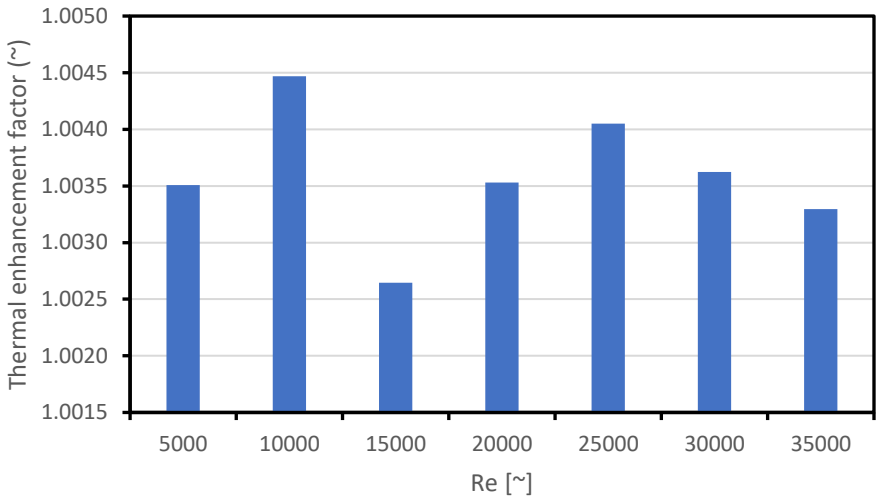

Fig. 5. 6: Thermal enhancement factor at 400 K inlet temperature

Considering the percentage thermal enhancement of both, it is apparent that an increase in inlet temperature reduces thermal enhancement factor. This is because the tremendous turbulence, that is, increase in fluid bulk velocity with temperature,

allows minimal time for heat transfer fluid to gain sufficient heat energy before exiting the absorber tube given its relatively shorter length.

Since examining just influence of 9-fins receiver at various turbulence state is not conclusive, it was necessary to test the impact of increasing the number of fins. The results are as presented in Fig. 5. 7.

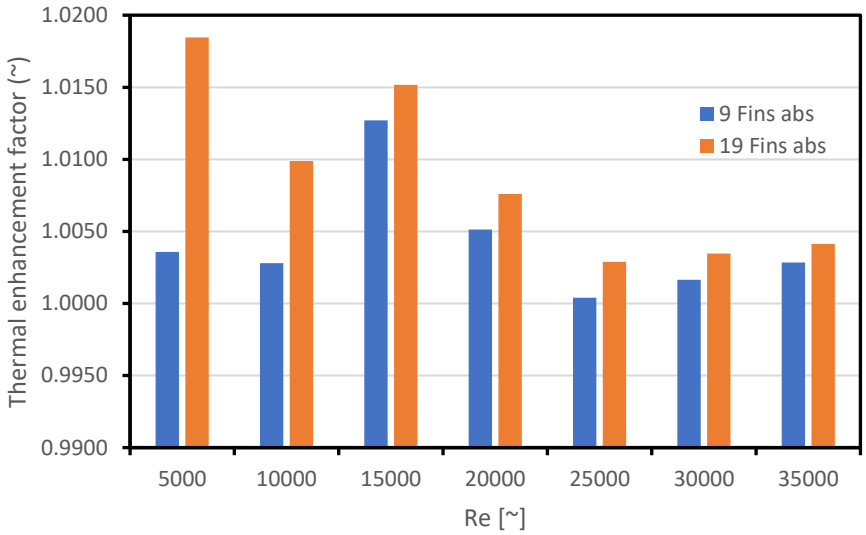

Fig. 5. 7: Comparison of thermal enhancement factors with 9 fins and 19 fins

As observed, an increase in the number of fins increases thermal enhancement factor. As shown in Fig. 5. 7, the thermal enhancement factor at the Reynolds number 5000 depicts the highest thermal enhancement factor and the average thermal enhancement factors for 9-fins and 19-fins absorber tube are 1.0042 and 1.0088 respectively, which comparatively implies enhancement percentage of 0.42% and 0.88%. Therefore, increasing the number of fins improves thermal performance of the receiver. This is because fins naturally increase the surface area that consequently increases the amount of heat flux absorbed by the absorber tube.

5.5. Thermal Loss, and Circumferential Temperature Gradient in Relation to Fin Variations

Thermal stress and strain are critical elements that determine failure of thermal system. This demands an attention to investigate factors that influence them. One of the factors is circumferential temperature gradient. What's more, in designing thermal

system, thermal loss is put into consideration. This section is examining the influence of fins on these two critical factors.

To objectively determine the influence of fins, a test is carried out at different outlet temperatures and Reynolds numbers. As shown in Fig. 5. 8 and Fig. 5. 9, thermal loss in smooth reciever is higher than the enhanced one. This is because although the fins increase the surface area that may inherently increase the radiative loss, the increased surface area also enhances heat conduction and the rate of heat absorption is relatively high hence reducing the losses.

In Fig. 5. 8, thermal loss for both smooth and enhanced reciever tested at *Re* = 5,000 steadly decreases from T_{in} = 350 - 450 K and exponentially increases after that point. Increasing the Reynolds number decreases the thermal loss and at the lower temperature and the functions of thermal loss in terms of inlet temperature transform into an a positive exponent. The increase of thermal loss with inlet temperature is due to the fact that an increase in inlet temperature increases the temperature gradient between inner wall of the glass cover and outer surface of the absorber thus increasing the heat loss due to radiation (the only considered heat loss mechanism in this study).

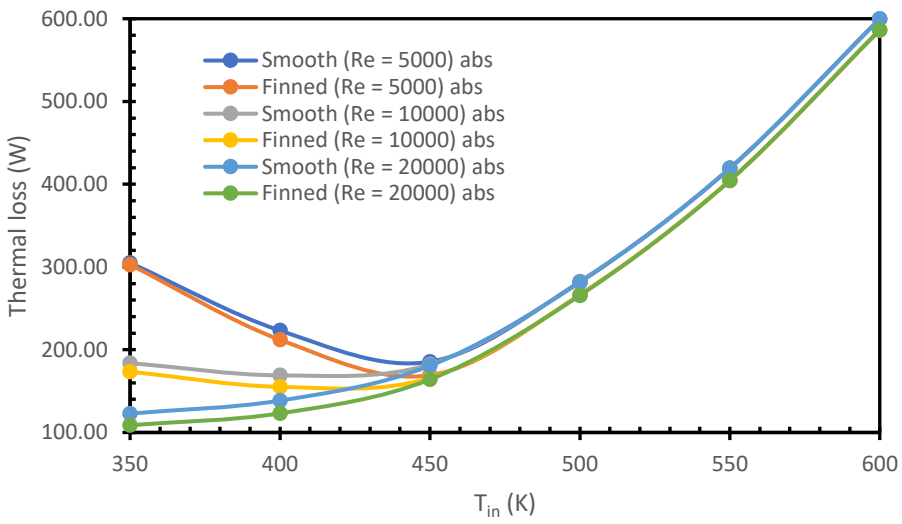

Fig. 5. 8: Thermal loss as function of inlet temperature tested at Re = 5000, 10,000, 20,000 for both smooth and finned absorber

For inlet temperatures of 350 K and 400 K, thermal loss decreases with Reynolds number as shown in Fig. 5. 9. This is because as Reynolds number increases, the turbulence of flow proportionally increases and therefore improving convective heat

transfer hence less heat loss. At higher inlet temperatures as tested at T_{in} = 500 K, no substantial change in thermal loss has been observed; it tends to be constant but higher that the one at lower inlet temperatures. This comparatively greater thermal loss is the relative higher temperature gradient between the two surfaces participating in the radiation.

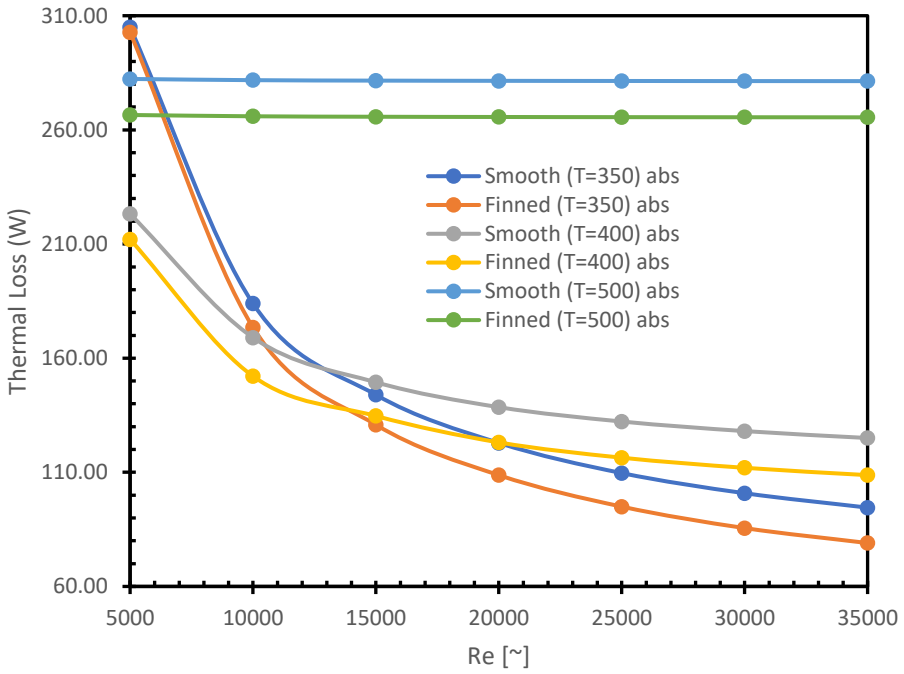

Fig. 5. 9: Thermal loss as functions of Reynold number test at T_{in} = 350 K, 400 K, 500 K for both smooth and finned absorber

As previously mentioned, circumferential temperature gradient influence performance of thermal system as it may lead to deformation of the reciever. At *Re* = 5000, 10000, and 20000, circumferential temperature gradient for both smooth and enhanced reciever has been examined as a function of inlet temperature as presented in Fig. 5. 10. As shown, the circumferential temperature gradient decreases with increase in inlet temperature. The observed trend is due to the fact that increasing inlet temperature leads to increase in fluid flow rate because of temperature-dependence of fluid properties which consequently ensure the higher convective heat transfer thus reducing temperature difference on the absorber tube.

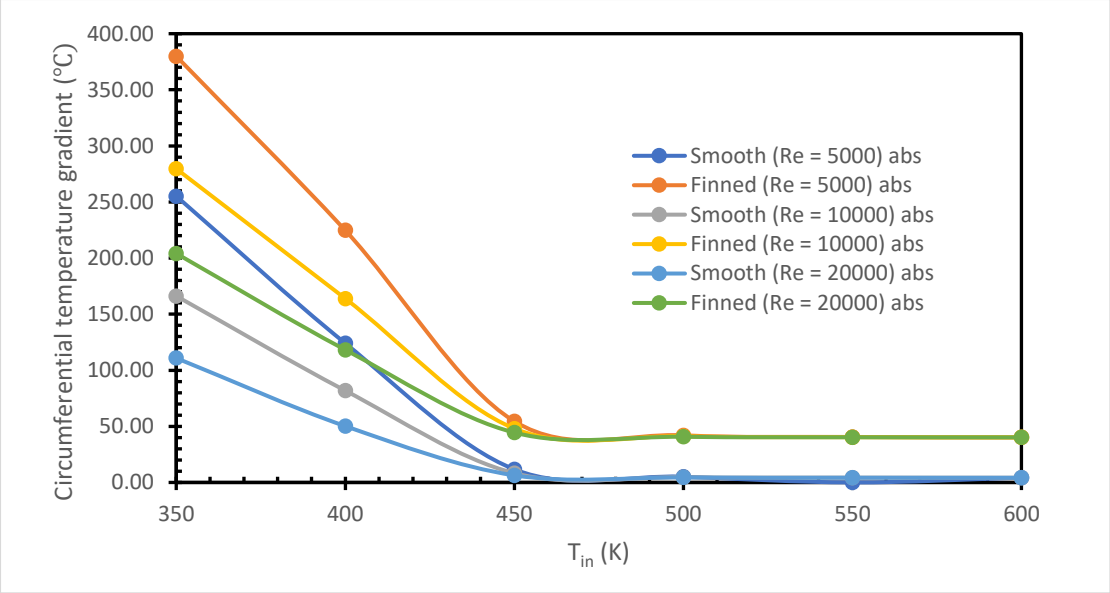

Fig. 5. 10: Circumferential temperature gradient as function of inlet temperature for Re = 5,000, 10,000, 20,000 for both smooth and finned absorber tube

Similar trend is observed with varying Reynolds number at inlet temperature 350 K, 400 K and 500 K. The reason for the decrease in the circumferential temperature gradient with increasing Reynolds number is owing to the increase turbulence that increases the flow rate which dampens the temperature difference on the absorber.

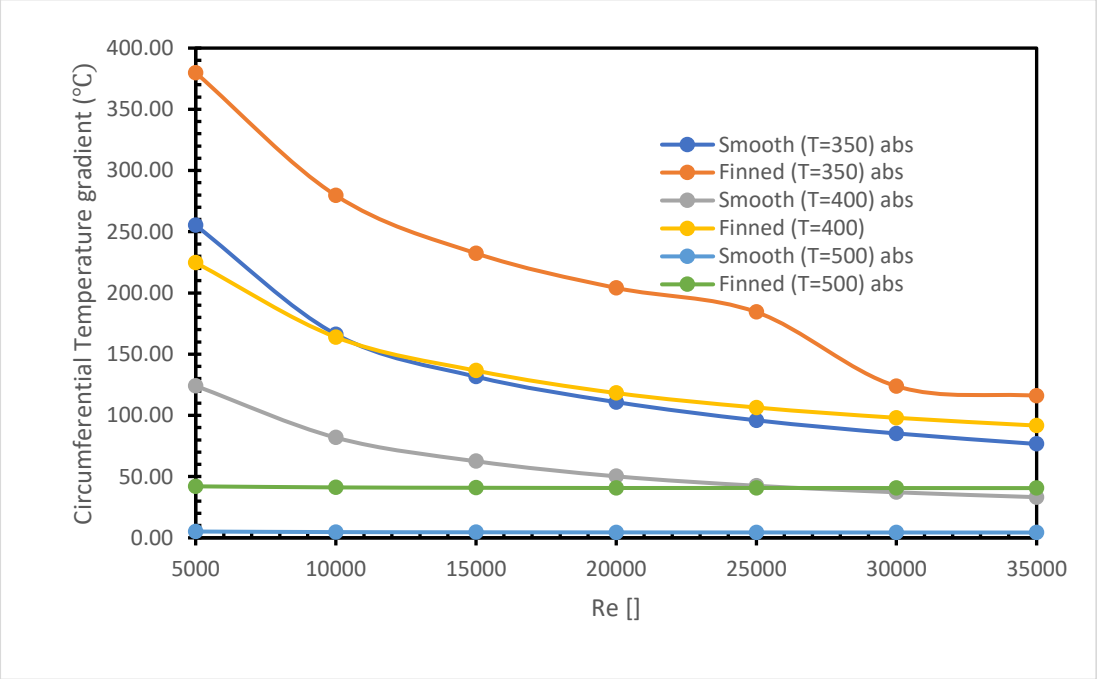

Fig. 5. 11: Circumferential temperature gradient as function of Reynolds number at T_{in} = 350 K, 400 K, 500 K for both smooth and finned absorber tube

In both cases of varying inlet temperatures and Reynolds numbers, it is observed that the circumferential temperature gradient is higher for the enhanced receiver than smooth one. It is also shown that low Reynolds numbers exhibit higher circumferential temperature gradient. The spike in the circumferential temperature gradient for enhanced receiver is because an induced extrusion that facilitates higher absorption of heat energy which raises temperature at this fin position thus increasing the maximum temperature there as shown in *appendix A.2*.

A variation of the fins number and fin length was done and their impact on circumferential temperature gradient and thermal loss observed. These tests were carried out at inlet temperature of 350 K.

As depicted in Fig. 5. 12, using fewer fins do not significantly impact the thermal loss, but significantly increasing number of fins leads to increase in the thermal loss. As observed, 19-fins reciever has the highest thermal loss compared to both smooth and 9-fins reciever. This increase in thermal loss with increased number of fins is due to inherent increase of surface area offered by additional fins which increases the radiative thermal loss.

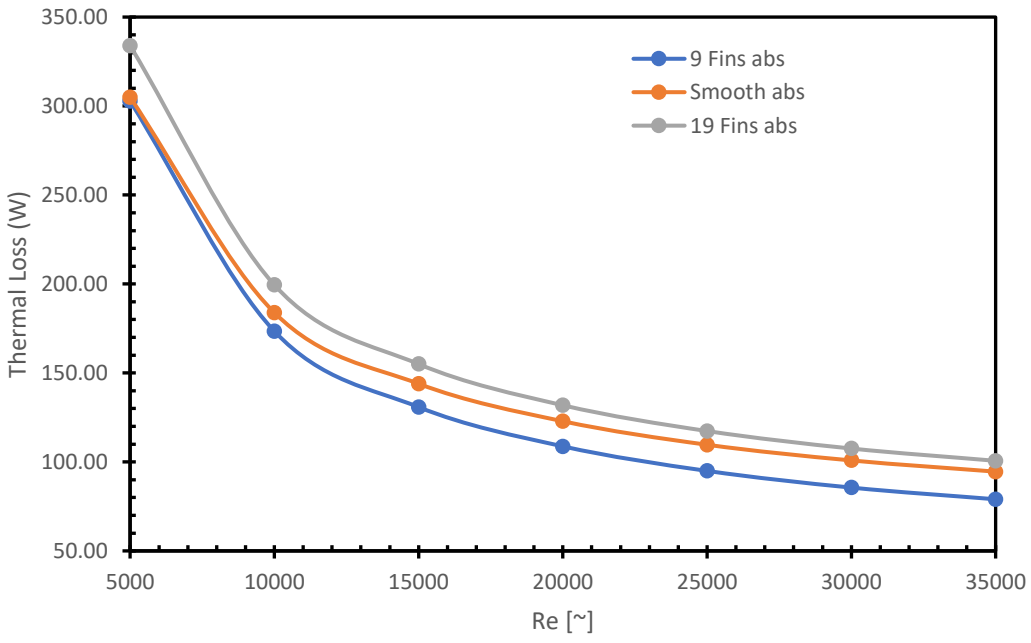

Fig. 5. 12: Thermal loss as examined for increased number of fins at T_{in} = 350 K for varied Reynold number

In Fig. 5. 13, circumferential temperature gradient increases with number of fins, with both 9 fins and 19 fins having higher but indistinguishable temperature differences from 5000-25000 Reynolds number range. After 25000 Reynolds number, the the reciever with larger number of fins acquires higher circumferential temperature gradient. This direct proportionality is due to varied convection due to increased amount of heat absorbed by the absorber tube.

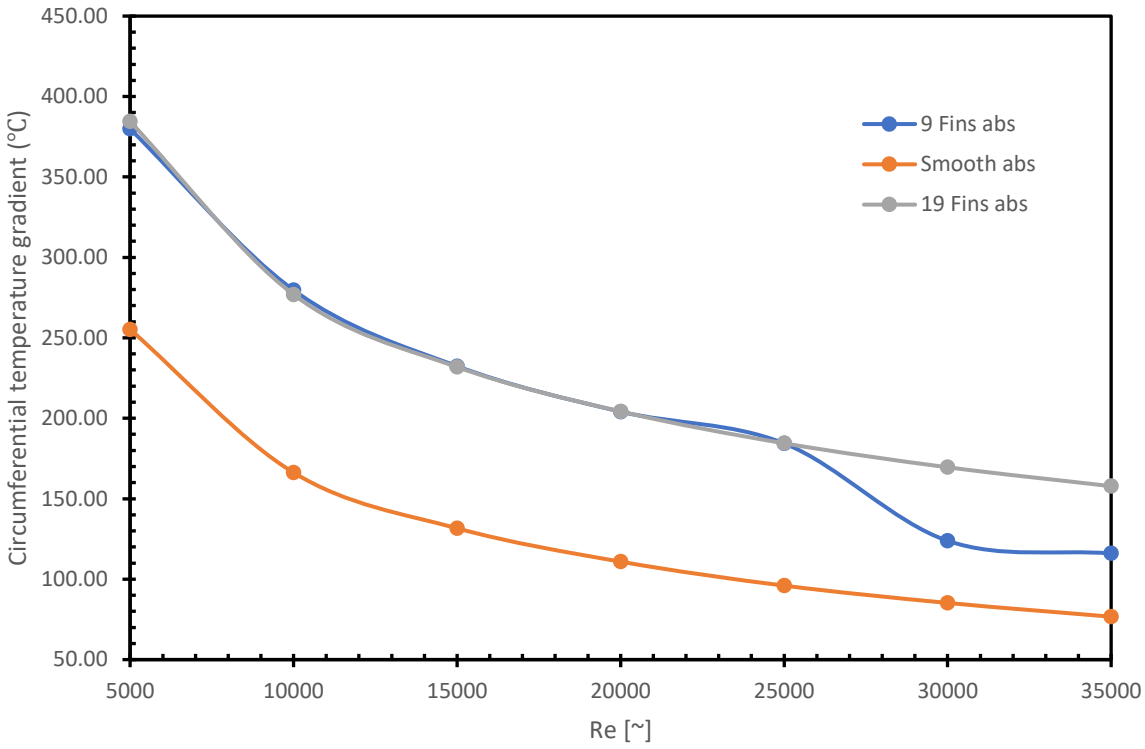

Fig. 5. 13: Circumferential temperature gradient examined for increased number of fins at T_{in} = 350 K for varied Reynolds number.

Increasing number of fins increases both thermal loss and circumferential temperature gradient, just as fins length influences. Fig. 5. 14 and Fig. 5. 15 show the highest thermal loss and circumferential temperature gradient for t = 10 mm and the lowest for smooth absorber tube.

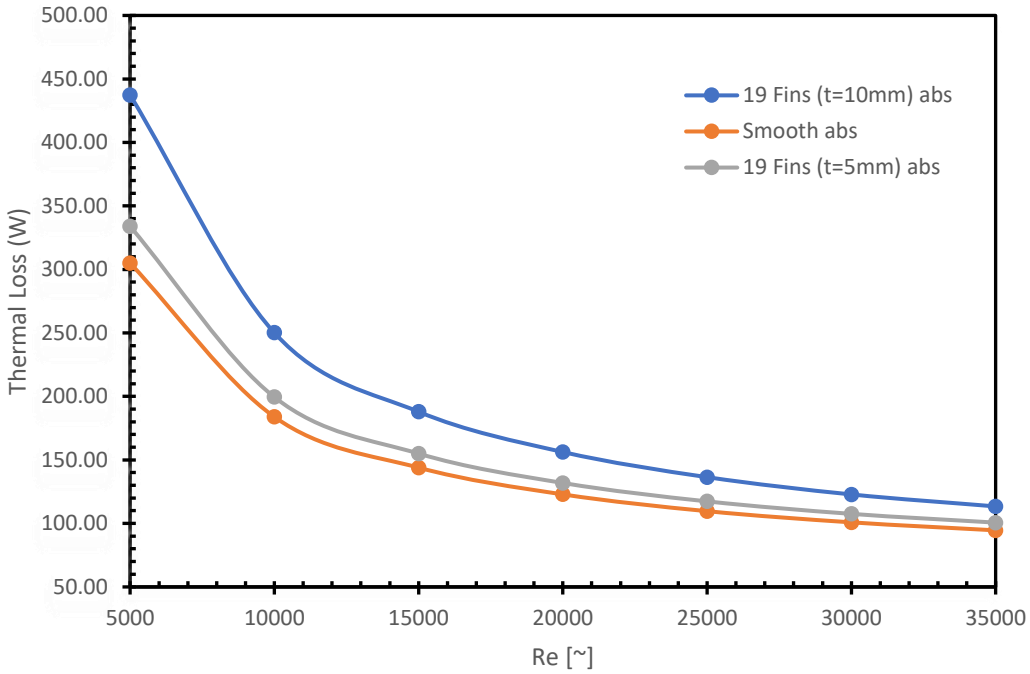

Fig. 5. 14: Influence of fins length for varied Reynold numbers tested at T_{in} = 350 K

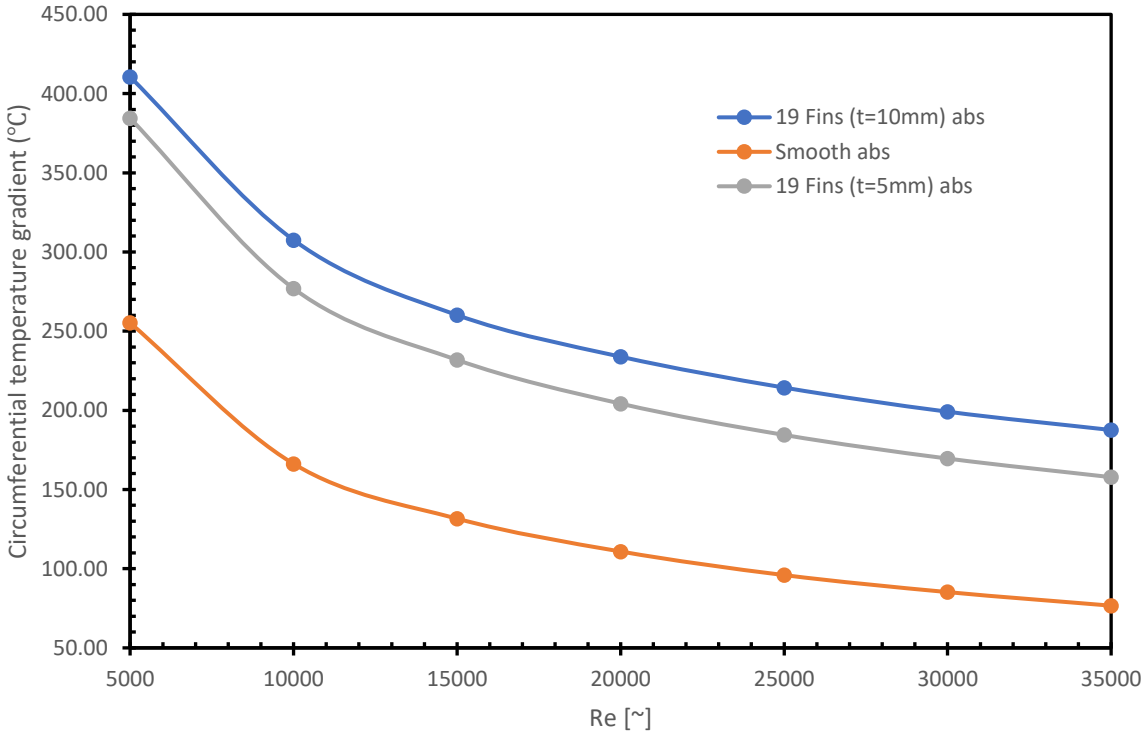

Fig. 5. 15: Influence of fins length for varied Reynold numbers tested at T_{in} = 350 K

The reason for this variation is due to the incremental influence of surface area on heat energy absorption of the system.

5.6. Nusselt Number and Fluid Friction

Nusselt number and fluid friction determine the flow regime as they model the flow resistance which has influence on the pressure variation. While the Nusselt number defined the degree of dominance of convective heat transfer over the conductive heat transfer, the fluid friction depicts the resistance in the flow.

Therefore, the Nusselt number and fluid friction has been considered in this work for the variation of the number of fins for different Reynolds numbers at T_{in} = 350. As shown in Fig. 5. 16 and Fig. 5. 17, the fluid friction and Nusselt number are respectively indistinguishable for varied number of fins. This means, the enhancement does not significantly impact these non-dimensional numbers.

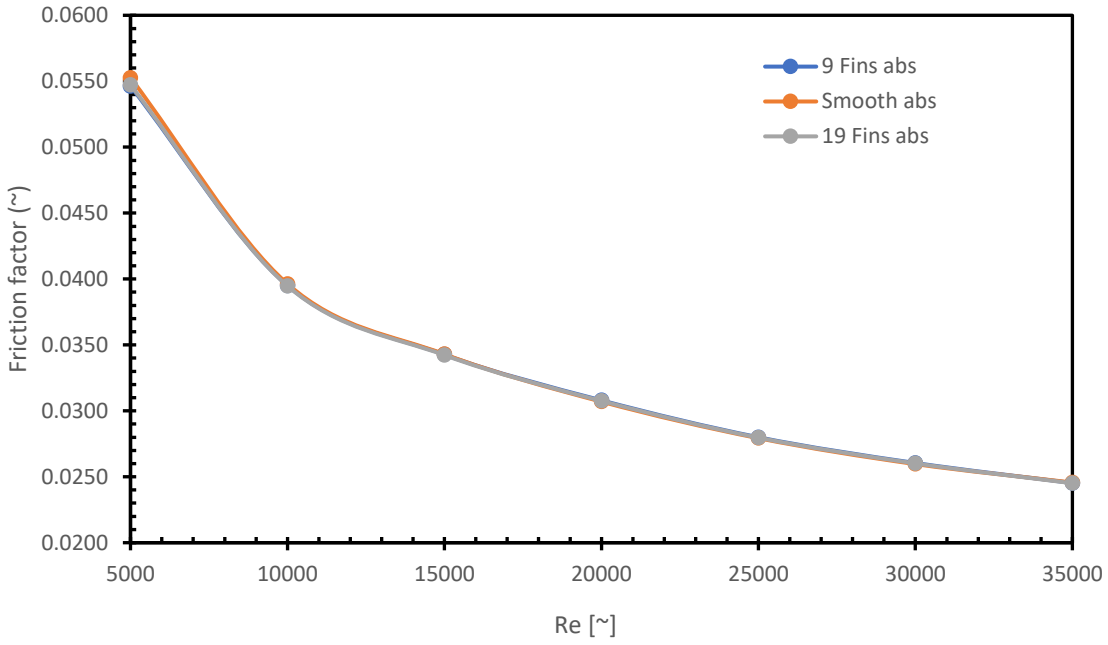

Fig. 5. 16: Impact of number of fins on the friction factor

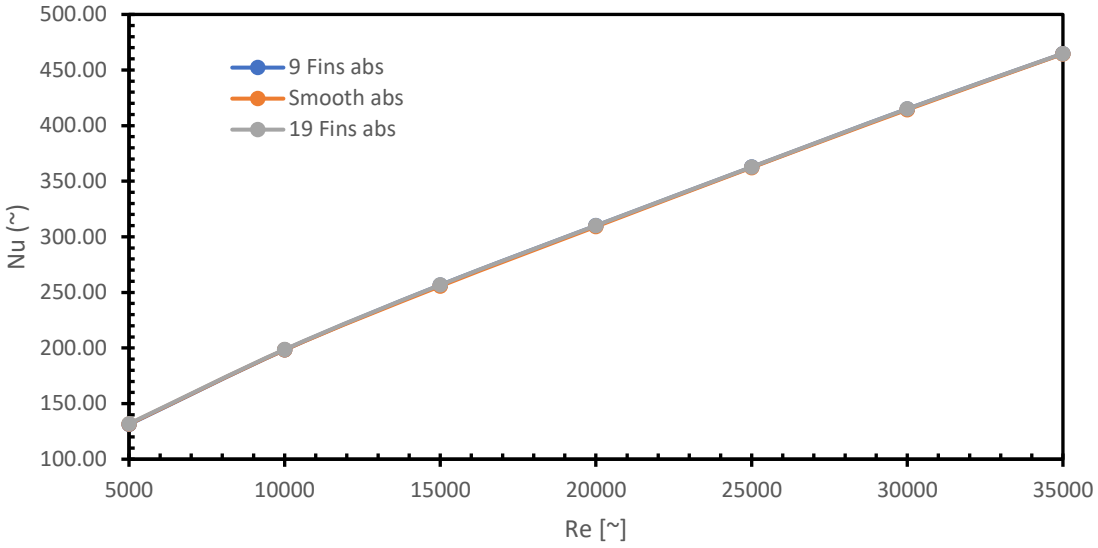

Fig. 5. 17:Influence of the number of fins on the Nusselt

The minimal variation in the Nusselt number and fluid friction is that the difference in temperature due to heat transfer fluid is not very significant. Therefore, the difference in the parameters is minimal.

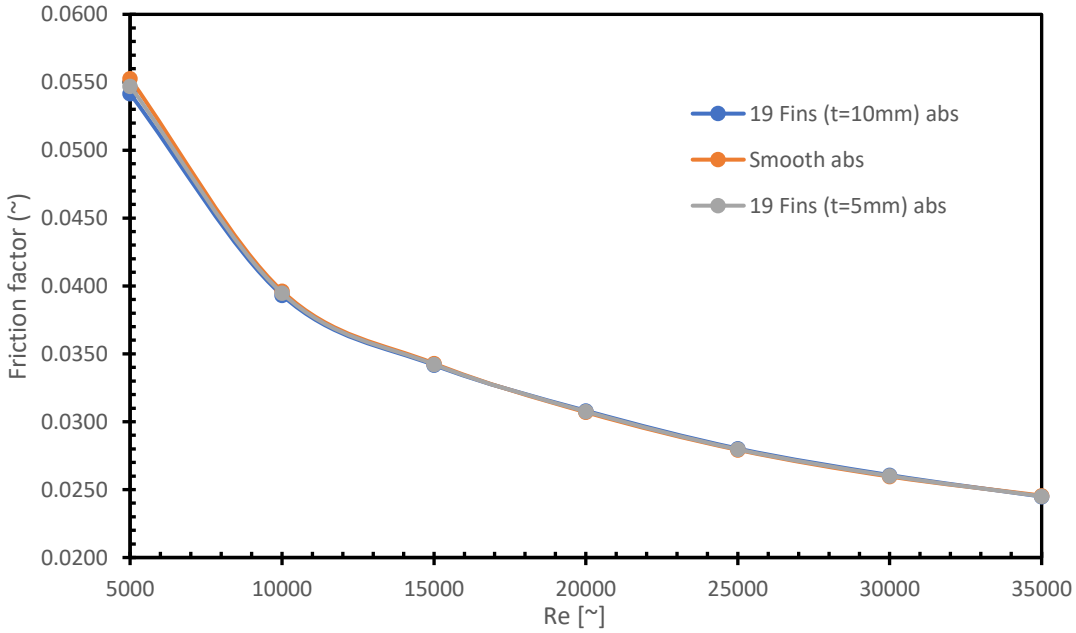

Fig. 5. 18: Influence of change of fin length on the friction factor

Changing the fin length at T_{in} = 350 K shows a similar trend. At lower Reynolds numbers, it is observed that the friction factor decreases with increase in the fin length. However, the increase in the turbulence as shown above makes the friction factor to

be indistinguishable. The indistinguishability of the friction factor at high Reynold number is that the viscosity tends to dissipate with increased turbulence and therefore making the friction factor near-zero relatively close.

5.7. Pumping Power and Pressure Drops

Pumping power and pressure drop interrelate and they are critically observed when designing a thermal system. They are mathematically related using eq. (2.21). As depicted in this equation and reflected in Fig. 5. 19 and Fig. 5. 20 , an increase in pressure drop demands higher pumping power. Since pumping power saps energy resources, it is necessary to minimize it. The minimization is achievable with trade-off of pressure.

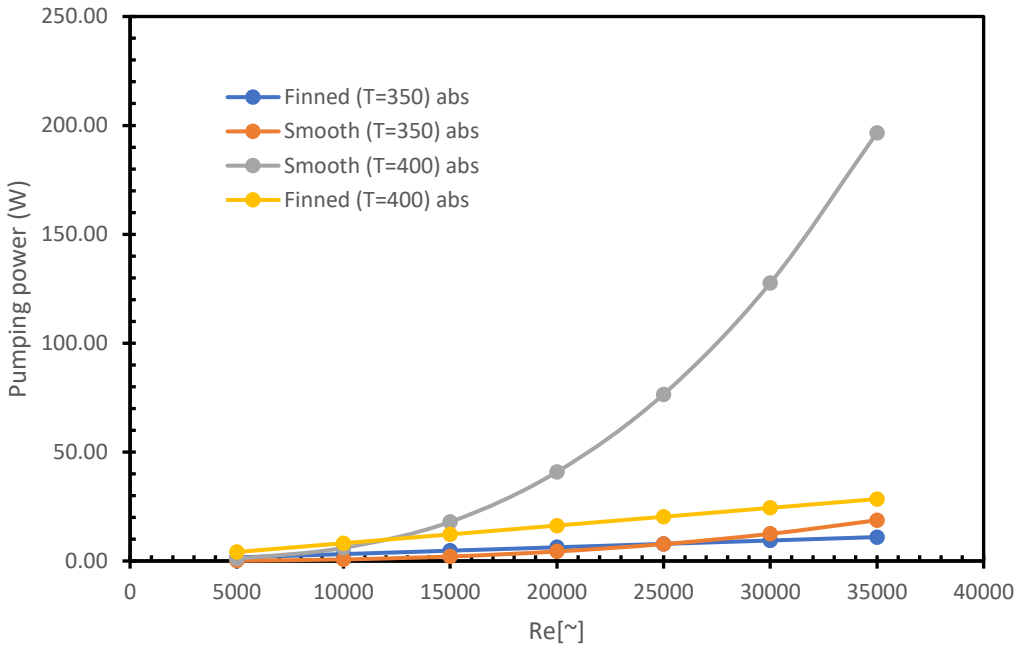

Fig. 5. 19:Variation of pumping power with inlet temperature

Fig. 5. 19 shows the increase in inlet temperature increases the pumping power. What's more, introducing fins reduces it. The reason for direct proportionality of the inlet temperature with pumping power is because the heat transfer fluid properties are dependent on temperature, and this consequently increases the pressure as shown in Fig. 5. 20

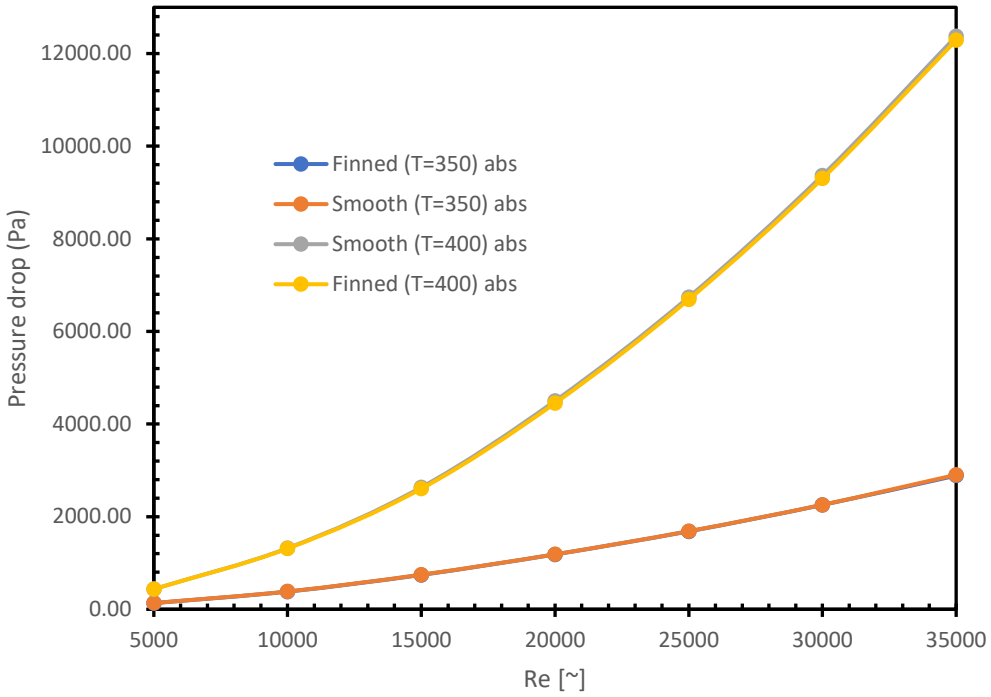

Fig. 5. 20: Variation of pressure with changing inlet temperature

Pressure drops and pumping power also increases with increase in Reynold number as shown above.

5.8. Summary and Conclusion

This chapter has examined some critical performance criteria based on the First Law of Thermodynamics. They include thermal efficiency, circumferential temperature gradient, thermal loss, thermal enhancement factor, Nusselt number, fluid friction, pressure drop and pumping power in varied Reynold numbers, inlet temperature, number of fins, and fin length.

The following conclusions were drawn:

- Both increase in the number of fins and fins length improve thermal efficiency. An increase of 2.26 % for T_{in} = 350 K, 2.21 % for T_{in} = 400 K and 2.22 % for T_{in} = 500 K and t = 5 mm was recorded. The increase is due to the increase in conductive heat transfer owing to increased surface area due to increased number of fins. Similar trend is observed with the efficiency in t = 10 mm being higher than the t = 5 mm with efficiencies lying in the range of 88 - 90.5 percent while unenhanced receiver falls in the range of 84 - 86 percent

- There is marginal increase in thermal enhancement factor, which implies the introduction of fins, and its variation is thermally favourable.
- It is observed the fins increase heat loss and this has adverse influence on thermal enhancement factor.
- Simultaneously increasing inlet temperature and Reynolds number increases thermal loss. This is because increased inlet temperature influences the HTF properties that contribute to thermal loss.
- Fins and their variations do not have significant influence on the Nusselt number and fluid friction. That is, the values of Nusselt number and friction factor of the enhanced and smooth absorber are relatively indistinguishable.
- Pumping power and pressure drop has been observed to be spiking with introduction of fins.

Chapter Six

Chapter 6: Performance Evaluation Based on the Second Law of Thermodynamics

6.1. Introduction

Despite effectiveness of the First Law of Thermodynamics in analysing the thermal performance of a system as far as energy conservation is concerned, it does not conclusively elaborate the dynamics of available useful work of the system. This demands utilization of the Second Law of Thermodynamics.

This section delves into the performance evaluation criteria based on the Second Law of Thermodynamics. The criteria have been divided into those that hinge on entropy generation and those dependent on the exergy of the system.

6.2. Entropy Generation Analysis

This sub-section examines entropy generation rate, entropy generation distribution along the length of the receiver, non-dimensional entropy generation number, and Bejan number as critical performance criteria of measuring entropy of the system. The results presented here are extracted from the simulation methodology discussed in *chapter five* of this work.

6.2.1. Entropy Generation Rate

Entropy generation influences the useful work of thermal system. This makes it a critical factor to consider when evaluating the system performance. The entropy generation rate is examined for the receiver (entire collector system).

The entropy generation rate for the entire collector system was determined by formulation derived from Gouy-Stodola Theorem as presented in Refs.([77], [78])

$$S_{gen} = \frac{Q_0}{T_0} + \frac{Q}{T_r} - \frac{Q^*}{T^*} \qquad (6.\ 1)$$

Where Q_o is heat loss, Q is energy gain by HTF, Q^* is Sun's heat discharge rate, T_0 is ambient temperature, T_r is average absorber temperature, T^* is adjusted Sun temperature.

Fig. 6. 1 shows the collector entropy generation rate for smooth receiver is greater than an enhanced one for all inlet temperatures for all considered Reynolds numbers. It also shows entropy generation rate steadily increases in range of 350 – 450 K inlet temperature for *Re* = 5000 and thereafter starts to decrease. The similar trend is observed for *Re* = 10000, but the increase of entropy generation rate is slow for lower inlet temperature and for *Re* = 20000 it tends to decrease from the onset with an increase in inlet temperature. The same graph also shows the entropy generation rate for higher Reynolds numbers is greater for lower inlet temperatures; while at higher inlet temperatures, the entropy generation rate for lower Reynolds numbers from 500-600 K inlet temperatures tends to be higher than the ones with higher Reynolds numbers.

Higher inlet temperatures tend to have lower entropy because higher inlet temperatures ensure high bulk temperature of the heat transfer fluid. At higher bulk temperatures, the entropy generation due to heat transfer is low because of their inverse proportionality. It is established that the entropy generation for *Re* = 5000 is reduced by 1.44 % across all inlet temperatures.

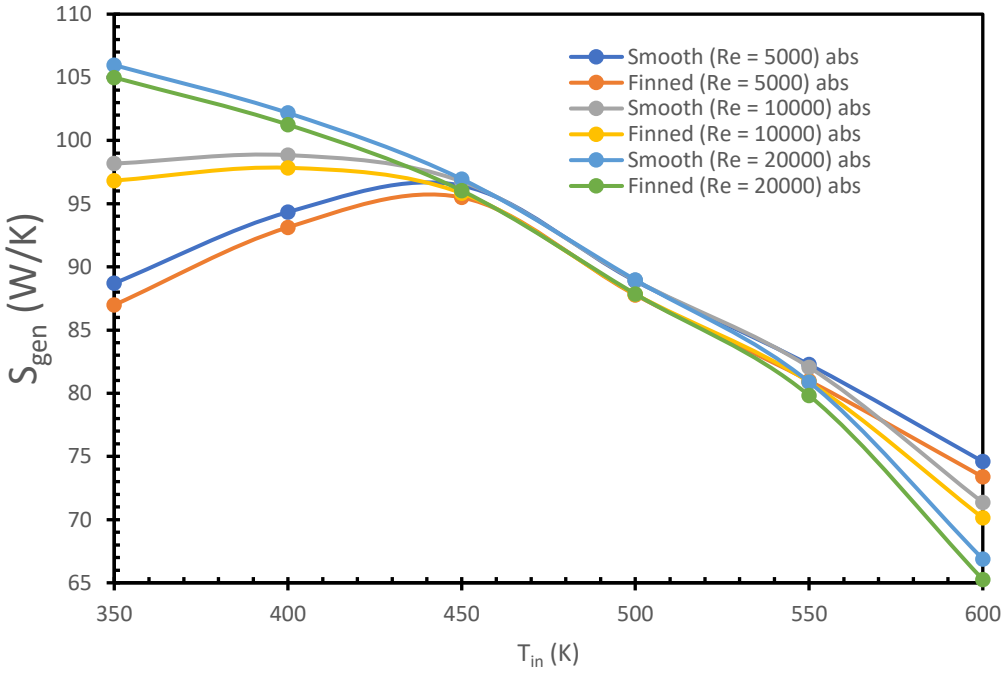

Fig. 6. 1: Collector entropy generation rate as function of inlet temperatures at Re = 5000, 10000, 20000 for smooth and finned absorber

To test the influence of fins on the collector's entropy generation rate, Reynolds number was varied for inlet temperature 350 K, 400 K and 500 K. As shown in Fig. 6. 2, the collector generation rate increases with increase in Reynolds number numbers for T_{in} = 350 K, 400 K with smooth absorber having higher entropy generation rate. For T_{in} = 500, no noticeable change is observed with increasing Reynolds number, but the smooth absorber tube similarly has higher entropy generation rate.

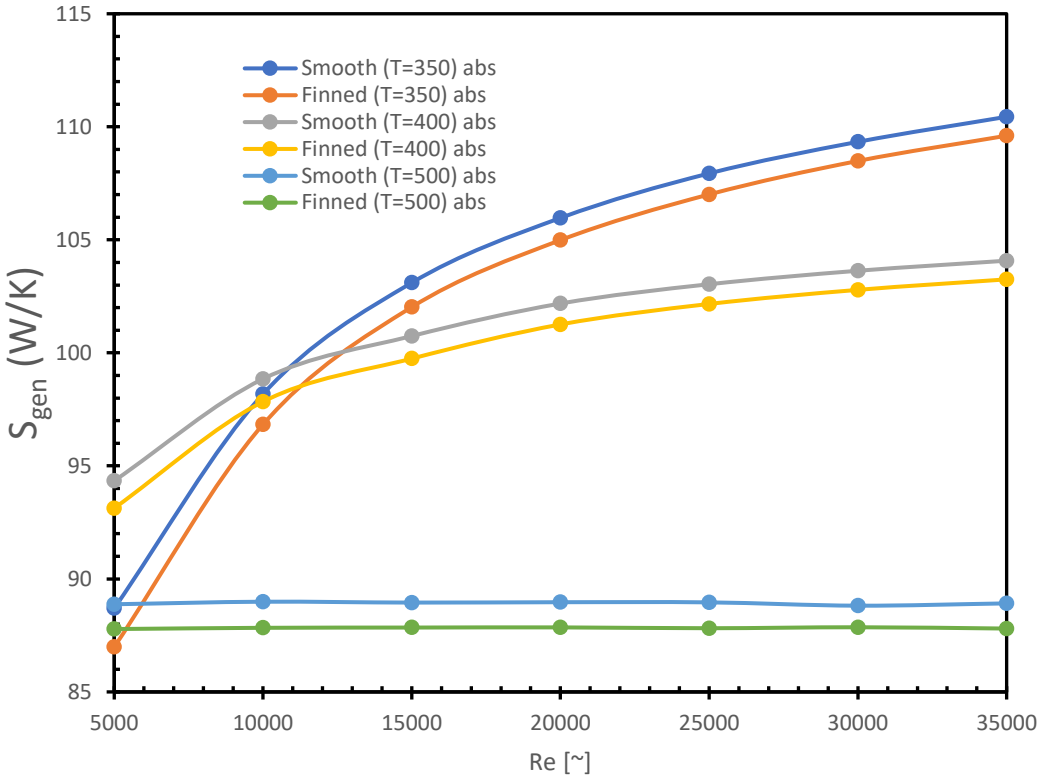

Fig. 6. 2: Collector entropy generation rate as function of Reynold number at T_{in} = 350 K, 400 K, 500 K for smooth and finned absorber

The entropy of the system increases with increasing turbulence for lower inlet temperature because as the Reynolds number increase, fluid thermal resistance relatively increases, and this generates entropy. As bulk temperatures increase, this resistance dissipate, and the entropy generation reduces and that is why the entropy generation rate for T_{in} = 500 K is comparatively low.

Changing fin length also has influence on the collector entropy generation rate. Increasing the fin length reduces the entropy generation rate as shown in Fig. 6. 3.

This is due to the increase in conductive heat transfer that elevates heat transfer rate, thus increasing useful energy.

To holistically determine the entropy generation behaviour of the receiver system a fin length was varied. As shown in Fig. 6. 3, the entropy generation rate decreases with increasing fin length. The smooth absorber tube has the highest entropy generation rate whereas the absorber tube with t = 10 mm has the lowest.

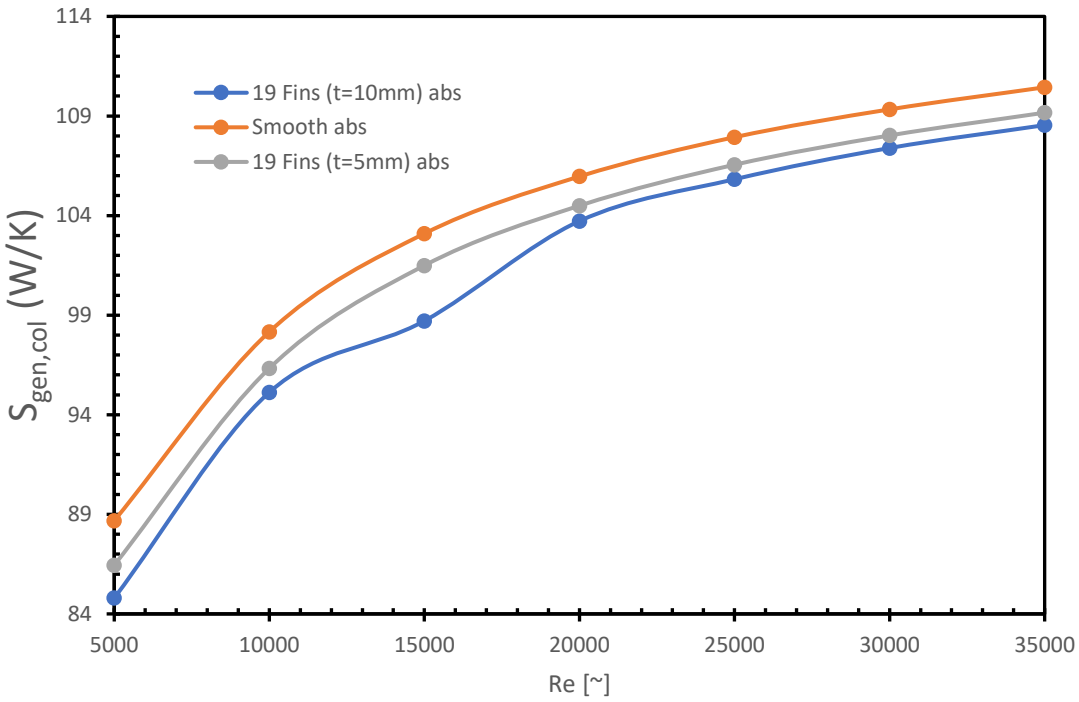

Fig. 6. 3: Collector entropy generation rate variation with different length of fins tested at T_{in} = 350 K

The trend is as discussed in this sub-section. Increasing the fin length augments the surface area that enables higher conductive heat transfer which consequently influence entropy generation as reflected by the presented results.

6.2.2. Entropy Variation Along the Length of the Receiver

In Fig. 6. 4, entropy distribution along the length of absorber tube as measure of heat transfer irreversibility is examined as a function of inlet temperature for *Re* = 5000, 10000, 20000 for smooth and enhanced geometry.

This local entropy generation in the absorber was computed using Adrian Bejan's formulation presented in Bejan [79].

$$S'_{gen} = \frac{q'^2}{\pi \lambda T_{bulk}^2 Nu} + \frac{32 \dot{m}^3 c_f}{\pi^2 \rho^2 T_{bulk} D^5} \quad (6.\ 2)$$

Where $c_f = \frac{\Delta P \rho D}{2G^2}$ and $G = \frac{4m}{\pi D}$

The first term of this formula represents the heat transfer irreversibility, and the second term represents fluid friction irreversibility.

As shown, the heat transfer irreversibility is dominant for lower inlet temperatures. The irreversibility gradually dissipates after T_{in} = 450 K, after which fluid friction irreversibility takes over. On the same graph, it is observed that the enhanced absorber tube exhibits higher heat transfer irreversibility compared to smooth one. It is also noted that as the turbulence increases, that is, as the Reynolds number increases, the entropy generation per unit length decreases.

The heat transfer irreversibility per unit length is pronounced in the enhanced absorber tube because of the high heat transfer to HTF because of the increased heat absorption due to increased surface area.

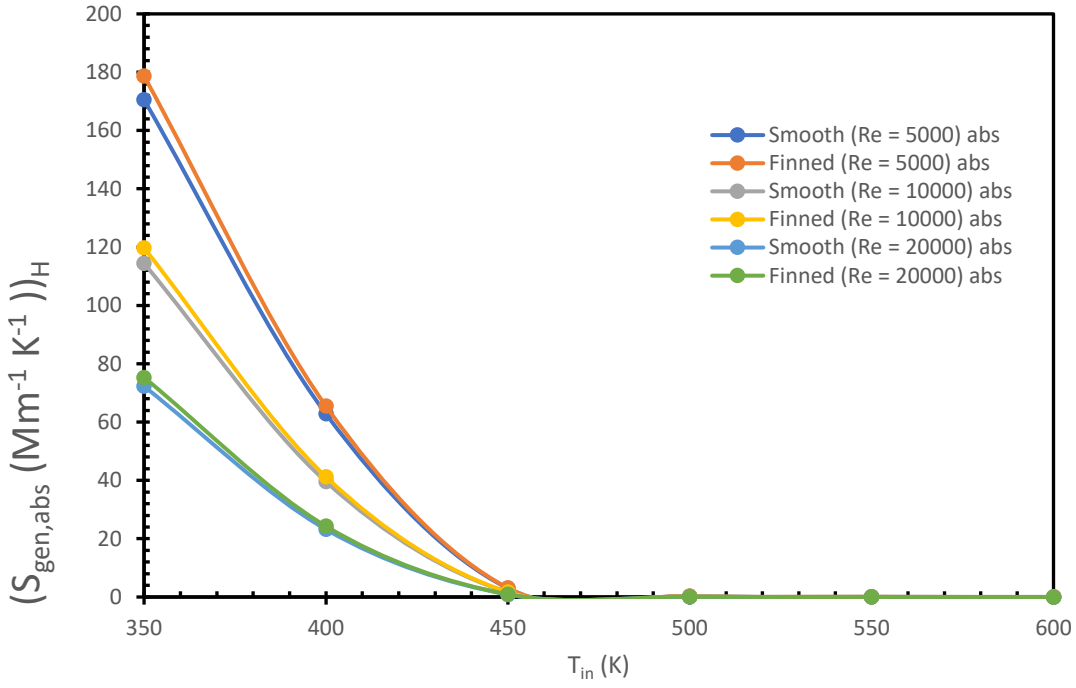

Fig. 6. 4: Heat transfer entropy distribution along length of absorber

Just as the entropy distribution along the absorber tube has been tested, the entropy generated along the length of the entire collector has equally been scrutinized. The

total entropy generated per unit length of collector has been tested by varying the Reynolds number at inlet temperatures 350 K, 400 K, 500 K.

As Fig. 6. 5 shows, the total entropy generation per unit length of the collector with enhanced absorber tube is lower than the one for with the smooth one. For T_{in} = 350 K, 400 K, the entropy generation per unit length increases with increase in Reynolds numbers. 500 K inlet temperature does not exhibit any noticeable change in the entropy generation per unit length—it remains constant.

The reason why there is no substantial change in entropy generation per unit length of the collector for higher inlet temperatures is that heat transfer rate is relatively low therefore both the heat transfer irreversibility and fluid flow irreversibility are equally low.

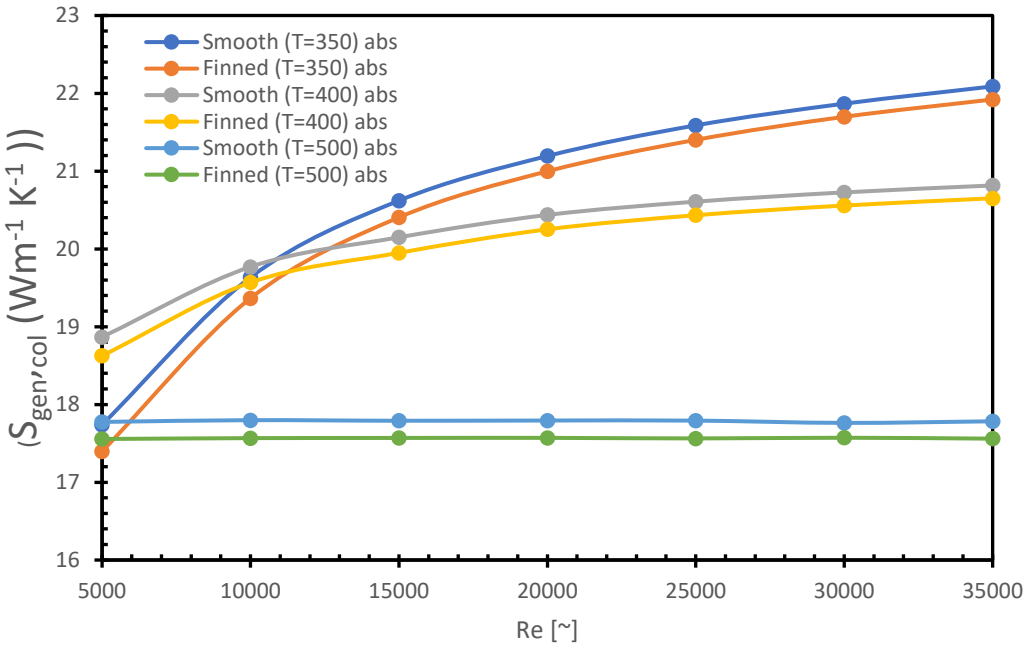

Fig. 6. 5: Total entropy distribution along the length of entire collector

With lower total entropy distribution along the length of enhanced collector, it implies that it is thermodynamically favourable as less exergy is destroyed. It therefore offers optimal available useful energy for the system.

6.2.3. Non-dimensional Entropy Generation Number

Non-dimensional entropy generation number is one of the holistic approaches to evaluate entropy generation. It evaluates entropy generation relative to inlet temperature and heat transfer rate. This offers quick glimpse of how entropy of the

system changes with change in heat transfer rate and inlet temperature of the fluid flow.

This entropy parameter is calculated according to this formulation.

$$N_s = \frac{S_{gen}}{q^{'} / T_{in}} \qquad 6.3$$

Following the similar test for entropy generation as discussed above, the entropy generation number is examined for an entire collector as function of Reynolds number and inlet temperature as shown in Fig. 6. 6 and Fig. 6. 7. As depicted in Fig. 6. 6, the trend for entropy generation number follows the similar trend with the entropy generation discussed in *sub-section 6.2.2*. The entropy numbers increase with increasing turbulence for lower inlet temperatures whereas it turns to be constant for all Reynolds numbers for T_{in} = 500 K. Notably, the entropy generation numbers for enhanced collector are lower than unenhanced one just as observed in the entropy parameters discussed.

This exhibition of lower entropy numbers in enhanced collector implies the enhancement improve thermodynamic performance of the collector, therefore it is thermodynamically sensible to introduce external fins to for thermodynamic enhancement.

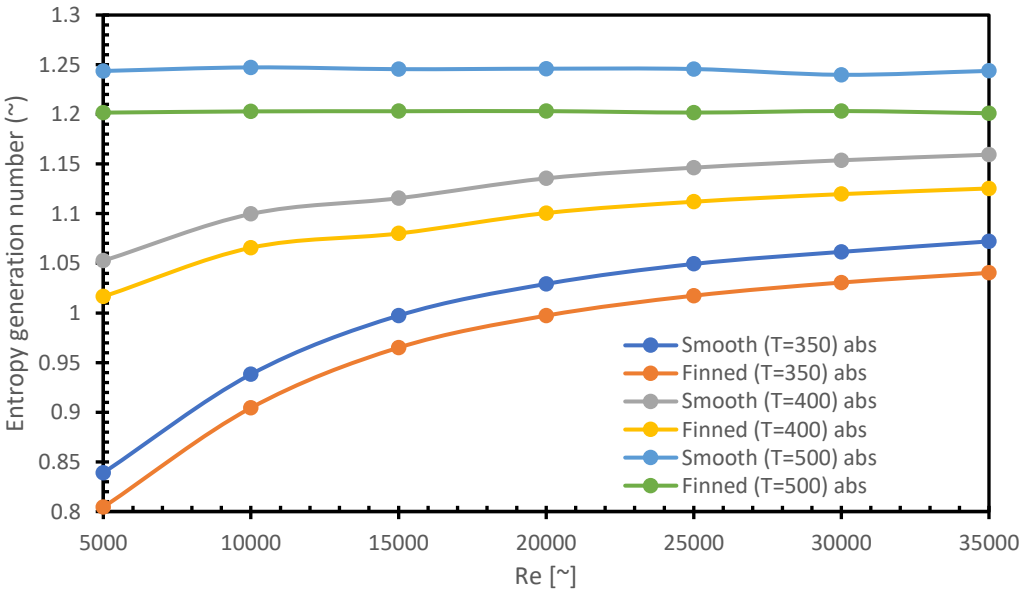

Fig. 6. 6: Non-dimensional entropy generation number as function of Reynolds number for entire collector

For lower inlet temperatures and lower Reynolds number, the entropy generation numbers are low as shown in Fig. 6. 7. This low entropy generation shows that more exergy is conserved therefore the thermodynamic performance of the system is appreciable.

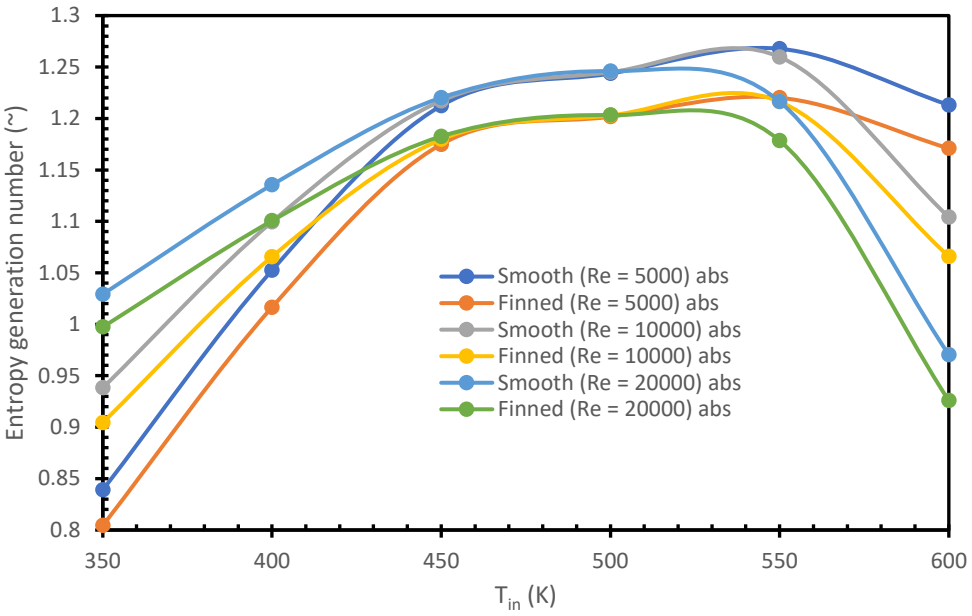

Fig. 6. 7: Non-dimensional entropy generation number as function of inlet temperature for entire collector

It is sensible to examine the parametric response to the change in fin length for both absorber as well as the collector.

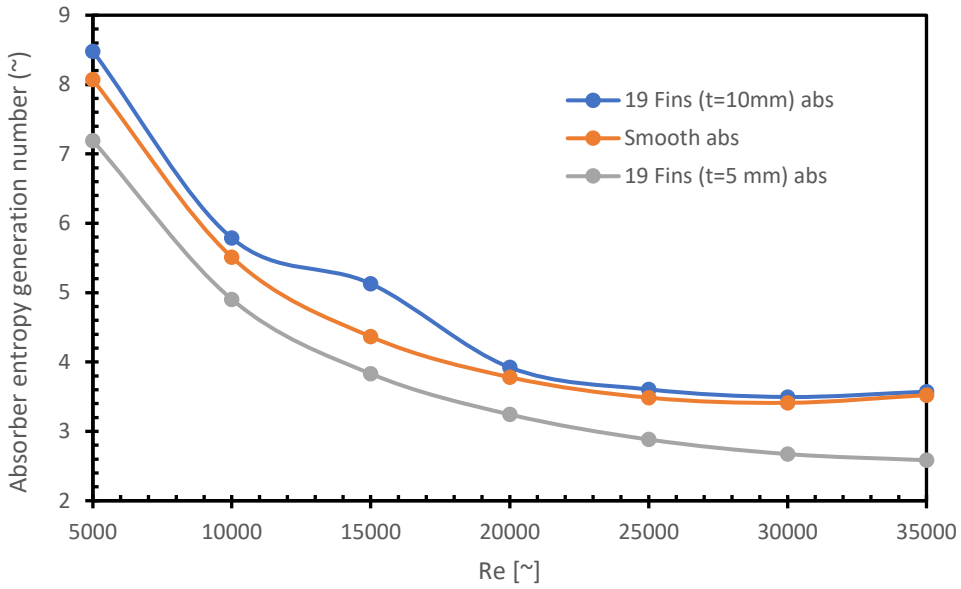

Fig. 6. 8: Non-dimensional entropy generation number as function of Reynolds number for absorber for double fin length for an absorber tested at T_{in} = 350 K

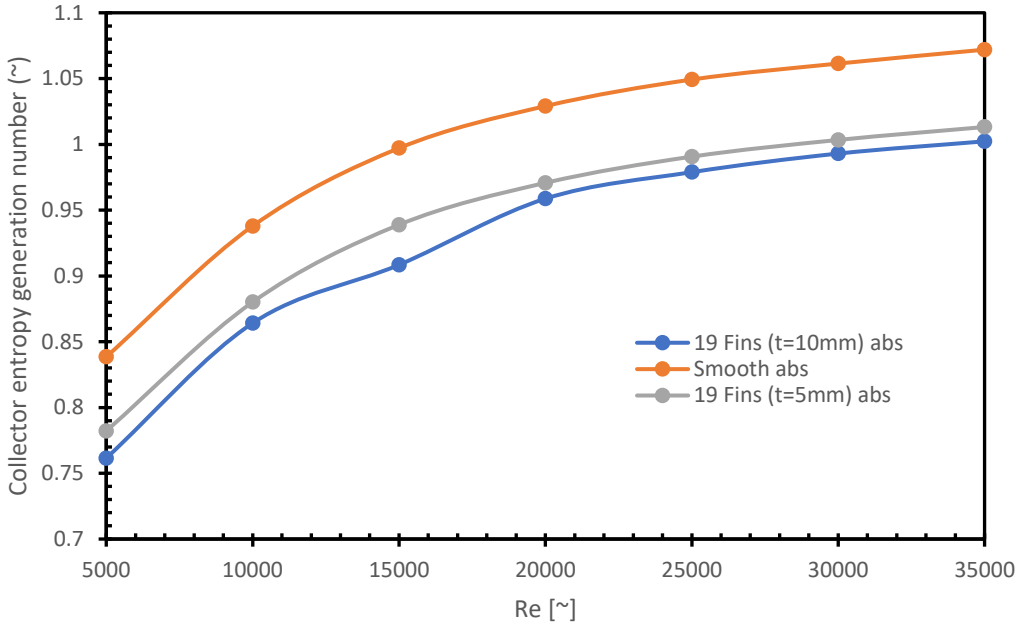

Fig. 6. 9: Non-dimensional entropy generation number as function of Reynolds number for double fin length for entire collector tested at T_{in} = 350 K

The results show the opposite behaviour of the entropy generation as function of Reynolds number for both absorber and the entire collector system as presented in Fig. 6. 8 and Fig. 6. 9. Just as conventional entropy generation rate exhibits, the non-dimensional entropy generation number of absorber decreases with increase in

turbulence. However, the entire collector's entropy generation number tells different story. This trend is due to the dominant influence of heat transfer rate in the collectors.

6.2.4. Bejan Number

Heat transfer irreversibility and fluid friction irreversibility are critical determinants of the performance of thermal systems and need examinations. To determine the dominance of these factors a Bejan number proves to be the most convenient parameter to visualize them. It is a ratio of heat transfer irreversibility to total entropy generation rate. This dimensionless number is presented by Adrian Bejan [77]

$$Be = \frac{(S_{gen})_H}{S_{gen}} \tag{6. 4}$$

As observed in Fig. 6. 10 and Fig. 6. 11, the heat transfer irreversibility is dominant at the lower Reynolds numbers and starts to dissipate at the higher turbulence as fluid friction irreversibility takes over.

From the same figures, it is also observed that both increase in number of fins and fin length reduces the heat transfer irreversibility which consequently minimises the entropy generation—a phenomenon which is thermodynamically favourable to the system.

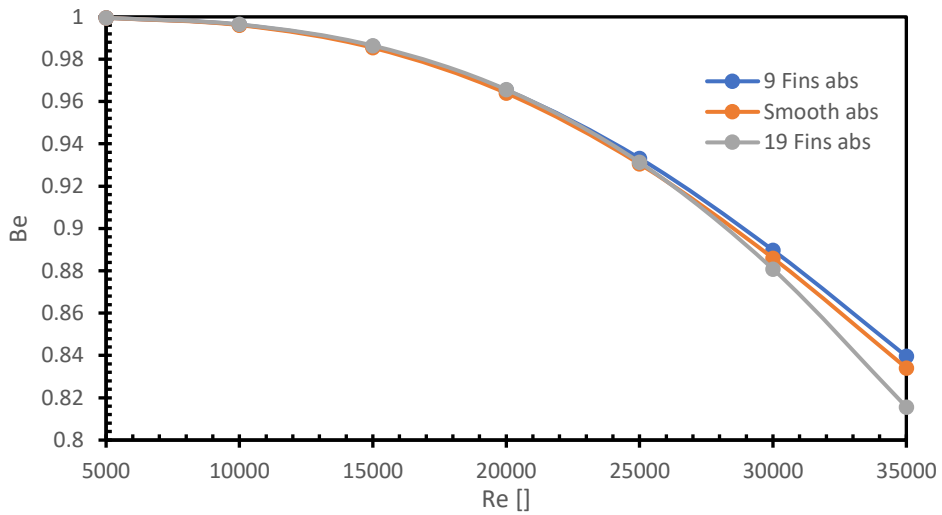

Fig. 6. 10: Bejan number as function of Reynold number for varied number of fins

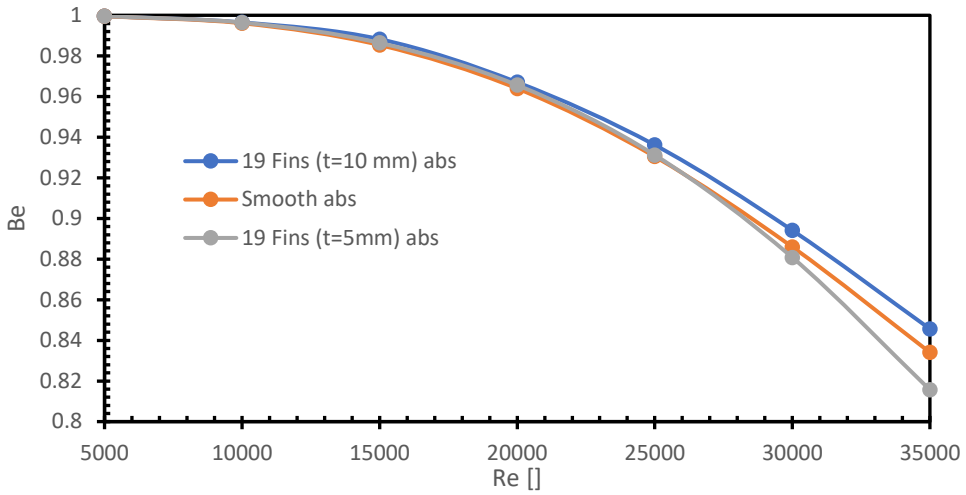

Fig. 6. 11: Bejan number as function of Reynold number for varied fin length

The degree at which the enhancement techniques achieve it varies. As shown Fig. 6. 11, the entropy generation minimization is more prominent in increasing fin length than varying fins numbers, which proves the thermodynamic favourability of increasing the fin length as mean of performance enhancement.

6.3. Exergy Analysis

Exergy quantifies the available useful work of a system. Since system as the one being studied here aims at maximizing the energy available to do work to generate electricity, exergy presents itself as potent tool to precisely determine its thermodynamic performance.

This subsection examines the global exergy efficiency of entire collector and the absorber, and the exergy destruction rate of both considering the applied enhancements. Like the discussion in the entropy generation, the results reported and discussed here are from the solution methodology presented in *chapter five* of this work.

6.3.1. Exergy Efficiency

Exergy efficiency captures the quality of the energy dynamics in the system. This makes it a useful tool in measuring the energy performance of a thermal system.

Like other performance criteria examined in this work, the global exergy efficiency of the entire collector has been examined. As depicted in Fig. 6. 12, the exergy efficiency is greater in the enhanced receiver compared to smooth one. It is also shown that the

exergy efficiency in lower inlet temperatures (350 K, 400 K) decreases with increase in Reynolds number whereas the one at inlet temperature 500 K has rather constant exergy. The exergy at 500 K inlet temperature is found to be larger than the rest.

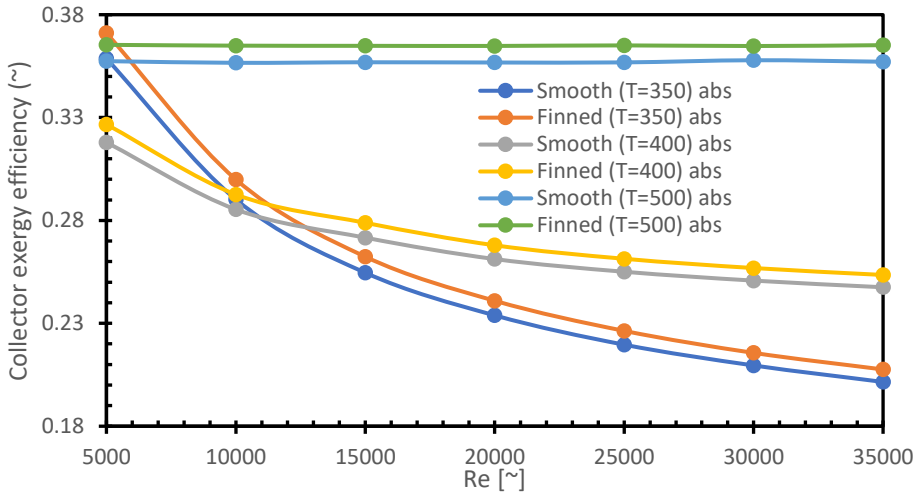

Fig. 6. 12: Collector exergy efficiency as function of Reynold numbers for various inlet temperature (350 K, 400 K, 500 K) for smooth and enhanced absorber

The decrease in exergy with increasing turbulence is because the flow rate at that point is too high that the energy loses its quality as the convective heat transfer is affected.

Fig. 6. 13 on the other hand shows the behaviour of the exergy as function of inlet temperature. It shows the exergy efficiency of 350 K inlet temperature and 5000 Reynolds number gradually decreases up to 450 K inlet temperature after which it starts to exponentially increase. It is also noted enhancement increases the exergy efficiency by 2.44 % for 5000 Reynold numbers, 2.30 % for *Re* = 10000, and 2.30 % for *Re* = 20000. It is also noted that exergy of the lower Reynolds number at lower inlet temperatures (350 -450 K) is higher than the one of higher Reynolds numbers. But at higher inlet temperatures (500-600 K) the exergy of the higher turbulence is observed to be higher than the lower turbulence.

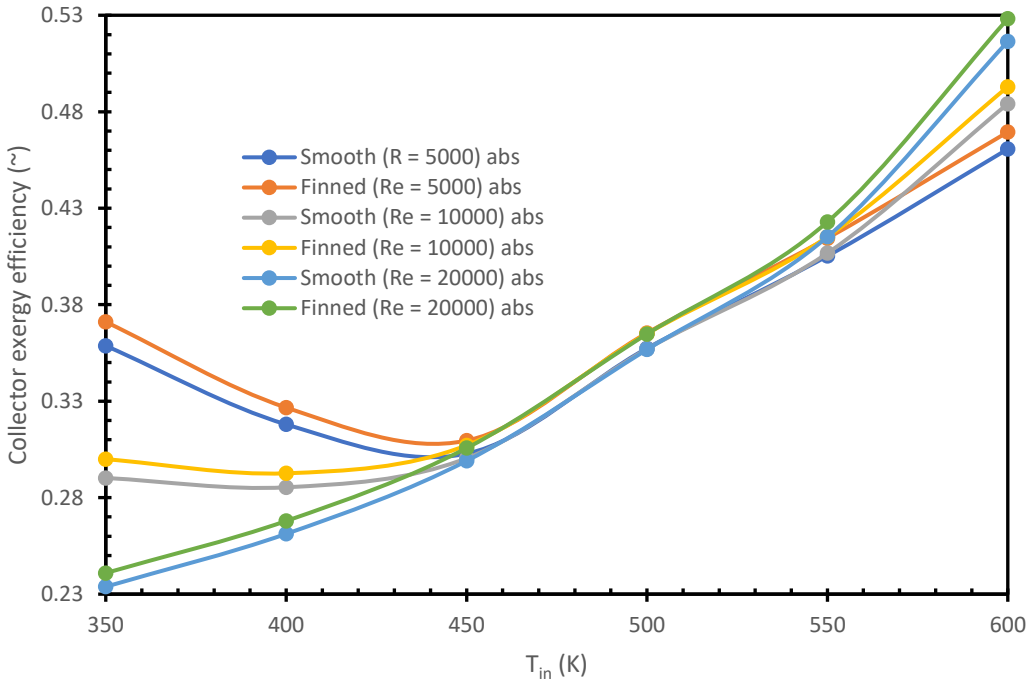

Fig. 6. 13: Collector exergy efficiency as function of inlet temperatures for various Reynold numbers (Re = 5000, 10000, 20000) for smooth and enhanced absorber

As inlet temperatures reaches 500 K, the energy transfer for the higher turbulence increases significantly because there is little energy loss through thermal radiation because of low temperature gradient between the interacting surfaces. This significantly improves the quality of the energy transferred to HTF thus higher exergy efficiency.

A test for the behaviour of exergy has been examined for exergy in the absorber tube. As shown in Fig. 6. 14, the trend is like global collector exergy efficiency presented in Fig. 6. 13. The difference however is that the exergy in this case is a slightly larger than for the entire collector.

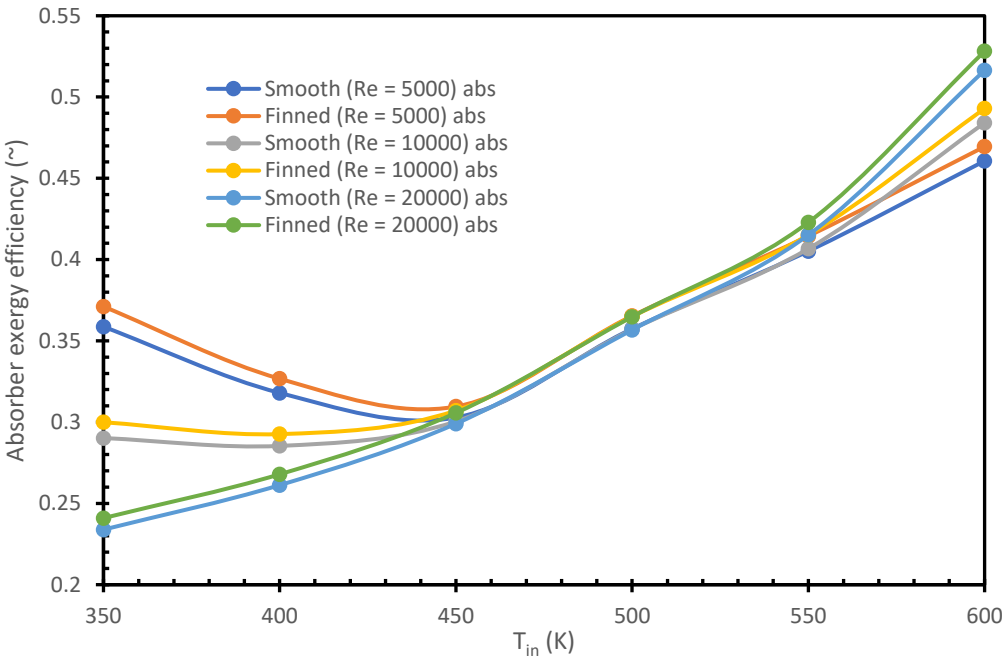

Fig. 6. 14: Absorber exergy efficiency as function of inlet temperatures for various Reynolds numbers (Re = 5000, 10000, 20000) for smooth and enhanced absorber

The reasons for that appreciable absorber exergy are because of less losses compared to collector's. For entire collector an optical loss occurs that contribute to exergy degradation, unlike in absorber that do not have that phenomenon.

Testing the influence of the varying fin length for both collector and absorber tube, the trend obtained is presented in Fig. 6. 15 and Fig. 6. 16. They show that increase in fin length improves the exergy of both the entire collector and the absorber. This is because the improved conductive heat transfer avails more useful energy that positively feeds into the exergy of the system.

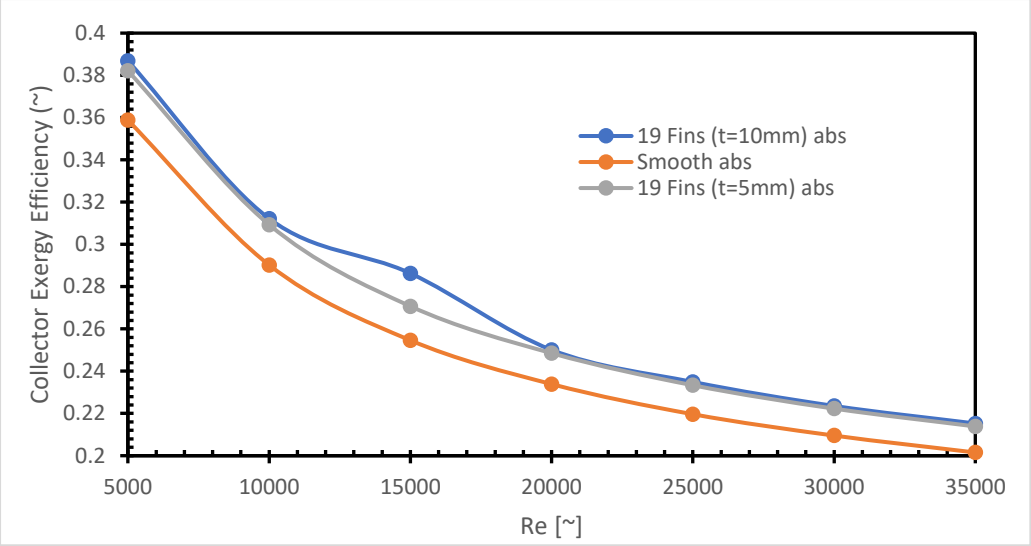

Fig. 6. 15: Influence of fins length on the exergy efficiency of the entire collector

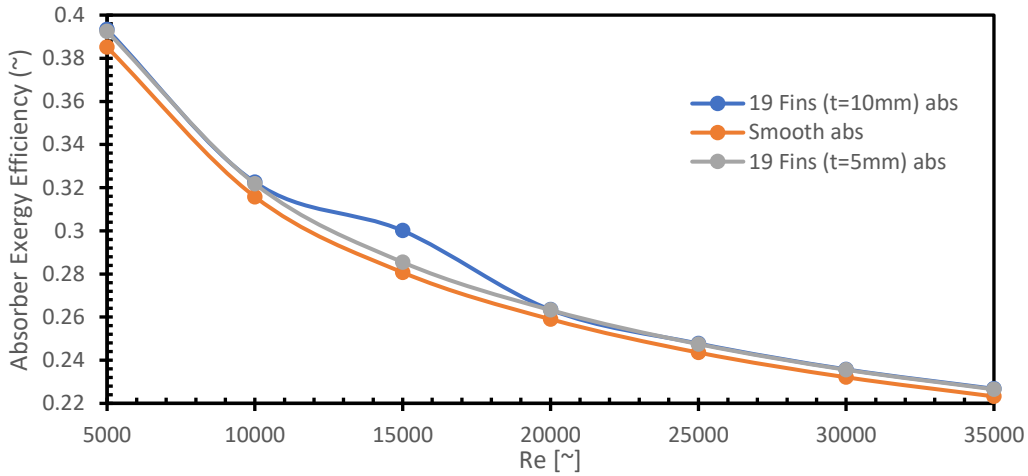

Fig. 6. 16: Influence of fiins length on the exergetic efficiency of the absorber tube

6.3.2. Exergy Destruction

Other criteria that determine the performance of the system is exergy destruction. This quantifies the exergy degradation in the system and thus influences the exergy efficiency discussed in the *subs-section 6.3.1*. As shown in Fig. 6. 17 and Fig. 6. 18, the destroyed exergy shows the opposite trend with the exergy efficiency. This makes sense because the greater the destroyed exergy, the lower the exergy efficiency of the system.

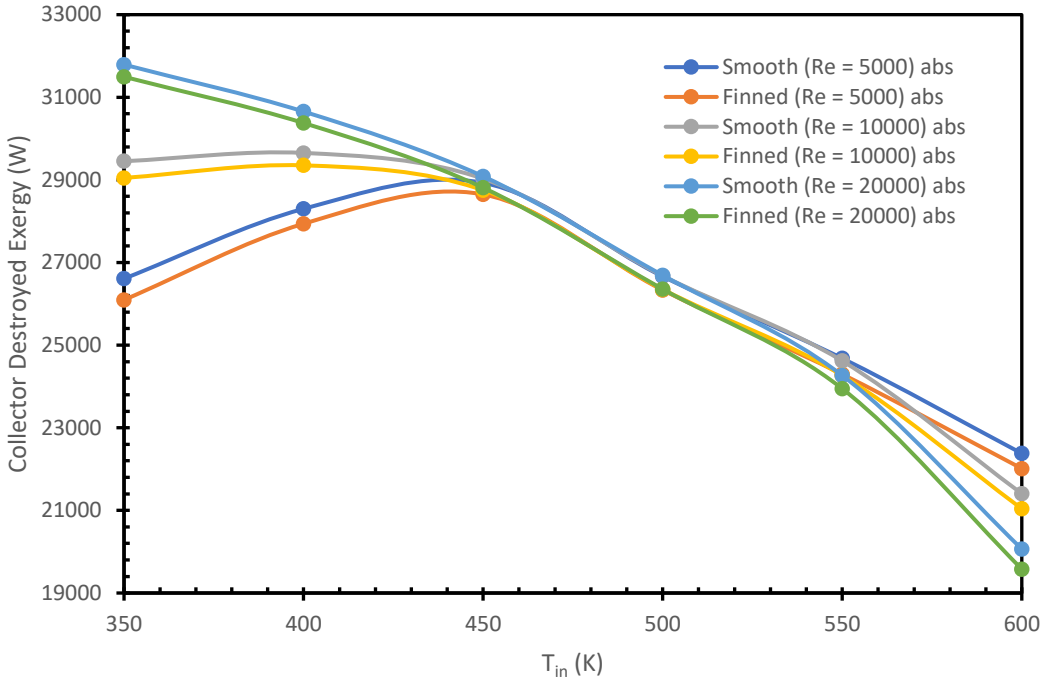

Fig. 6. 17: Collector exergy destruction as function of inlet temperature

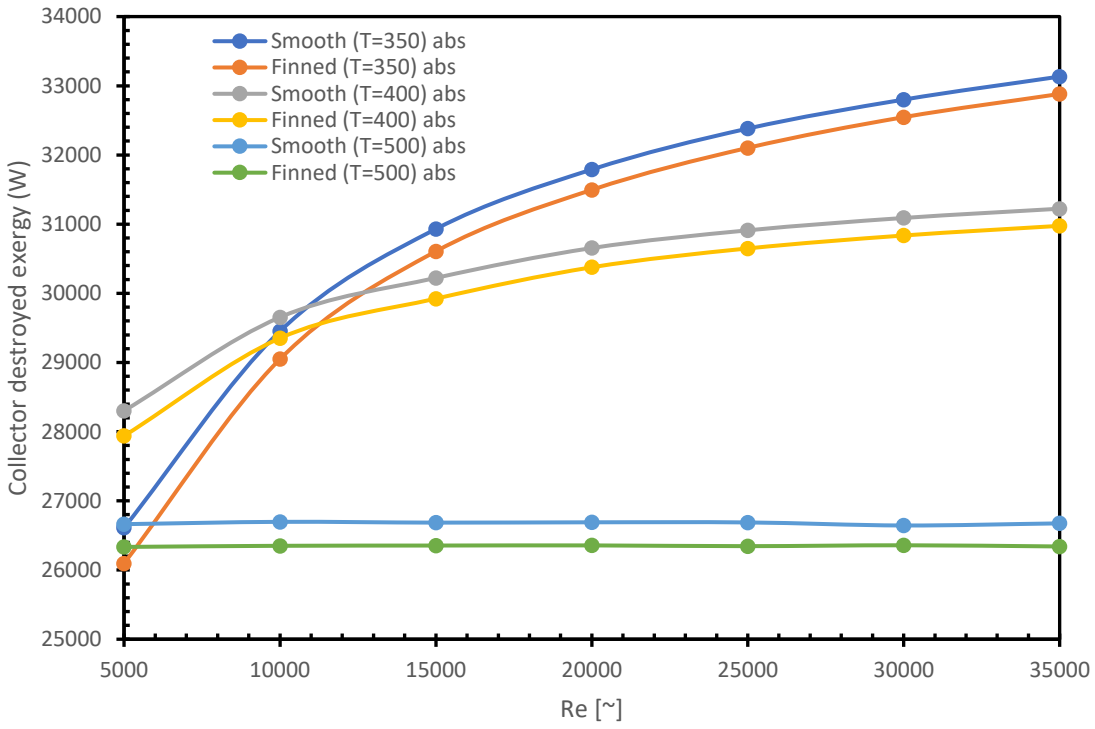

Fig. 6. 18: Exergy destruction as function of Reynold numbers

It is observed in both graphs above that unenhanced collector has higher destroyed exergy. This is because the unenhanced collector at lower inlet temperatures and

lower turbulence tend to generate high heat transfer irreversibility. It contributes to the destruction of the system exergy.

6.4. Summary and Conclusion

Entropy and exergy are critical factors in the thermal system design and analysis as they depict the available useful energy and its quality respectively. Therefore, this chapter has been devoted to examining performance criteria based on these factors. The PECs examined include entropy generation rate, entropy distribution along the length of absorber and collector, Bejan number, exergy efficiency, and exergy destruction rate.

The following critical conclusions were drawn from the entropy and exergy analysis:

- Enhancement by external fins minimizes the entropy generation. An entropy generation reduction of 1.44 % has been established for *Re* = 5000 across all inlet temperatures.
- Exergy is favored by the modification. It is also noted enhancement increase the exergy efficiency by 2.44 % for 5000 Reynold numbers, 2.30 % for *Re* = 10000, and 2.30 % for *Re* = 20000. It is also noted that exergy of the lower Reynolds number at lower inlet temperatures (350-450 K) is higher than the one of higher Reynolds numbers. But at higher inlet temperatures (500-600 K) the exergy of the higher turbulence is observed to be higher than the lower turbulence.

Chapter Seven

Chapter 7: Summary, Conclusions, and Recommendations

7.1. Summary

This work started with statements of the motivation of the study, which has been provided as the need to design a receiver system with an improved performance. The need for optimizing the performance of the receiver system is to enable the design of a stand-alone reliable parabolic trough collector power plants. It is necessary for a shift to renewable energy which will preempt the looming existential threats of climate change.

To identify the gap in literature, relevant studies have been studied. From the literature, it was established that much of the works are on enhancing performance by inserts or through passive introductions of internal fins to augment convective heat transfer. Other focus has been placed on manipulating the geometrical parameters of the collectors such concentration ratio, aperture area, and rim angle. Little has been done on the external modification of the tubular receiver. This was found to be the gap that needs to be bridged. The work was niched on introducing novel annular external fins to improve conductive heat transfer.

For that objective to be achieved, fluid flow and thermal models were developed and with simplifying assumptions was implemented in commercial ANSYS Fluent software. The simulations were carried out in Reynolds numbers range of 5000-35000 and inlet temperatures of 350-600 K with varying number of fins and fin length.

The analysis of the results was subjected to performance evaluation criteria based on both the First and Second Laws of Thermodynamics. The considered PECs based on the First Law include thermal efficiency, thermal enhancement factor, thermal loss, and circumferential temperature gradient. On the other hand, the Second Law's PECs are based on entropy and exergy. They include entropy generation rate, entropy

distribution along the length of absorber and collector, non-dimensional entropy number, Bejan number, exergy efficiency, and exergy destruction rate.

Some of the critical observations and conclusions are elaborated in *sub-section 7.2* of this work.

7.2. Conclusions

This study set out to investigate the influence of the external annular fins on the thermal and thermodynamic performance of the receiver by conducting numerical simulations.

The results were analysed on the performance criteria based on the First and Second Law of Thermodynamics. Following conclusions were generated from the analysis.

- Introduction of fins increases thermal efficiency of the receiver. An increase of 2.26 % for T_{in} = 350 K, 2.21 % for T_{in} = 400 K and 2.22 % for T_{in} = 500 K was recorded for varying Reynolds numbers. Similar trend is observed with doubling of the fin length. The efficiency in t = 10 mm is higher than t = 5 mm with values in the range of 88 - 90.5 % while unenhanced receiver falls in the range of 84 - 86 %
- Thermal enhancement factor with the variation of the fin length and Reynolds numbers appreciably increases. The result of 400 K inlet temperature shows an average thermal enhancement factor at 1.0036 which reflects 0.36 % thermal enhancement.
- Variation of annular fins increase the exergy efficiency. It is observed that enhancement increase the exergy efficiency by 2.44 % for *Re*= 5000, 2.30 % for *Re* = 10000, and 2.30 % for *Re* = 20000. It is also noted that exergy of the lower Reynolds numbers at lower inlet temperatures (350-450 K) is higher than the one of higher Reynolds numbers.
- Entropy generation rate and entropy generation numbers responded favourably with the enhancement. The entropy generation rate decreases with increasing fin length. The smooth absorber tube has the highest entropy generation rate whereas the absorber tube with t = 10 mm has the lowest.
- Heat transfer irreversibility has been found to be dominant at lower turbulence and variation of annular fin length and numbers reduces it.

Since the aim of designing thermal system is to minimize entropy while improving other thermal and thermodynamic performances, the observations outlined prove the favourable influence of the external fins on the thermal and thermodynamic performance of the receiver.

7.3. Recommendations for Future Study

The thermal model developed in this was a simplified one. Some of the simplifying assumptions made here can be improved in the future work to see how they will influence performance. For future work, it is recommended that:

- Heat flux can be modeled using Monte Carlo Ray Tracing and couple with the model using UDF, instead of using uniform heat flux as done in this work.
- The shape of annular fin can be changed to elongated prism and studied how it influences the performance criteria tested here.
- Convective loss due to wind and radiative loss on the exterior of the glass cover can be included in the model.
- The external annular fins can be combined with inserts and internal fins to model the receiver's performance.
- Optimization of different parameters of the receiver can be done to determine optimal design of the system.
- Special coatings can be applied to the absorber to augment its optical performance.

References

[1] Y. Wang, Q. Liu, J. Lei, and H. Jin, “Performance analysis of a parabolic trough solar collector with non-uniform solar flux conditions,” *Int. J. Heat Mass Transf.*, vol. 82, pp. 236–249, 2015, doi: 10.1016/j.ijheatmasstransfer.2014.11.055.

[2] J. G. Backes, A. D’Amico, N. Pauliks, S. Guarino, M. Traverso, and V. Lo Brano, “Life Cycle Sustainability Assessment of a dish-Stirling Concentrating Solar Power Plant in the Mediterranean area,” *Sustain. Energy Technol. Assessments*, vol. 47, no. February, 2021, doi: 10.1016/j.seta.2021.101444.

[3] E. Casati, F. Casella, and P. Colonna, “Design of CSP plants with optimally operated thermal storage,” *Sol. Energy*, vol. 116, pp. 371–387, 2015, doi: 10.1016/j.solener.2015.03.048.

[4] A. Mwesigye, İ. H. Yılmaz, and J. P. Meyer, “Numerical analysis of the thermal and thermodynamic performance of a parabolic trough solar collector using SWCNTs-Therminol®VP-1 nanofluid,” *Renew. Energy*, vol. 119, pp. 844–862, 2018, doi: 10.1016/j.renene.2017.10.047.

[5] A. Bruch, J. F. Fourmigué, and R. Couturier, “Experimental and numerical investigation of a pilot-scale thermal oil packed bed thermal storage system for CSP power plant,” *Sol. Energy*, vol. 105, pp. 116–125, 2014, doi: 10.1016/j.solener.2014.03.019.

[6] M. M. Aboelmaaref *et al.*, “Hybrid solar desalination systems driven by parabolic trough and parabolic dish CSP technologies: Technology categorization, thermodynamic performance and economical assessment,” *Energy Convers. Manag.*, vol. 220, no. June, p. 113103, 2020, doi: 10.1016/j.enconman.2020.113103.

[7] R. Naveenkumar *et al.*, “Comprehensive review on various parameters that influence the performance of parabolic trough collector,” *Environ. Sci. Pollut. Res.*, vol. 28, no. 18, pp. 22310–22333, 2021, doi: 10.1007/s11356-021-13439-y.

[8] O. A. Jaramillo, M. Borunda, K. M. Velazquez-Lucho, and M. Robles,

"Parabolic trough solar collector for low enthalpy processes: An analysis of the efficiency enhancement by using twisted tape inserts," *Renew. Energy*, vol. 93, pp. 125–141, 2016, doi: 10.1016/j.renene.2016.02.046.

[9] A. Mwesigye, T. Bello-Ochende, and J. P. Meyer, "Heat transfer and entropy generation in a parabolic trough receiver with wall-detached twisted tape inserts," *Int. J. Therm. Sci.*, vol. 99, pp. 238–257, 2016, doi: 10.1016/j.ijthermalsci.2015.08.015.

[10] B. Vahedi, E. Golab, A. Nasiri Sadr, and K. Vafai, "Thermal, thermodynamic and exergoeconomic investigation of a parabolic trough collector utilizing nanofluids," *Appl. Therm. Eng.*, vol. 206, no. October 2021, p. 118117, 2022, doi: 10.1016/j.applthermaleng.2022.118117.

[11] F. Dinter and D. M. Gonzalez, "Operability, reliability and economic benefits of CSP with thermal energy storage: First year of operation of ANDASOL 3," *Energy Procedia*, vol. 49, pp. 2472–2481, 2014, doi: 10.1016/j.egypro.2014.03.262.

[12] I. Bendato, L. Cassettari, M. Mosca, and R. Mosca, "Stochastic techno-economic assessment based on Monte Carlo simulation and the Response Surface Methodology: The case of an innovative linear Fresnel CSP (concentrated solar power) system," *Energy*, vol. 101, pp. 309–324, 2016, doi: 10.1016/j.energy.2016.02.048.

[13] A. Mwesigye and İ. H. Yılmaz, "Thermal and thermodynamic benchmarking of liquid heat transfer fluids in a high concentration ratio parabolic trough solar collector system," *J. Mol. Liq.*, vol. 319, 2020, doi: 10.1016/j.molliq.2020.114151.

[14] J. Coventry and C. Andraka, "Dish systems for CSP," *Sol. Energy*, vol. 152, pp. 140–170, 2017, doi: 10.1016/j.solener.2017.02.056.

[15] J. Subramani, P. K. Nagarajan, C. Subramaniyan, and N. Anbuselvan, "Performance studies on solar parabolic dish collector using conical cavity receiver for community heating applications," *Mater. Today Proc.*, vol. 45, pp. 1862–1866, 2021, doi: 10.1016/j.matpr.2020.09.062.

[16] A. Msaddak, E. Sediki, and M. Ben Salah, “Assessment of thermal heat loss from solar cavity receiver with Lattice Boltzmann method,” *Sol. Energy*, vol. 173, no. August, pp. 1115–1125, 2018, doi: 10.1016/j.solener.2018.08.059.

[17] S. Wang, C. A. Asselineau, Y. Wang, J. Pye, and J. Coventry, “Performance enhancement of cavity receivers with spillage skirts and secondary reflectors in concentrated solar dish and tower systems,” *Sol. Energy*, vol. 208, no. May, pp. 708–727, 2020, doi: 10.1016/j.solener.2020.08.008.

[18] S. Benmarraze, D. Itskhokine, M. Benmarraze, E. Alasis, M. Tawalbeh, and W. Shahin, “Status of implementation of the first Linear Fresnel solar thermal power plant in the Middle East - WECSP solar project in the Kingdom of Jordan,” *Energy Procedia*, vol. 69, pp. 1586–1596, 2015, doi: 10.1016/j.egypro.2015.03.113.

[19] D. R. Mills, “Linear Fresnel reflector (LFR) technology,” *Conc. Sol. Power Technol.*, no. June, pp. 153–196, 2012, doi: 10.1533/9780857096173.2.153.

[20] D. Schlipf, M. Dohn, and J. Lehner, *Model-based feedforward control for CSP plants with linear fresnel technology for a flexible renewable power generation*, vol. 8, no. PART 1. IFAC, 2012.

[21] M. J. Montes, C. Rubbia, R. Abbas, and J. M. Martínez-Val, “A comparative analysis of configurations of linear fresnel collectors for concentrating solar power,” *Energy*, vol. 73, pp. 192–203, 2014, doi: 10.1016/j.energy.2014.06.010.

[22] M. J. Montes, R. Barbero, R. Abbas, and A. Rovira, “Performance model and thermal comparison of different alternatives for the Fresnel single-tube receiver,” *Appl. Therm. Eng.*, vol. 104, pp. 162–175, 2016, doi: 10.1016/j.applthermaleng.2016.05.015.

[23] R. Abbas, A. Sebastián, M. J. Montes, and M. Valdés, “Optical features of linear Fresnel collectors with different secondary reflector technologies,” *Appl. Energy*, vol. 232, no. July, pp. 386–397, 2018, doi: 10.1016/j.apenergy.2018.09.224.

[24] M. Oukili, S. Zouggar, M. Seddik, F. Vallée, M. El Hafyani, and T. Ouchbel,

"Evaluation of the moroccan power grid adequacy with introduction of concentrating solar power (CSP) using solar tower and parabolic trough mirrors technology," *Energy Procedia*, vol. 42, pp. 113–122, 2013, doi: 10.1016/j.egypro.2013.11.011.

[25] M. Binotti, M. Astolfi, S. Campanari, G. Manzolini, and P. Silva, "Preliminary Assessment of sCO2 Power Cycles for Application to CSP Solar Tower Plants," *Energy Procedia*, vol. 105, pp. 1116–1122, 2017, doi: 10.1016/j.egypro.2017.03.475.

[26] A. B. Awan, K. V. V. Chandra Mouli, and M. Zubair, "Performance enhancement of solar tower power plant: A multi-objective optimization approach," *Energy Convers. Manag.*, vol. 225, no. September, p. 113378, 2020, doi: 10.1016/j.enconman.2020.113378.

[27] S. A. Kalogirou, "A detailed thermal model of a parabolic trough collector receiver," *Energy*, vol. 48, no. 1, pp. 298–306, 2012, doi: 10.1016/j.energy.2012.06.023.

[28] W. Fuqiang, T. Zhexiang, G. Xiangtao, T. Jianyu, H. Huaizhi, and L. Bingxi, "Heat transfer performance enhancement and thermal strain restrain of tube receiver for parabolic trough solar collector by using asymmetric outward convex corrugated tube," *Energy*, vol. 114, pp. 275–292, 2016, doi: 10.1016/j.energy.2016.08.013.

[29] H. L. Zhang, J. Baeyens, J. Degrève, and G. Cacères, "Concentrated solar power plants: Review and design methodology," *Renew. Sustain. Energy Rev.*, vol. 22, pp. 466–481, 2013, doi: 10.1016/j.rser.2013.01.032.

[30] C. Prieto and L. F. Cabeza, "Thermal energy storage (TES) with phase change materials (PCM) in solar power plants (CSP). Concept and plant performance," *Appl. Energy*, vol. 254, no. August, p. 113646, 2019, doi: 10.1016/j.apenergy.2019.113646.

[31] J. Pacio, C. Singer, T. Wetzel, and R. Uhlig, "Thermodynamic evaluation of liquid metals as heat transfer fluids in concentrated solar power plants," *Appl. Therm. Eng.*, vol. 60, no. 1–2, pp. 295–302, 2013, doi: 10.1016/j.applthermaleng.2013.07.010.

[32] N. Bhuiyan, W. Ullah, R. Islam, T. Ahmed, and N. Mohammad, “Performance optimisation of parabolic trough solar thermal power plants–a case study in Bangladesh,” *Int. J. Sustain. Energy*, vol. 39, no. 2, pp. 113–131, 2020, doi: 10.1080/14786451.2019.1649263.

[33] L. Qoaider and A. Liqreina, “Optimization of dry cooled parabolic trough (CSP) plants for the desert regions of the Middle East and North Africa (MENA),” *Sol. Energy*, vol. 122, pp. 976–985, 2015, doi: 10.1016/j.solener.2015.10.021.

[34] M. Hajjaj, A. Mellaikhafi, A. Tilioua, and C. Messaoudi, “Numerical Investigation and Control The Thermal Storage System in A Single- Tank for CSP Plants Numerical Investigation and Control The Thermal Storage System in A Single-Tank for CSP Plants,” no. February 2021, 2020.

[35] M. E. Burulday, M. S. Mert, and N. Javani, “Thermodynamic analysis of a parabolic trough solar power plant integrated with a biomass-based hydrogen production system,” *Int. J. Hydrogen Energy*, vol. 47, no. 45, pp. 19481–19501, 2022, doi: 10.1016/j.ijhydene.2022.02.163.

[36] I. Afgan, “Enhancement Techniques of Parabolic Trough Collectors: A Review of Past and Recent Technologies,” *Adv. Civ. Eng. Technol.*, vol. 3, no. 3, pp. 1–6, 2019, doi: 10.31031/acet.2019.03.000563.

[37] A. A. Hachicha, Z. Said, S. M. A. Rahman, and E. Al-Sarairah, “On the thermal and thermodynamic analysis of parabolic trough collector technology using industrial-grade MWCNT based nanofluid,” *Renew. Energy*, vol. 161, pp. 1303–1317, 2020, doi: 10.1016/j.renene.2020.07.096.

[38] R. V. Padilla, A. Fontalvo, G. Demirkaya, A. Martinez, and A. G. Quiroga, “Exergy analysis of parabolic trough solar receiver,” *Appl. Therm. Eng.*, vol. 67, no. 1–2, pp. 579–586, 2014, doi: 10.1016/j.applthermaleng.2014.03.053.

[39] M. H. Abedini-Sanigy, F. Ahmadi, E. Goshtasbirad, and M. Yaghoubi, “Thermal Stress Analysis of Absorber Tube for a Parabolic Collector under Quasi-Steady State Condition,” *Energy Procedia*, vol. 69, pp. 3–13, 2015, doi: 10.1016/j.egypro.2015.03.002.

[40] T. Fahim, S. Laouedj, A. Abderrahmane, S. Alotaibi, O. Younis, and H. M. Ali,

"Heat Transfer Enhancement in Parabolic through Solar Receiver: A Three-Dimensional Numerical Investigation," *Nanomaterials*, vol. 12, no. 3, pp. 1–19, 2022, doi: 10.3390/nano12030419.

[41] A. Mwesigye, T. Bello-Ochende, and J. P. Meyer, "Multi-objective and thermodynamic optimisation of a parabolic trough receiver with perforated plate inserts," *Appl. Therm. Eng.*, vol. 77, pp. 42–56, 2015, doi: 10.1016/j.applthermaleng.2014.12.018.

[42] A. Mwesigye, T. Bello-Ochende, and J. P. Meyer, "Minimum entropy generation due to heat transfer and fluid friction in a parabolic trough receiver with non-uniform heat flux at different rim angles and concentration ratios," *Energy*, vol. 73, pp. 606–617, 2014, doi: 10.1016/j.energy.2014.06.063.

[43] A. Mwesigye, T. Bello-Ochende, and J. P. Meyer, "Numerical investigation of entropy generation in a parabolic trough receiver at different concentration ratios," *Energy*, vol. 53, pp. 114–127, 2013, doi: 10.1016/j.energy.2013.03.006.

[44] B. Zou, J. Dong, Y. Yao, and Y. Jiang, "A detailed study on the optical performance of parabolic trough solar collectors with Monte Carlo Ray Tracing method based on theoretical analysis," *Sol. Energy*, vol. 147, pp. 189–201, 2017, doi: 10.1016/j.solener.2017.01.055.

[45] A. J. Abdulhamed, N. M. Adam, M. Z. A. Ab-Kadir, and A. A. Hairuddin, "Review of solar parabolic-trough collector geometrical and thermal analyses, performance, and applications," *Renew. Sustain. Energy Rev.*, vol. 91, no. April, pp. 822–831, 2018, doi: 10.1016/j.rser.2018.04.085.

[46] E. Bellos and C. Tzivanidis, "Assessment of the thermal enhancement methods in parabolic trough collectors," *Int. J. Energy Environ. Eng.*, vol. 9, no. 1, pp. 59–70, 2018, doi: 10.1007/s40095-017-0255-3.

[47] H. Adun *et al.*, "Multi-objective optimization and energy/exergy analysis of a ternary nanofluid based parabolic trough solar collector integrated with kalina cycle," *Sol. Energy Mater. Sol. Cells*, vol. 231, no. August, p. 111322, 2021, doi: 10.1016/j.solmat.2021.111322.

[48] E. Vengadesan, S. Thameenansari, E. J. Manikandan, and R. Senthil,

"Experimental study on heat transfer enhancement of parabolic trough solar collector using a rectangular channel receiver," *J. Taiwan Inst. Chem. Eng.*, vol. 135, p. 104361, 2022, doi: 10.1016/j.jtice.2022.104361.

[49] E. Bellos, C. Tzivanidis, I. Daniil, and K. A. Antonopoulos, "The impact of internal longitudinal fins in parabolic trough collectors operating with gases," *Energy Convers. Manag.*, vol. 135, pp. 35–54, 2017, doi: 10.1016/j.enconman.2016.12.057.

[50] E. Bellos, C. Tzivanidis, K. A. Antonopoulos, and G. Gkinis, "Thermal enhancement of solar parabolic trough collectors by using nanofluids and converging-diverging absorber tube," *Renew. Energy*, vol. 94, pp. 213–222, 2016, doi: 10.1016/j.renene.2016.03.062.

[51] B. Kurşun, "Thermal performance assessment of internal longitudinal fins with sinusoidal lateral surfaces in parabolic trough receiver tubes," *Renew. Energy*, vol. 140, pp. 816–827, 2019, doi: 10.1016/j.renene.2019.03.106.

[52] S. Akbarzadeh and M. S. Valipour, "Energy and exergy analysis of a parabolic trough collector using helically corrugated absorber tube," *Renew. Energy*, vol. 155, pp. 735–747, 2020, doi: 10.1016/j.renene.2020.03.127.

[53] A. Mwesigye, T. Bello-Ochende, and J. P. Meyer, "Heat transfer and thermodynamic performance of a parabolic trough receiver with centrally placed perforated plate inserts," *Appl. Energy*, vol. 136, pp. 989–1003, 2014, doi: 10.1016/j.apenergy.2014.03.037.

[54] B. Abdullahi, R. K. AL-Dadah, S. Mahmoud, and R. Hood, "Optical and thermal performance of double receiver compound parabolic concentrator," *Appl. Energy*, vol. 159, pp. 1–10, 2015, doi: 10.1016/j.apenergy.2015.08.063.

[55] E. Bellos, C. Tzivanidis, and K. A. Antonopoulos, "Parametric analysis and optimization of a solar assisted gas turbine," *Energy Convers. Manag.*, vol. 139, pp. 151–165, 2017, doi: 10.1016/j.enconman.2017.02.042.

[56] M. A. Hassan *et al.*, "Internally shielded receivers for parabolic trough solar concentrators operating with supercritical carbon dioxide: Analytical assessment," *Energy Convers. Manag.*, vol. 280, no. February, p. 116789,

2023, doi: 10.1016/j.enconman.2023.116789.

[57] K. Zhao, H. Jin, Z. Gai, and H. Hong, “A thermal efficiency-enhancing strategy of parabolic trough collector systems by cascadingly applying multiple solar selective-absorbing coatings,” *Appl. Energy*, vol. 309, no. September 2021, p. 118508, 2022, doi: 10.1016/j.apenergy.2021.118508.

[58] T. U. Shinde, V. H. Dalvi, R. G. Patil, C. S. Mathpati, S. V. Panse, and J. B. Joshi, “Thermal performance analysis of novel receiver for parabolic trough solar collector,” *Energy*, vol. 254, p. 124343, 2022, doi: 10.1016/j.energy.2022.124343.

[59] H. A. Mohammed, H. B. Vuthaluru, and S. Liu, “Thermohydraulic and thermodynamics performance of hybrid nanofluids based parabolic trough solar collector equipped with wavy promoters,” *Renew. Energy*, vol. 182, pp. 401–426, 2022, doi: 10.1016/j.renene.2021.09.096.

[60] S. Samiezadeh, R. Khodaverdian, M. H. Doranehgard, H. Chehrmonavari, and Q. Xiong, “CFD simulation of thermal performance of hybrid oil-Cu-Al2O3 nanofluid flowing through the porous receiver tube inside a finned parabolic trough solar collector,” *Sustain. Energy Technol. Assessments*, vol. 50, no. August 2021, p. 101888, 2022, doi: 10.1016/j.seta.2021.101888.

[61] A. A. Alnaqi, J. Alsarraf, and A. A. A. A. Al-Rashed, “Hydrothermal effects of using two twisted tape inserts in a parabolic trough solar collector filled with MgO-MWCNT/thermal oil hybrid nanofluid,” *Sustain. Energy Technol. Assessments*, vol. 47, no. June, p. 101331, 2021, doi: 10.1016/j.seta.2021.101331.

[62] F. H. Sani, M. Pourfallah, and M. Gholinia, “The effect of MoS2–Ag/ H2O hybrid nanofluid on improving the performance of a solar collector by placing wavy strips in the absorber tube,” *Case Stud. Therm. Eng.*, vol. 30, no. October 2021, p. 101760, 2022, doi: 10.1016/j.csite.2022.101760.

[63] M. Ibrahim, A. Abidi, E. A. Algehyne, T. Saeed, G. Cheraghian, and M. Sharifpur, “Improvement of the energy and exergy efficiencies of the parabolic solar collector equipped with a twisted turbulator using SWCNT-Cu/water two-phase hybrid nanofluid,” *Sustain. Energy Technol. Assessments*, vol. 49, no.

October 2021, p. 101705, 2022, doi: 10.1016/j.seta.2021.101705.

[64] Y. Khetib, A. Alzaed, A. Alahmadi, G. Cheraghian, and M. Sharifpur, “Application of hybrid nanofluid and a twisted turbulator in a parabolic solar trough collector: Energy and exergy models,” *Sustain. Energy Technol. Assessments*, vol. 49, no. October 2021, p. 101708, 2022, doi: 10.1016/j.seta.2021.101708.

[65] A. Allouhi, M. Benzakour Amine, R. Saidur, T. Kousksou, and A. Jamil, “Energy and exergy analyses of a parabolic trough collector operated with nanofluids for medium and high temperature applications,” *Energy Convers. Manag.*, vol. 155, no. October 2017, pp. 201–217, 2018, doi: 10.1016/j.enconman.2017.10.059.

[66] R. Goyal and K. S. Reddy, “Numerical investigation of entropy generation in a solar parabolic trough collector using supercritical carbon dioxide as heat transfer fluid,” *Appl. Therm. Eng.*, vol. 208, no. September 2021, p. 118246, 2022, doi: 10.1016/j.applthermaleng.2022.118246.

[67] R. 14. . ANSYS®, Academic Research, “ANSYS FLUENT Theory Guide,” *ANSYS Inc, USA*, vol. 15317, no. November, p. 814, 2013, [Online]. Available: http://www.afs.enea.it/project/neptunius/docs/fluent/html/th/main_pre.htm.

[68] Y. Y. Bae, E. S. Kim, and M. Kim, “Application of compressible Reynolds-averaged governing equations to turbulent mixed convection in supercritical fluids in heated vertical tubes,” *Int. J. Heat Fluid Flow*, vol. 76, no. December 2018, pp. 85–99, 2019, doi: 10.1016/j.ijheatfluidflow.2018.12.003.

[69] H. K. V. and W. Malalasekera, *An Introduction to Computational Fluid Dynamics: THE FINITE VOLUME METHOD*, vol. 10, no. 01. 2007.

[70] B. Zhang, J. Zhu, L. Gong, K. Jia, and L. Gao, “Topology optimization of heat sink in turbulent natural convection using k-ω turbulent model,” *Appl. Math. Model.*, vol. 118, pp. 272–302, 2023, doi: 10.1016/j.apm.2023.01.028.

[71] H. J. Xu, Z. B. Xing, F. Q. Wang, and Z. M. Cheng, “Review on heat conduction, heat convection, thermal radiation and phase change heat transfer of nanofluids in porous media: Fundamentals and applications,” *Chem. Eng.*

Sci., vol. 195, pp. 462–483, 2019, doi: 10.1016/j.ces.2018.09.045.

[72] N. Zhan, R. Chen, and Y. You, “Three-dimensional high-order finite-volume method based on compact WENO reconstruction with hybrid unstructured grids,” *J. Comput. Phys.*, vol. 490, p. 112300, 2023, doi: 10.1016/j.jcp.2023.112300.

[73] J. P. Pontaza, “A least-squares finite element formulation for unsteady incompressible flows with improved velocity-pressure coupling,” *J. Comput. Phys.*, vol. 217, no. 2, pp. 563–588, 2006, doi: 10.1016/j.jcp.2006.01.013.

[74] R. Forristall, “Heat Transfer Analysis and Modeling of a Parabolic Trough Solar Receiver Implemented in Engineering Equation Solver,” *Natl. Renew. Energy Lab.*, no. October, p. 164, 2003, doi: NREL/TP-550-34169.

[75] E. Dudley, J. Kolb, A. Mahoney, T. Mancini, S. M, and D. Kearney, “Test results: SEGS LS-2 solar collector. Sandia National Laboratory. Report: SAND94- 1884,” *Sandia Natl. Lab.*, p. 140, 1994.

[76] A. Mwesigye, Z. Huan, T. Bello-Ochende, and J. P. Meyer, “Influence of optical errors on the thermal and thermodynamic performance of a solar parabolic trough receiver,” *Sol. Energy*, vol. 135, pp. 703–718, 2016, doi: 10.1016/j.solener.2016.06.045.

[77] A. Bejan, “Entropy generation minimization: The new thermodynamics of finite-size devices and finite-time processes,” *J. Appl. Phys.*, vol. 79, no. 3, pp. 1191–1218, 1996, doi: 10.1063/1.362674.

[78] R. Pal, “On the Gouy-Stodola theorem of thermodynamics for open systems,” *Int. J. Mech. Eng. Educ.*, vol. 45, no. 2, pp. 194–206, 2017, doi: 10.1177/0306419017697413.

[79] A. Bejan, “General criterion for rating heat-exchanger performance,” *Int. J. Heat Mass Transf.*, vol. 21, no. 5, pp. 655–658, 1978, doi: 10.1016/0017-9310(78)90064-9.

Appendices

A.1. Scaled residuals for smooth absorber tube subjected to T_{in} = 350 K for Re = 5000

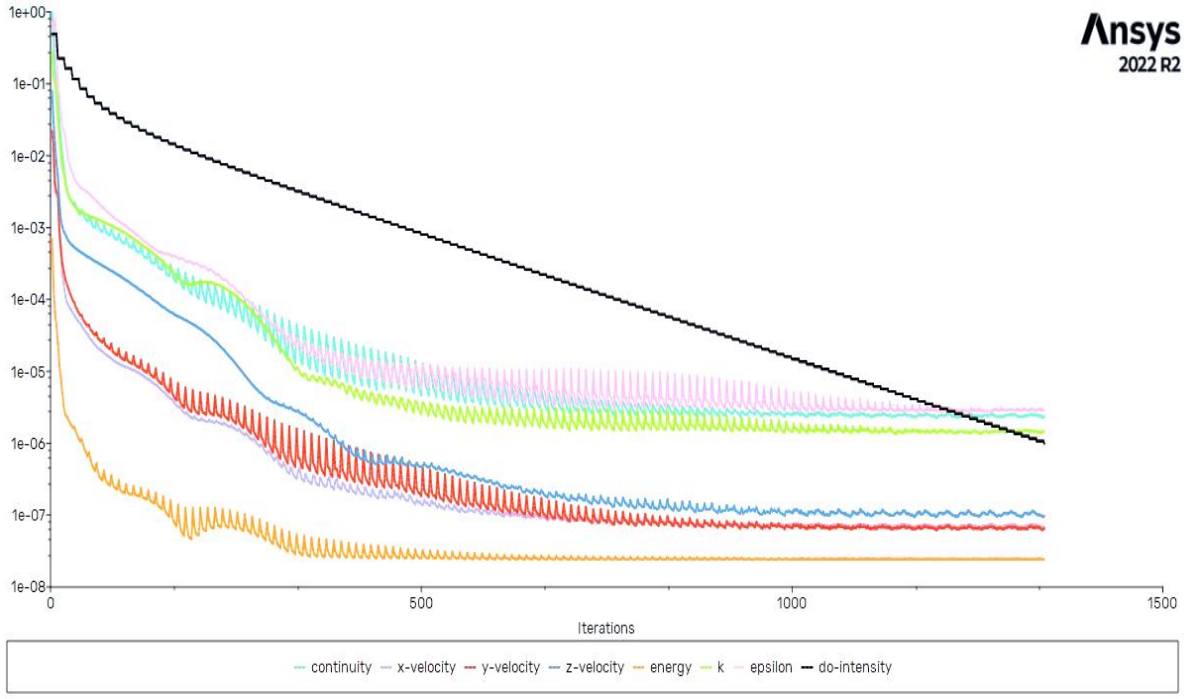

A.2. Temperature contour of the enhanced absorber tube for Re = 5000 at T_{in} = 350 K

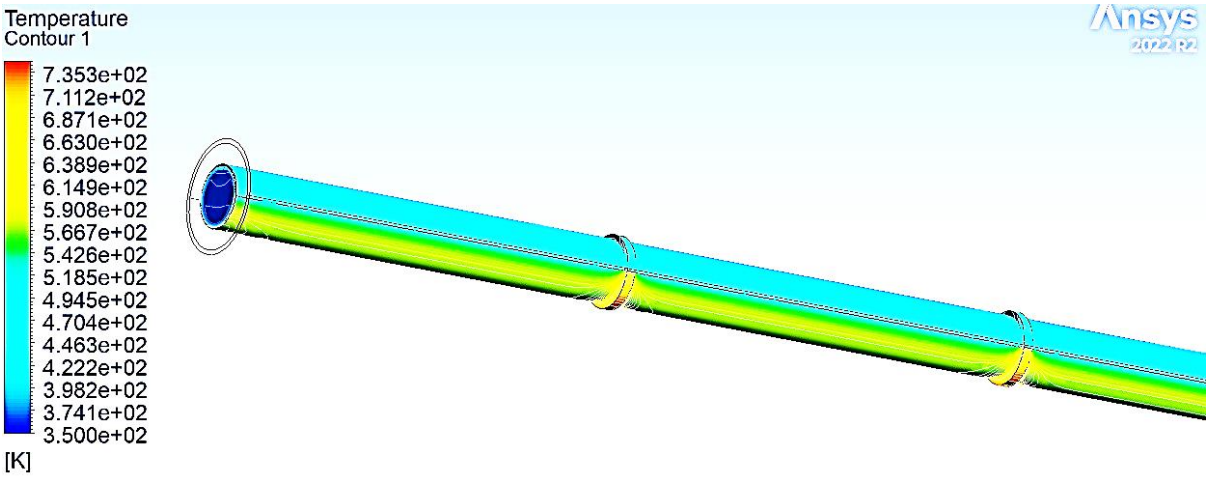

A.3. Temperature distribution on the absorber tube and glass cover for T_{in} = 350 K and Re = 15000

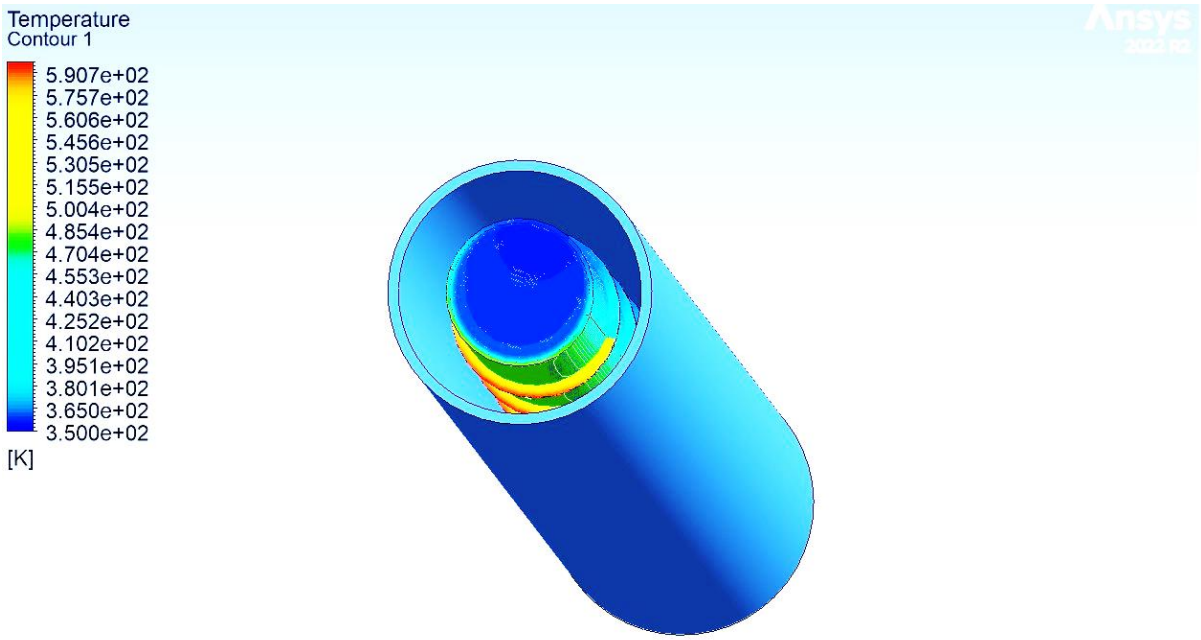

A.4. Radiation distribution on absorber tube and glass cover for T_{in} = 350 K and Re = 5,000

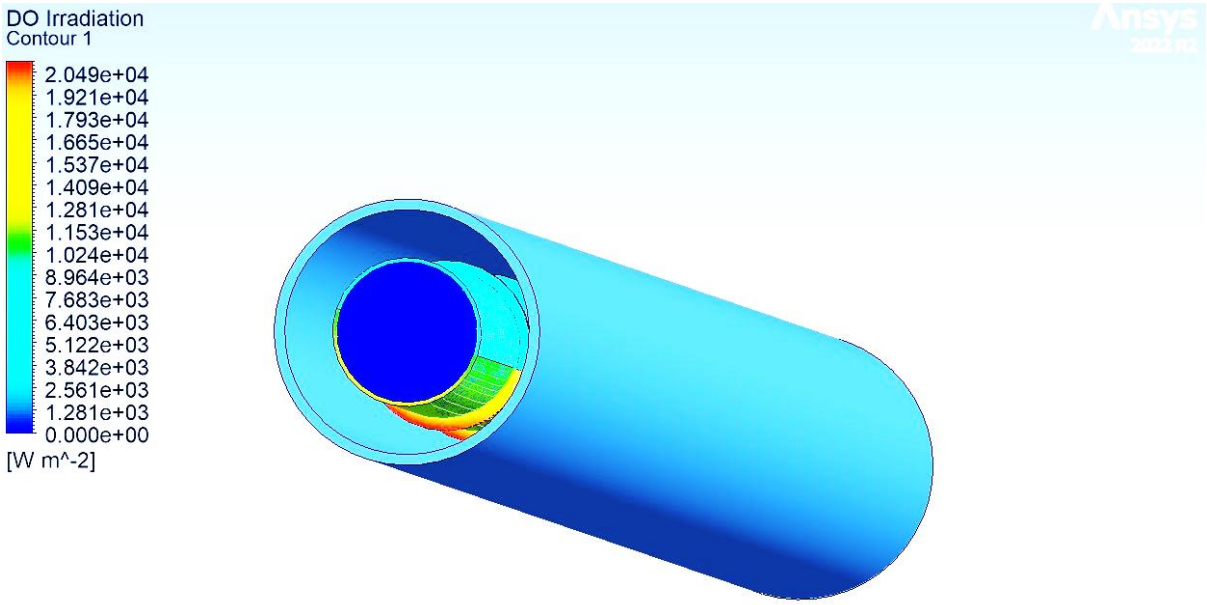

A.5. Pressure distribution in an enhanced absorber tube for T_{in} = 400 K, Re = 15,000, and t = 5 mm

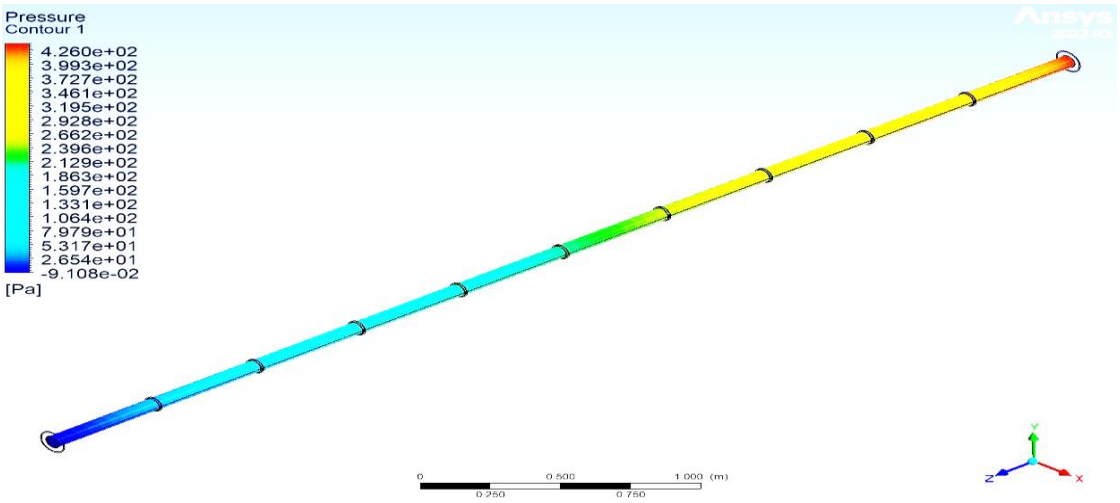

A.6.1. Sample section of the modelled absorber tube and glass cover done in ANSYS Fluent R2

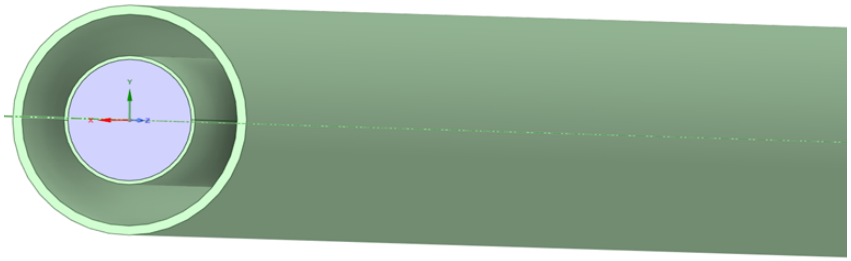

A.6.2. Sample section of an enhanced absorber tube done in ANSYS Fluent R2

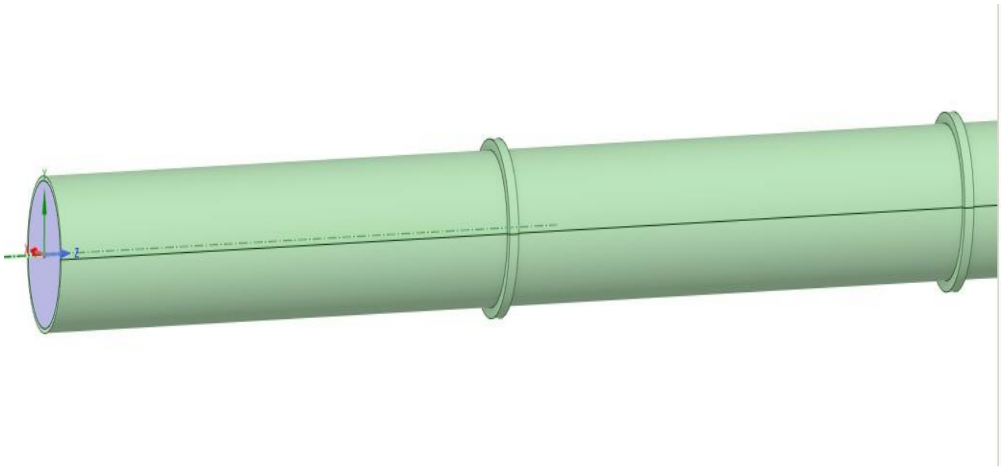

A.6.3. Sample section of generated mesh as done in ANSYS Fluent R2 mesh environment.

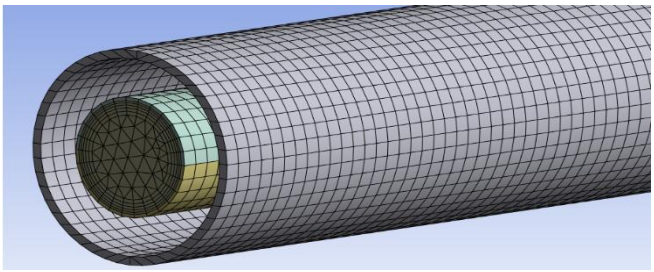

A.7. Faculty Ethic Clearance

UNIVERSITY OF CAPE TOWN
IYUNIVESITHI YASEKAPA • UNIVERSITEIT VAN KAAPSTAD

PRE-SCREENING QUESTIONNAIRE OUTCOME LETTER

STU-EBE-2023-PSQ000225
2023/03/14

Dear Jacob Aketch,

Your Ethics pre-screening questionnaire (PSQ) has been evaluated by your departmental ethics representative. Based on the information supplied in your PSQ, it has been determined that you do not need to make a full ethics application for the research project in question.

You may proceed with your research project titled:

Performance evaluation of PTC receiver with external fins

Please note that should aspect(s) of your current project change, you should submit a new PSQ in order to determine whether the changed aspects increase the ethical risks of your project. It may be the case that project changes could require a full ethics application and review process.

Regards,

Faculty Research Ethics Committee